

**Identification of Fucose- $\alpha$ (1-2)-Galactose  
Binding Proteins in the Mammalian  
Brain**

Thesis by  
Arif Wibowo

In Partial Fulfillment of the Requirements for the  
degree of  
Doctor of Philosophy



CALIFORNIA INSTITUTE OF TECHNOLOGY  
Pasadena, California  
2013  
(Defended 30 May 2013)

© 2013  
Arif Wibowo  
All Rights Reserved

*Knowledge Speaks but Wisdom Listens ~ Jimi Hendrix*

## ACKNOWLEDGEMENTS

First and foremost, I want to thank God, whose many blessings have made me who I am today. My Caltech experience, both scientific and personal, has been bittersweet. I would not be where I am today if not for my family, friends and coworkers at Caltech. Sincerely, I would like to thank everyone who has been part of my life for the past 7 years.

Specifically, I would like to thank my advisor, Linda Hsieh-Wilson, for the opportunity to do great science. She taught me many things but most importantly to always strive for excellence. When I leave Caltech, I am a better scientist because of you. To my committee members: Peter Dervan, Jack Beauchamp and Bob Grubbs, I can't thank you enough for all your guidance and kind support. You have inspired many scientists throughout your career and I feel privileged to have this experience first-hand. I would also like to thank David Tirrell for his advice and generous support and for his valuable input on the dendritic protein synthesis work. To my undergraduate advisor, Richmond Sarpong, thank you for giving me a chance to start in research.

My colleagues in the Hsieh-Wilson lab, both past and present, have been truly invaluable. In particular, I am greatly indebted to Manish Rawat, Song Gil Lee and Wen Yi for being an excellent teacher and even better friend. I would also like to thank Cristal Gama and Jessica Rexach for teaching me how to work with neurons. I have to give special mention to my classmates, Chithra Krishnamurthy and Young In Oh, for being available, especially during a moment of personal tragedy. In addition, I would like to thank Abby Pulsipher, Matt Griffin and Elizabeth Jensen for reading my thesis and

correcting my mistakes. To the rest of the Hsieh-Wilson lab, I am honored to work with a group of talented scientists like all of you.

I am lucky to have had many excellent sources of support in the Caltech community. I would like to thank Anne Penney, Agnes Tong, Joe Drew, Rick Gerhart, Chris Smith, Michael Werner, Susan Mucha, Laura Flower Kim, and Natalie Gilmore for making my life as a graduate student so much easier. For the Caltech staff: Scott Ross, David VanderVelde, Mona Shahgoli, Naseem Torian, Scott Wang and Jennifer Costanza, thank you for helping me do great science. I would also like to thank Michael Bethune, Jiang Xia, Yan Xia, John Matson, Ishu Saraogi and Lea Goentoro for your valuable advice on my career path.

To my friends from Caltech and outside of the campus, your friendship has kept me where I am today. I can't name all of you but I want to thank you for your prayers and encouragements, especially when my heart was heavy. For the friends that have put some normalcy into to my life outside of science, thank you. To my Berkeley, Singapore and Indo friends both at Caltech and elsewhere, I am grateful to have developed such a lasting friendship with all of you. Finally, I want to thank my family for their unconditional love. Levina, I hope I can inspire you. Mom, thank you for being my rock. Dad, I know you're smiling down from heaven.

## ABSTRACT

Fucose- $\alpha$ (1-2)-galactose (Fuc $\alpha$ (1-2)Gal) carbohydrates have been implicated in cognitive functions. However, the underlying molecular mechanisms that govern these processes are not well understood. While significant progress has been made towards identifying glycoconjugates bearing this carbohydrate epitope, a major challenge remains the discovery of interactions mediated by these sugars. Here, we employ the use of multivalent glycopolymers to enable the proteomic identification of weak affinity, low abundant Fuc $\alpha$ (1-2)Gal-binding proteins (i.e., lectins) from the brain. End-biotinylated glycopolymers containing photoactivatable crosslinkers were used to capture and enrich potential Fuc $\alpha$ (1-2)Gal-specific lectins from rat brain lysates. Candidate lectins were tested for their ability to bind Fuc $\alpha$ (1-2)Gal, and the functional significance of the interaction was investigated for one such candidate, SV2a, using a knock-out mouse system. Our results suggest an important role for this glycan-lectin interaction in facilitating synaptic changes necessary for neuronal communication. This study highlights the use of glycopolymer mimetics to discover novel lectins and identify functional interactions between fucosyl carbohydrates and lectins in the brain.

## TABLE OF CONTENTS

Acknowledgements .....	iv
Abstract .....	vi
Table of Contents .....	vii
List of Illustrations Tables .....	viii
Nomenclature .....	xi
<b>Chapter 1: Carbohydrate-Mediated Interactions in Animals .....</b>	<b>1</b>
Introduction.....	1
The Nature of Glycan-Protein Interactions.....	3
Mammalian Lectins and Their Functions .....	6
<b>Chapter 2: The Role of Fucose<math>\alpha</math>(1-2)Galactose Carbohydrates in     Neuronal Communications.....</b>	<b>16</b>
Cellular Fucosylation.....	16
Fucosylation in Neuronal Development .....	18
Fucose- $\alpha$ (1-2)-Galactose and Lectin Association in the Brain.....	22
<b>Chapter 3: Synthesis of Photoactivatable Glycopolymers.....</b>	<b>30</b>
Synthetic Probes for Lectin Isolation.....	30
Design and Synthesis of Photoactivatable Glycovalent Probes.....	33
Methods and Materials .....	45
<b>Chapter 4: Proteomic Identification of Fucose<math>\alpha</math>(1-2)Gal Lectins.....</b>	<b>62</b>
Lectin Discovery by Mass Spectrometry.....	62
Lectin Capture with Biotinylated Multivalent Probes.....	63
Identification of Fucose $\alpha$ (1-2)Gal Lectins in the Brain .....	65
Experimental Methods .....	73
<b>Chapter 5: Validation of Fucose<math>\alpha</math>(1-2)Gal-Lectin Candidates .....</b>	<b>80</b>
Biological Impact of MS-Based Proteomics .....	80
Validating Lectin Binding towards Fucose $\alpha$ (1-2)Gal Carbohydrates .....	82
Structural Analysis of Lectin Candidate SV2a.....	86
Characterization of SV2a Function in FUT KO Mice .....	90
Experimental Methods .....	95
Appendix 1: Spectra For Polymer Synthesis .....	104
Appendix 2: Proteomics Data.....	117

## LIST OF ILLUSTRATIONS TABLES

<i>Chapter 1</i>		<i>Page</i>
Figure 1.1	Major Types of Animal Lectins	6
Figure 1.2	Cellular Functions of Lectins	9
 <i>Chapter 2</i>		
Figure 2.1	Biosynthesis of Complex Fuc $\alpha$ (1-2)Gal Carbohydrates	18
Figure 2.2	Chemical Structures of Fucosyl Derivatives	20
Figure 2.3	Inhibition of Fuc $\alpha$ (1-2)Gal Linkages with 2-dGal	21
Figure 2.4	Fuc $\alpha$ (1-2)Gal PAA Stimulates Neurite Outgrowth	23
Figure 2.5	Multivalent Interaction between Fuc $\alpha$ (1-2)Gal and Its Associated Lectin	23
Figure 2.6	Treatment of Hippocampal Neurons with 2-dGal Inhibits Neuronal Growth	24
 <i>Chapter 3</i>		
Figure 3.1	Lectin Capture from the Brain Using Monovalent Probe	32
Figure 3.2	Design of Multivalent Biotinylated Capture Probe	33
Figure 3.3	Isolation of Lectin Using Multivalent Capture Probe	34
Scheme 3.1	Synthesis of Fuc $\alpha$ (1-2)Gal Glycomonomer	36
Scheme 3.2	Directing Stereoselectivity with Protecting Group Manipulation	38

Scheme 3.3	Anomeric Effect on Glycan Linkage	38
Scheme 3.4	Synthesis of Phenyl Azide Crosslinker Monomer	40
Scheme 3.5	Synthesis of Biotin-Arylamine Initiator	40
Scheme 3.6	Mechanism of Biotin-Chain-Terminated Glycopolymer Synthesis	41
Table 3.1	Characterization of Biotin-Functionalized Polymer	42
Scheme 3.7	Synthesis of Biotin-Functionalized Photoactivatable Glycopolymer	43
 <i>Chapter 4</i>		
Figure 4.1	UEAI Capture with Multivalent Glycopolymer Probes	65
Figure 4.2	Multivalent Capture Probes are Non-Toxic to Hippocampal Neurons	66
Figure 4.3	Multivalent Capture Probes Stimulates Neuronal Growth	66
Figure 4.4	Strategies for Fuc $\alpha$ (1-2)Gal Lectins Identification	68
Figure 4.5	Representative Gel of Captured Lectins from Various Neuronal Fractions	69
Figure 4.6	Lectin Capture Enrichment from the Synaptosome and Membrane Fractions	69
Figure 4.7	Functional Classifications of the Fuc $\alpha$ (1-2)Gal Lectins	70
Table 4.1	Fuc $\alpha$ (1-2)Gal-Lectin Candidates from the Brain	71
 <i>Chapter 5</i>		
Figure 5.1	Profiling PKC $\epsilon$ and SV2a Binding on Mammalian Glycan Arrays	83

Figure 5.2	Fuc $\alpha$ (1-2)Gal Enhances the Binding Affinity of PKC $\epsilon$ and SV2a	84
Figure 5.3	Binding Validation of Lectin Candidates with Enzyme-Linked Lectin Assay	86
Figure 5.4	Predicted Topology of SV2 Protein	87
Figure 5.5	SV2a Sequence Homology with the C-type Lectin Superfamily	89
Figure 5.6	Chemoenzymatic Strategy for Fuc $\alpha$ (1-2)Gal Glycan Labeling	91
Figure 5.7	Functional Interaction between SV2a and Fuc $\alpha$ (1-2)Gal Carbohydrates	92

## LIST OF ABBREVIATIONS

1D	one-dimensional
2D	two-dimensional
2-dGal	2-deoxy-D-galactose
2-fucosyllactose	L-fucose $\alpha$ (1-2)galactose $\beta$ (1-4)glucose
3-dGal	3-deoxy-D-galactose
Ab	antibody
Ac	acetyl, acetate
Ac <sub>2</sub> O	acetic anhydride
AgNO <sub>3</sub>	silver nitrite
AgOTf	silver (I) triflate
ANB-NOS	<i>N</i> -5-azido-2-nitrobenzylsuccinimide
ASGR1	Asialoglycoprotein receptor 1
aq	aqueous
BSA	bovine serum albumin
°C	degree Celsius
CaCl <sub>2</sub>	calcium chloride
Cat	catalytic
CAN	ceric ammonium nitrate
CH <sub>3</sub> N	acetonitrile
CHCl <sub>3</sub>	chloroform
CH <sub>2</sub> Cl <sub>2</sub>	dichloromethane
(CH <sub>3</sub> S) <sub>2</sub>	dimethyl disulfide
CMF-HBSS	Calcium and Magnesium-Free Hank's Balanced Salt Solution
CNS	central nervous system
CO <sub>2</sub>	carbon dioxide
CRD	carbohydrate recognition domain
CS	chondroitin sulfate
Ct	control polymer III
CTLD	C-type lectin domain
DCLK1	double cortin-like kinase 1
DC-SIGN	dendritic cell-specific ICAM 3-grabbing non-integrin
ddH <sub>2</sub> O	double distilled water
D-Gal	D-galactose
DIV	days in vitro
DMEM	Dulbecco's Minimal Eagle's Medium
DMF	dimethylformamide
DMSO	dimethylsulfoxide
E18	embryonic day 18

EDTA	ethylenediaminetetraacetic acid
EGTA	ethylene glycol tetraacetic acid
Et <sub>2</sub> O	diethyl ether
Et <sub>3</sub> N	triethyl amine
FG	fucose $\alpha$ (1-2)galactose polymer II
Fuc	L-fucose
Fuc $\alpha$ (1-2)Gal	fucose $\alpha$ (1-2) galactose
FUT	fucosyltransferase
FUT1	$\alpha$ (1-2) fucosyltransferase 1
FUT2	$\alpha$ (1-2) fucosyltransferase 1
g	gram, gravitational force
G $\alpha$ O	guanine nucleotide-binding protein alpha subunit
Gal	galactose
GalNAc	<i>N</i> -acetylgalactosamine
GDP-fucose	guanosine diphosphatyl-fucose
GlcN	D-glucosamine
GlcNAc	<i>N</i> -acetylglucosamine
Gluc	glucose
GluR1	glutamate receptor 1
GTP	guanosine triphosphate hour
HBF <sub>4</sub>	tetrafluoroboric acid
HIO <sub>4</sub>	periodate
HMDS	hexamethyldisilane
HRP	horse-radish peroxidase
HS	heparan sulfate
ICAM	intercellular cell adhesion molecule
IDCP	Iodonium di-sym-collidine perchlorate
IgG	immunoglobulin
IP	immunoprecipitated
K <sup>+</sup>	potassium ion
K <sub>a</sub>	association constant
KCl	potassium chloride
kDa	kilodalton
L	liter
LTP	long-term potentiation
M	molar
MALDI-TOF	matrix-assisted laser desorption/ionization time-of-flight
MALLS	multi-angle laser light spectroscopy
MAP2	microtubule associated protein 2
MAPK	mitogen-associated protein kinase
MEM	Minimal Eagle's Medium
MeCN	acetonitrile
MeOH	methanol

$\mu\text{g}$	microgram
$\text{MgCl}_2$	magnesium chloride
min	minutes
m	milli or meter
$\mu$	micro
mol	mole
MS	mass spectrometry
n	nano
N	normal
$\text{Na}^+$	sodium ion
NaCl	sodium chloride
NaH	sodium hydride
NaOCN	sodium cyanate
NaOH	sodium hydroxide
NaOMe	sodium methoxide
$\text{NaNO}_2$	sodium nitrite
NeuAc	N-acetyl-neuraminic acid
$\text{NH}_4\text{HCO}_3$	ammonium bicarbonate
NIS	n-iodosuccinimide
NP-40	nonidet P-40 detergent
OEt	<i>O</i> -ethyl
P2	insoluble fraction 2
PAA	polyacrylamide
PAGE	polyacrylamide gel electrophoresis
PBS	phosphate buffered saline
PDI	polydispersity index
PKC $\epsilon$	protein kinase C epsilon subunit
PMB	p-methoxy benzyl
PTM	post-translation modification
PVDF	polyvinylidene difluoride
Pol	polymer
Pyr	pyridine
Rel	relative
RNA	ribonucleic acid
rpm	revolutions per minute
RSL	rattle snake lectin
rt	room temperature
SDS	sodium dodecyl sulfate
SEC	size-exclusion column
SEM	standard error of the mean
SV2a	synaptic vesicle glycoprotein a
Syt1	synaptotagmin 1
TBAF	tetrabutylammonium fluoride

TCEP	tris(2-carboxyethyl)phosphine
TBST	tris buffered saline with Tween-20
THF	tetrahydrofuran
TMSSPH	(phenylthio)trimethylsilane
Tris-Cl	tris chloride
U	unit
UEA I	<i>Ulex europaeus</i> agglutinin I
UV	ultraviolet
vol	volume
w/v	weight per volume
WT	wild type
ZnI <sub>2</sub>	zinc iodide

## *Chapter 1*

### CARBOHYDRATE-MEDIATED INTERACTIONS IN ANIMALS

#### **1.1. Introduction**

Complex cellular processes are regulated by networks of interacting biomolecules both inside and outside of cells. These interactions contribute to the structure and function of a living cell and are mediated by various cellular components, such as proteins, DNA, RNA and small molecules.<sup>1,2</sup> An important component of this network is characterized by the interactions between carbohydrates and their corresponding binding partner(s). The various combinations of the naturally occurring monosaccharides, joined through numerous possible linkages and branch points, have the potential to generate complex sets of oligosaccharide structures. These oligosaccharides are covalently bound to lipids and proteins, forming glycolipids and glycoproteins, respectively. With such structural diversity, these sugars carry enormous potential for encoding molecular information significant for modulating complex processes in living organisms.

Glycoconjugates (e.g., glycoproteins, GPI-anchored glycans and glycolipids) are abundant in every organism from bacteria, fungi, virus and plants to mammals. Approximately more than 50% of all proteins are modified with glycans.<sup>3</sup> Even though carbohydrate architectures are structurally diverse, they are exposed to the same glycosylation machinery. As such, carbohydrate biosynthesis must be tightly regulated by the concerted actions of cellular enzymes and substrates. Gene transcription has a major

impact on glycan formation, as reflected by the cell type-specific and developmentally modulated expression of many glycosyltransferases and glycosidases. Furthermore, subcellular localization of these enzymes and their nucleotide sugar donor substrates could facilitate the formation of different saccharide linkages in the endoplasmic reticulum (ER) and Golgi. Changes in the glycome in response to environmental and genetic stimuli are potentially associated with the acquisition of altered cellular phenotypes. Vertebrates, especially mammals, have evolved a highly complex glycan repertoire that is structurally distinct from that of invertebrates, lower eukaryotes and prokaryotes. As a result, the variation in glycomes among vertebrates may serve as the molecular basis for mediating different cellular functions.

Glycans serve important biological roles in protein maturation and turnover, cell adhesion and trafficking and receptor binding and activation.<sup>4-7</sup> In addition, aberrant glycosylation can lead to various diseases. The congenital disorders of glycosylation (CDGs) affect children by causing severe morphogenic and metabolic defects due to a general failure in glycan formation.<sup>8,9</sup> Alterations in glycosylation profiles are a common feature of tumor cells and may affect any types of cell glycoconjugates such as glycoproteins, glycolipids or glycosaminoglycans.<sup>10</sup> In fact, overexpression of the sialyl, fucosyl and Tn antigens have been observed in malignant tissues throughout the body, including the brain, colon, breast and prostate.<sup>11-16</sup> Carbohydrate-mediated interactions in the nervous system also play important roles during development, regeneration and synaptic plasticity.<sup>17,18</sup> Therefore, glycan-mediated interactions are involved in a number of

cellular functions, including protein folding and trafficking, cell-cell communication, receptor activation and signal transduction.

## **1.2. The Nature of Glycan-Protein Interactions**

Glycosylation produces different types of glycoconjugates that are typically attached to cellular proteins and lipids. Glycoproteins, glycosaminoglycans and MUCINS exhibit glycans that are covalently attached to protein backbones in various linkages. There are two broad groups of glycoproteins, N-glycans and O-glycans, which differ in the nature of their linkage to the protein backbone. N-glycans are attached to asparagine residues of proteins, specifically a subset residing in the Asn-X-Ser/Thr motif, whereas O-glycans are attached to a subset of serine and threonine residues.<sup>19,20</sup> Glycosaminoglycans are also linked to serine and threonine residues, but they are made up of structurally linear oligosaccharide polymers that can often be highly sulfated.<sup>21</sup> Glycolipids are characterized by a membrane-embedded ceramide moiety that anchors the extracellular glycan component of the glycolipid to the cell. Neutral and sialylated glycosphingolipids (GSLs) exist as the major glycolipid constituents in mammals. Neutral GSLs are derived from the core glycosylceramides precursor and are implicated in cellular homeostasis and tissue development, while the sialylated forms, often termed gangliosides, are relatively enriched in the brain and participate in cellular adhesion and signaling.<sup>22,23</sup> Extensive carbohydrate presentations from these glycoconjugates indicate that glycans are involved in modulating many cellular functions. As such, glycan receptor(s) identification is critical for understanding the molecular mechanism of carbohydrate-mediated signaling events.

Structural information encoded by glycans is recognized by specific glycan binding proteins (GBPs). A class of these proteins, lectins, binds mono- and oligosaccharides reversibly and with high specificity, are devoid of catalytic activity and are not products of the immune response. Lectins, like their glycoconjugate counterparts exist in most organisms, ranging from viruses and bacteria to plants and animals.<sup>24</sup> The interactions between glycans and lectins typically occur with weak affinity ( $K_a = 10^3\text{--}10^6 \text{ M}^{-1}$ )<sup>25</sup> but with significant avidity, given that most lectins can simultaneously bind multiple glycan moieties. In nature, the typically weak binding interactions between GBPs and individual glycans are compensated by their multivalent displays on glycoprotein scaffolds.<sup>26,27</sup> In many instances, the glycan structure alone is not sufficient enough to generate a recognition event below a certain epitope density threshold. As a result, the multivalent binding activities of carbohydrate-lectin interactions are extremely important because they lead to the augmentation of glycoprotein organization (clustering).<sup>28</sup> In turn, glycoprotein clustering contributes to the regulatory mechanism by which cell-surface glycan epitope density is maintained for downstream signaling events.<sup>29</sup>

The multivalency of glycoproteins is also exhibited in GBPs, as they frequently possess more than one glycan-binding site (subsite multivalency). The involvement of secondary binding interactions in regions of the receptor other than the primary binding site have been shown to provide substantial affinity enhancements.<sup>30</sup> In addition, lectins can oligomerize to form multiple receptor binding sites for increased binding interactions. Furthermore, the chelating effects between multivalent ligands and multiple receptors decrease the binding off-rate because the translational entropy expenditure is made with the

first receptor-ligand contact.<sup>31</sup> Nevertheless, the apparent affinity of a multivalent interaction often is less than might be expected, presumably due to the conformational entropy restrictions incurred by multipoint binding. As a consequence, there are a number of different modes through which GBPs and glycoproteins can engage each other

Lectins undergo few changes in conformation upon binding to sugar.<sup>32</sup> Carbohydrate binding sites are typically broad and shallow, characterized by several general principles. First, the epimeric -OH that distinguishes particular sugars is involved in hydrogen bonding to the lectin, providing a direct read-out towards glycan affinity. Next, specificity is established by the steric exclusion of disfavored ligands, rather than the mere loss of contact within the binding sites. The combination of hydrogen bonding of the -OH groups and the van der Waals packing of the hydrophobic face of each sugar ring impose geometric constraints on the oligosaccharides, evoking the desired energetic conformation that leads to a substantial binding enhancement for multivalent ligands. Higher selectivity is further achieved through an extended binding pocket which recognizes the protein domain contribution of the glycoconjugate, in addition to its glycan structure.<sup>33-35</sup> Finally, the selectivity and enhanced affinity between the glycan and lectin pair can be achieved by bridging water molecules and/or divalent cations. In particular,  $\text{Ca}^{2+}$  and  $\text{Mn}^{2+}$  have been shown to stabilize the lectin binding site by coordinating the interactions between specific amino acids and carbohydrate ligands.<sup>32</sup>

### 1.3. Mammalian Lectins and Their Functions

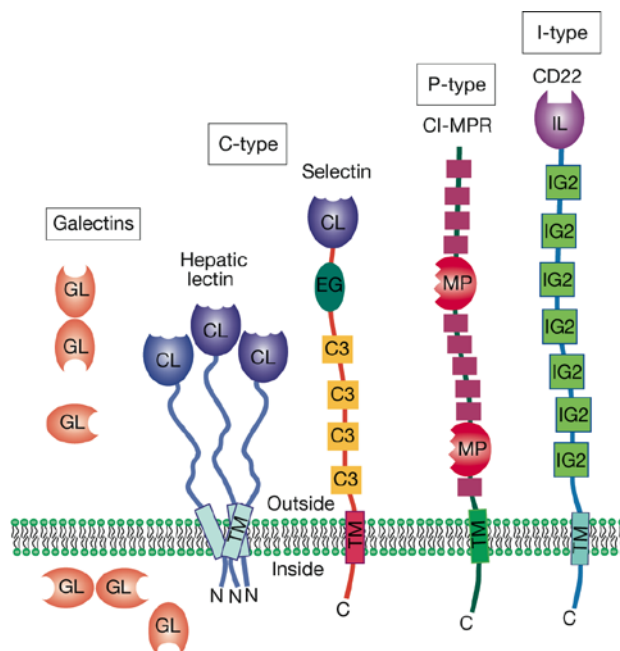


**Fig 1.1.** Schematic examples of major types of animal lectins. Reproduced with permission from *Essentials of Glycobiology*, 2<sup>nd</sup> Edition, Chapter 26.

Mammalian lectins have been identified and classified by their carbohydrate recognition domain (CRD) motif, such as those that define the C-, S-, P-, and I-type lectins (Fig 1.1).<sup>36</sup> C-type lectins (CTLs) are the most abundant of all animal lectins, and the CTL superfamily is grouped into three families: selectins, collectins and endocytic lectins.<sup>37,38</sup> A majority of CTLs are large, asymmetric, possess one or more CRD and exist as  $\text{Ca}^{2+}$ -dependent proteins found in secreted or membrane-bound forms.<sup>37,39</sup> The collectin family of CTLs mediates pathogen neutralization through soluble collagenous lectins, such as mannose-binding proteins (MBPs), pulmonary surfactant SP-A and SP-D and conglutinin. The selectin family consisting of the E-, L- and P-selectins, is directly involved in adaptive immune response by mediating transient interactions between leukocytes and the

endothelium. These selectins have a single epidermal growth (EGF)-like domain, an extracellular CRD, a cytoplasmic tail, a transmembrane domain and two to nine short consensus repeat units that may participate in cellular adhesion.<sup>40,41</sup> The physiological ligands for the selectins contain fucosylated core trisaccharides designated as Lewis<sup>x</sup> (Le<sup>x</sup>) and Lewis<sup>a</sup> (Le<sup>a</sup>) and their corresponding sialylated counterparts (sLe<sup>x</sup> and sLe<sup>a</sup>).<sup>37,40</sup> Finally, the other families of CTLs include the macrophage mannose receptor, DC-SIGN and the hepatic asialoglycoprotein receptor (ASGR). These receptors have all been implicated in pathogen recognition, leading to the cellular uptake and subsequent processing of its endocytic contents.<sup>42,43</sup>

In contrast, the S-type lectins (galectins) are generally small, non-glycosylated, soluble and exist as Ca<sup>2+</sup> independent proteins that are found both inside and outside of cells.<sup>37,44</sup> To date, 15 galectins have been identified in mammals, most with wide tissue distribution, and many bind N-acetyllactosamine (Gal $\beta$ 1-nGlcNAc-R) through  $\beta$ -gal residue recognition.<sup>39</sup> Most galectins are either bivalent or multivalent with regard to their carbohydrate-binding activities, which allows them to recognize multiple binding partners for activating distinct signaling pathways. Galectins display an intriguing combination of intra- and extracellular activities and are implicated in the regulation of immunity and inflammation,<sup>45</sup> progression in cancer<sup>46</sup> and in specific developmental processes.<sup>47</sup>

The I-type lectins are a class of carbohydrate-recognizing proteins that belong to the immunoglobulin (Ig) superfamily. A major component of the I-type lectin family is the Siglec, a type 1 transmembrane protein that bind to sialic acid epitopes with low affinity

( $K_d = 0.1 - 3 \text{ mM}$ ) through its N-terminal V-set Ig domain.<sup>48</sup> Ten Siglecs have been identified in mammals, most with unique expression patterns in different cell types, implicating roles in highly specialized and specific cellular processes.<sup>49</sup> In fact, most Siglecs present an immunoreceptor tyrosine-based motif from their intracellular domain, suggesting roles in both cell-cell interactions and cellular signaling events.<sup>50</sup> Other members of the I-type lectins have also been reported to recognize different glycan epitopes and include a family of adhesion molecules, such as the L1-cell adhesion molecule (L1-CAM), neural cell adhesion molecule (NCAM) and intercellular adhesion molecule 1 (ICAM-1).<sup>49</sup> Efforts are currently underway to identify the endogenous ligand(s) for the I-type lectin family and their functions in cellular activity.

The P-type lectins serve an essential role in the generation of functional lysosomes within the cells of higher eukaryotes. The recruitment of soluble acid hydrolases to newly synthesized lysosomes is initiated by the formation of mannose 6-phosphate (M6P) residues, which become a targeting signal for the P-type lectin receptors.<sup>51</sup> Following M6P recognition, the hydrolase-receptor complex is transported to pre-lysosomal compartments, where the low-pH environment induces release of the enzymes from the receptors. This trafficking process is mediated by two P-type lectin receptor families located in the trans-Golgi network (TGN): the cation-dependent mannose 6-phosphate receptor (CD-MPR) and the insulin-like growth factor II/cation-independent mannose 6-phosphate receptor (IGF-II/CI-MPR). Both receptors contain a single transmembrane-spanning segment, a C-terminal cytoplasmic region and an N-terminal ligand-binding region.<sup>52</sup> In contrast to the CD-MPR, the multifunctional IGF-II/CI-MPR binds to several distinct nonglycosylated

ligands, including IGF-II, in addition to mannose 6-phosphorylated proteins.<sup>53–55</sup> As a result, CI-MPR is also implicated in other cellular processes, including apoptosis, viral entry and proteolytic activation of enzyme and growth factor precursors.

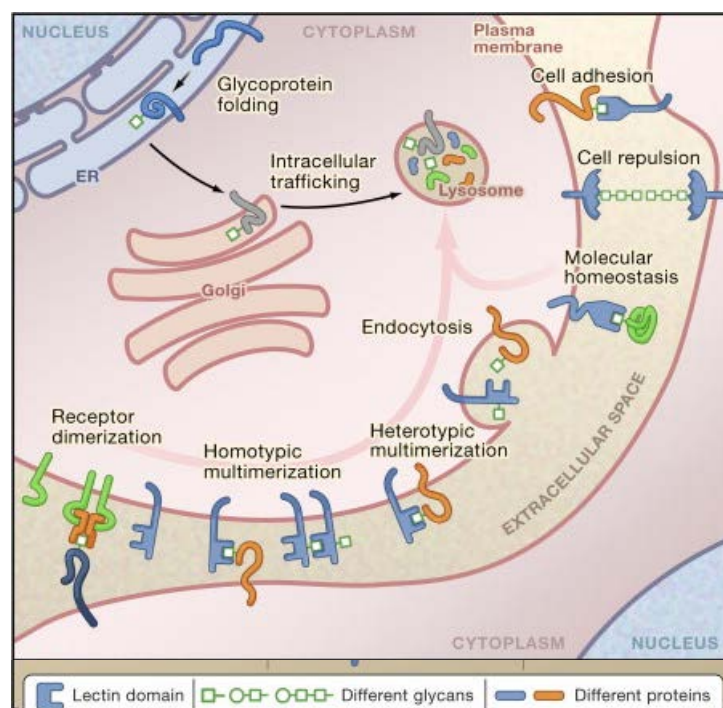


**Fig 1.2.** Glycan-receptor interaction encompasses a number of cellular functions including protein folding, trafficking, adhesion and signal transduction. Adapted with permission from (56).

The biological activities of mammalian lectins are due to their carbohydrate-binding properties. The success of deciphering carbohydrate-encoded information is based on lectin selectivity towards the different glycan epitopes and the corresponding interaction between specific glycan-receptor pairs. By binding to lectins and sterically modulating molecular interactions, mammalian glycans participate in multiple cellular activities, such

as protein folding, cell recognition and adhesion, trafficking, receptor activation, signal transduction and endocytosis (Fig 1.2).<sup>56</sup> Conversely, these functional roles are dependent on the nature of the interactions, specifically, the formation or disruption of intra- and intermolecular binding involving both homotypic and heterotypic substrates. In addition, the biological relevance of glycan-mediated interactions is determined by the spatiotemporal control of the lectin-glycoconjugate pair. Thus, although the glycan structure is expressed on many glycoproteins, the subcellular localization of the lectin and its glycoconjugate exclude other glycoproteins from being physiologically relevant.

Mammalian lectin involvement in cell-cell adhesion is best characterized by the selectins and their glycan ligands, which include a key fucose linkage on the sLe<sup>x</sup> oligosaccharide. This cell adhesion system is highly regulated on the cell-surface endothelium and on most leukocytes, thereby contributing to leukocyte trafficking during an immune-system response and inflammation.<sup>57</sup> Glycan recognition by mammalian lectin is also critical in pathogenic infection. A key example of this phenomenon involves DC-SIGN, a C-type lectin expressed by dendritic cells (DCs), which functions as a receptor for several viruses, including the Ebola virus, cytomegalovirus (CMV), hepatitis C virus, human immunodeficiency virus (HIV) and dengue virus.<sup>58</sup> In particular, DC-SIGN recognizes many different viral envelope glycoproteins expressing relatively large numbers of N-linked carbohydrates. One such example involves the DC-SIGN capture of HIV-1 at low titers through its increased affinity interaction due to high mannose expression on its envelope glycoprotein (gp120).<sup>59</sup> Interestingly, DC-SIGN does not facilitate HIV-1

processing by DCs but protects the virus from intracellular degradation, a process which is not completely understood.<sup>60</sup>

The plasma membrane is organized into various subdomains of clustered macromolecules. These clusters are organized by specialized scaffolding proteins including caveolins, which stabilize lipid rafts, and galectins, which crosslink multiple glycoproteins to form lattice microdomains. The crosslinking of these cell-surface glycoconjugates facilitates protein-protein interactions within various subdomains, triggering a cascade of transmembrane signaling events.<sup>46,61</sup> Indeed, galectins are implicated in different steps of tumorigenic processes, including tumour cell transformation, cell-cycle regulation and apoptosis.<sup>62</sup> For example, galectin-1 and galectin-3 are involved in tumorigenesis through their interactions with oncogenic Ras, which promotes Ras-mediated signal transduction involving the phosphatidylinositol-3-kinase (PI3K) and extracellular signal-regulated kinase (ERK) 1/2 pathways.<sup>63,64</sup> Similarly, the activation of several C-type lectin receptors (CLRs) family leads to a cascade of signaling events mediated by the action of protein kinases and phosphatases at their cytoplasmic domains.<sup>65</sup> Dectin-1, a member of the CLR family, is activated when it recognize the  $\beta$ -1,3-glucan epitope during fungal infection, resulting in the phosphorylation of its cytoplasmic domain and subsequent NF- $\kappa$ B pathway activation.<sup>66</sup> While mammalian lectin function is generally ascribed to cellular recognition, its involvement in cellular signaling is undoubtedly becoming more evident.

Studies have found that mammalian glycans produced in the Golgi modulate the endocytosis of cell-surface glycoproteins, which in turn, regulate receptor expression and

thereby, influencing cell signaling. The poly N-acetyllactosamine, for example, retards EGF and TGF- $\beta$  receptor endocytosis, thus altering receptor activation and signaling among epithelial carcinoma cells.<sup>67</sup> The hepatic ASGR, an endocytic recycling receptor belonging to the CTL family, is responsible for the molecular trafficking and removal of desialylated glycoprotein from circulation.<sup>68</sup> Furthermore, intracellular animal lectins have played important roles in glycoprotein sorting along the secretory pathway. Calnexin and calreticulin operate as chaperones to ensure the proper folding and oligomerization of many glycoproteins in the ER. The mannose lectin ERGIC-53 behaves as a cargo receptor, mediating the transport of glycoproteins from the ER to the Golgi, while the homologous lectin VIP36 controls the glycosylation events within the Golgi.<sup>69</sup>

Research on the function of mammalian glycosylation demonstrates that glycans and their associated lectins are involved in host-pathogen interactions, cellular homeostasis and transmembrane signaling. With such diverse functions, it is increasingly evident that carbohydrate-lectin interactions play critical roles in biology and in medicine. As a result, identifying functional glycan-receptor interactions is key to understanding how glycobiology governs and affects cellular physiology and disease. Therefore, technological advances in glycan-based methodologies should be capitalized for the identification of bioactive carbohydrate ligands and their corresponding lectins. We will discuss our efforts towards identifying functional glycan-receptor interactions in the next chapter. In particular, we will focus on the role of Fucose- $\alpha$ (1-2)-Galactose in mediating neuronal communication in the brain.

## REFERENCES

1. Wells, J.A.; McClendon, C.L. *Nature*. **2007**, 450, 1001
2. Barabasi, A-L.; Oltvai, Z.N. *Nat. Rev. Genet.* **2004**, 5, 101
3. Apweiler, R.; Hermjakob, H.; Sharon, N. *Biochim. Biophys. Acta.* **1999**, 1473, 4
4. Caramelo, J.J.; Parodi, A.J. *Semin. Cell Dev. Biol.* **2007**, 18, 732
5. Varki, A. *Cell*. **2006**, 126, 841
6. Helenius, A.; Aebi, M. *Annu. Rev. Biochem.* **2004**, 73, 1019
7. Lowe, J.B.; Marth, J.D. *Annu. Rev. Biochem.* **2003**, 72, 643
8. Jaeken, J.; Carchon, H. *Curr. Opin. Pediatr.* **2004**, 16, 434
9. Jaeken, J.; Matthijs, G. *Annu. Rev. Genomics Hum. Genet.* **2001**, 2, 129
10. Adamczyk, B.; Tharmalingam, T.; Rudd, P.M. *Biochim. Biophys. Acta.* **2012**, 1820, 1347
11. Hakomori, S. *Proc. Natl. Acad. Sci. USA.* **2002**, 99, 10231
12. Sell, S. *Human. Path.* **1990**, 21, 1003
13. Hakomori, S.; Zhang, Y. *Chem. Biol.* **1997**, 4, 97
14. Taylorpapadimitriou, J.; Epenetos, A.A. *Trends. Biotech.* **1994**, 12, 227
15. Gabius, H. J. *Angew. Chem.* **1988**, 27, 1267
16. Orntoft, T. F.; Vestergaard, E. M. *Electrophoresis.* **1999**, 20, 362
17. Kleene, R.; Schachner, M. *Nat. Rev. Neurosci.* **2004**, 5, 195
18. Murrey, H.E.; Hsieh-Wilson, L.C. *Chem. Rev.* **2008**, 108, 1708
19. Schachter, H. *Glycoconj. J.* **2000**, 17, 465
20. Yan, A.; Lennarz, W.J. *J. Biol. Chem.* **2005**, 280, 3121
21. Esko, J.D.; Selleck, S.B. *Annu. Rev. Biochem.* **2002**, 71, 435
22. Hakomori, S-I. *Proc. Natl. Acad. Sci. USA.* **2002**, 99, 225
23. Schnaar, R.L.; Suzuki, A.; Stanley, P. Glycosphingolipids. In: Varki, A.; Cummings, R.D.; Esko, J.D. et al. *Essentials of Glycobiology. 2nd edition.* Cold Spring Harbor (NY): Cold Spring Harbor Laboratory Press; **2009**. Chapter 10.
24. Lis, H.; Sharon, N. *Chem. Rev.* **1998**, 98, 637
25. Sears, P.; Wong, C.H. *Angew. Chem. Int. Ed.* **1999**, 38, 2300
26. Kitov, P.I.; Bundle, D.R. *J. Am. Chem. Soc.* **2003**, 125, 16271
27. Lee, R.T.; Lee, Y.C. *Glycoconj. J.* **2000**, 17, 543
28. Lundquist, J.J.; Toone, E.J. *Chem. Rev.* **2002**, 102, 555
29. Dam, T.K.; Brewer, C.F. *Glycobiology.* **2010**, 20, 270
30. Rini, J.M. *Annu. Rev. Biophys. Biomol. Struct.* **1995**, 24, 551
31. Kiessling, L.L.; Splain, L.A. *Annu. Rev. Biochem.* **2010**, 79, 619
32. Weis, W.I.; Drickamer, K. *Annu. Rev. Biochem.* **1996**, 65, 441
33. Katayama, Y.; Hidalgo, A.; Chang, J.; Peired, A.; Frenette, P.S. *J. Exp. Med.* **2005**, 201, 1183

34. Satoh, T.; Kaneko, M.; Wu, M.H.; Yokozeki, H.; Nishioka, K. *Eur. J. Immunol.* **2002**, 32, 1274
35. Somers, W.S.; Tang, J.; Shaw, G.D.; Camphausen, R.T. *Cell.* **2000**, 103, 467
36. Kilpatrick, D.C. *Handbooks of Animal Lectins*. John Wiley, Chichester, New York; **2000**.
37. Sharon, N.; Lis, H. *Glycobiology.* **2004**, 14, 53
38. Kerrigan, A.M.; Brown, G.D. *Immunobiol.* **2009**, 214, 562
39. Gorelick, E.; Galili, U.; Raz, A. *Cancer. Metastasis. Rev.* **2001**, 20, 245
40. Varki, A. *Proc. Natl. Acad. Sci. USA.* **1994**, 91, 7390
41. Tedder, T.F.; Steeber, D.A.; Chen, A.; Engel, P. *FASEB. J.* **1995**, 9, 866
42. Figdor, C.G.; van Kooyk, Y.; Adema, G.J. *Nat. Rev. Immunol.* **2002**, 2, 77
43. Zelensky, A.N.; Gready, J.E. *FEBS. J.* **2005**, 272, 6179
44. Cooper, D.N.; Barondes, S.H. *Glycobiology.* **1999**, 9, 979
45. Rabinovich, G.A.; Toscano, M.A. *Nat. Rev. Immunol.* **2009**, 9, 338
46. Liu, F-T.; Rabinovich, G.A. *Nat. Rev. Cancer.* **2005**, 5, 29
47. Leffler, H.; Carlsson, S.; Hedlund, M.; Qian, Y.; Poirier, F. *Glyconconj. J.* **2002**, 19, 433
48. Crocker, P.R.; Paulson, J.C.; Varki, A. *Nat. Rev. Immunol.* **2007**, 7, 255
49. Angata, T.; Brinkman-Van der Linden, E.C.M. *Biochim. Biophys. Acta.* **2002**, 1572, 294
50. Varki, A.; Angata, T. *Glycobiology*, **2006**, 16, 1R
51. Dahms, N.M.; Hancock, M.K. *Biochim. Biophys. Acta.* **2002**, 1572, 317
52. Dahms, N.M.; Olson, L.J.; Kim, J-J.P. *Glycobiology*, **2008**, 18, 664
53. Morgan, D.O.; Edman, J.C.; Standring, D.N.; Fried, V.A. et al. *Nature.* **1987**, 329, 301
54. MacDonald, R.G.; Pfeffer, S.R.; Coussens, L.; Tepper, M.A. et al. *Science.* **1988**, 239, 1134
55. Tong, P.Y.; Tollefsen, S.E.; Kornfeld, S. *J. Biol. Chem.* **1988**, 263, 2585
56. Ohtsubo, K.; Marth, J.D. *Cell.* **2006**, 126, 855
57. Rosen, S. *Annu. Rev. Immunol.* **2004**, 20, 129
58. van Kooyk, Y.; Geijtenbeek, T.B.H. *Nat. Rev. Immunol.* **2003**, 3, 697
59. Geijtenbeek, T.B.H.; Kwon, D.S.; Torensma, R.; van Vliet, S.J. et al. *Cell.* **2000**, 100, 587
60. Kwon, D.S.; Gregorio, G.; Bitton, N.; Hendrickson, W.A.; Littman, D.R. *Immunity.* **2002**, 16, 135
61. Lajoie, P.; Goetz, J.G.; Dennis, J.W.; Nabi, I.R. *J. Cell. Biol.* **2009**, 185, 381
62. Ghazarian, H.; Idoni, B.; Oppenheimer, S.B. *Acta. Histochem.* **2011**, 113, 236
63. Elad-Sfadia, G.; Haklai, R.; Ballan, E.; Kloog, Y. *J. Biol. Chem.* **2004**, 279, 34922
64. Elad-Sfadia, G.; Haklai, R.; Ballan, E.; Gabius, H.; Kloog, Y. *J. Biol. Chem.* **2002**, 277, 37169
65. Geijtenbeek, T.B.H.; Gringhuis, S.I. *Nat. Rev. Immunol.* **2009**, 9, 465
66. Gross, O.; Gewies, A.; Finger, K.; Schafer, M. et al. *Nature.* **2006**, 442, 651

67. Partridge, E.A.; Le Roy, C.; Di Guglielmo, G.M.; Pawling, J. et al. *Science*. **2004**, 306, 120
68. Weigel, P.H.; Yik, J.H.N. *Biochim. Biophys. Acta*. **2002**, 1572, 341
69. Hauri, H-P.; Appenzeller, C.; Kuhn, F.; Nufer, O. *FEBS. Letter*. **2000**, 476, 32

## *Chapter 2*

### THE ROLE OF FUCOSE $\alpha(1-2)$ GALACTOSE CARBOHYDRATES IN NEURONAL COMMUNICATION

#### **2. 1. Cellular Fucosylation**

Fucosylation is one of the most prevalent modifications involving oligosaccharides on glycoproteins or glycolipids. Fucosylation represents the attachment of fucose residue to the terminal or core glycan structures of N-glycans, O-glycans and glycolipids. Fucose is distinct from other naturally occurring sugars because it is a deoxyhexose sugar that exists exclusively in the L-configuration. In mammals, fucose-containing glycans serve important roles as blood group antigen determinants, in selectin-mediated leukocyte-endothelial adhesion and in host–microbe interactions.<sup>1-5</sup> Increased levels of fucosylation and the expression of the corresponding fucosyl transferases have been reported in a number of pathological conditions, including inflammation and cancer.<sup>6-13</sup> Therefore, the upregulation of tumor-associated fucosyl carbohydrates can serve as biomarkers for detection of cancer malignancy and metastatic potential. Importantly, the correlations between carbohydrate expression and disease progression can be utilized for therapeutic purposes.

In contrast to the modification of terminal oligosaccharides, fucose may also be directly linked to the hydroxyl groups of serine and threonine residues. Indeed, O-fucosylation of the mammalian Notch receptor is implicated in many developmental processes and cellular differentiation.<sup>14,15</sup> The binding of specific ligands to the extracellular domain of the Notch receptor leads to the proteolytic cleavage of its intracellular domain, which results in the transcriptional activation of several

developmental genes. Interestingly, Notch signaling and its ligand binding are regulated by O-fucosylation.<sup>16</sup> Indeed, disruption of O-fucose glycan synthesis causes severe Notch signaling defects in drosophila and mammals, resulting in acute developmental disorders.<sup>17-20</sup>

To date, thirteen fucosyltransferase genes have been identified in the human genome. Given the structural diversity of fucosylated glycans, it is not surprising that more than a dozen different glycosyltransferases are involved in the formation of fucose linkages, most of which exist in the terminal Golgi compartments.<sup>21</sup> In particular, a family of human  $\alpha(1,2)$ -fucosyltransferases, FUT1 and FUT2, is responsible for transferring fucose onto the galactose of type 1 (Gal $\beta$ 3GlcNAc) or type 2 (Gal $\beta$ 4GlcNAc) disaccharide precursors to form the H blood group antigen (Fuc $\alpha(1-2)$ Gal glycans).<sup>22-24</sup> A gene homologous to FUT1 and FUT2, termed Sec1, contains translational frameshifts and stop codons that interrupt potential open reading frames and thus appears to be a pseudogene.<sup>25</sup> The H antigen is further modified by the ABO locus-encoded glycosyltransferase to form the A and B blood group antigens, while the unmodified H antigen is expressed on the cell surface of type O individuals (Fig 2.1).<sup>26</sup> FUT1 and FUT2 knock-out (KO) mice appear viable and healthy, but their  $\alpha(1,2)$ fucosyl expression is downregulated in the epididymal cell surface and uterine, epithelium, respectively.<sup>27</sup> In addition, FUT1 and FUT2 -deficient mice have been shown to differentially regulate Fuc $\alpha(1-2)$ Gal expression in the olfactory bulb and gastrointestinal tract.<sup>28,29</sup> Therefore, FUT1 and FUT2 genes may act individually in specific tissues, retain a redundant function, or have compensatory mechanisms when the other gene is knocked out.

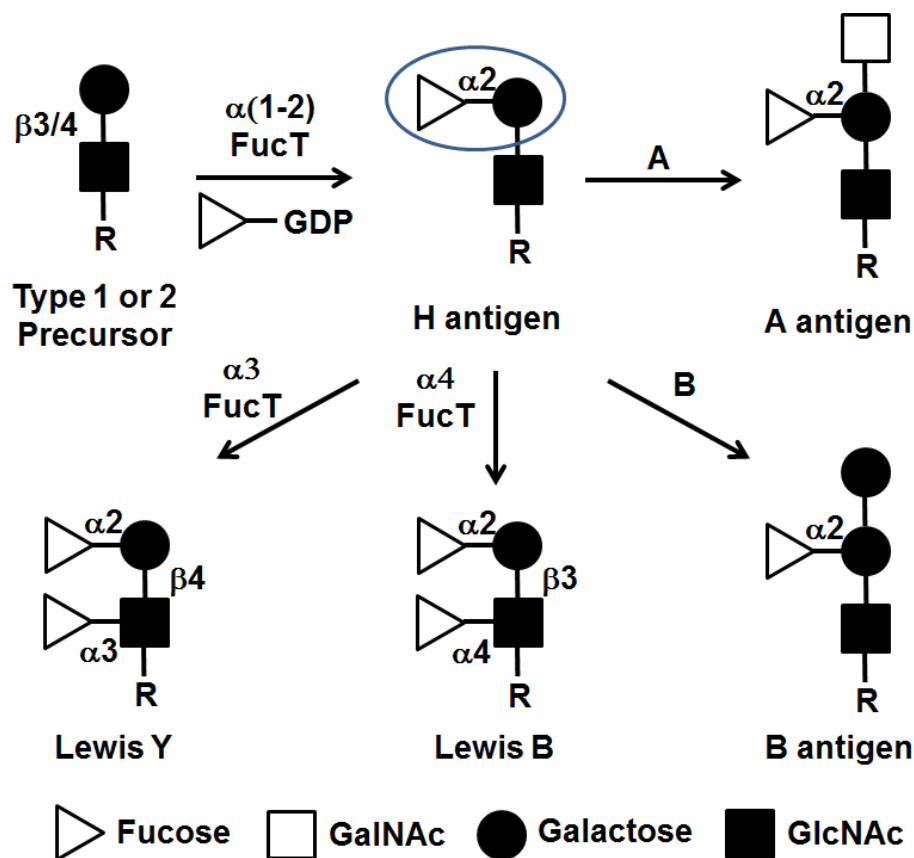


**Figure 2.1.** Biosynthesis of complex Fuc $\alpha$ (1-2)Gal glycans from the H antigen precursors.

## 2. 2. Fucosylation in Neuronal Development

Pivotal roles for glycans in regulating the nervous system during development, regeneration and synaptic plasticity, have recently emerged. Glycan function in cellular adhesion and recognition is critical for the maintenance of the specific molecular architecture responsible for neural cell interactions.<sup>30</sup> For instance, glycosylation influences various neuronal processes, such as neurite outgrowth and morphology, and may contribute to the molecular events that underlie learning and memory.<sup>31,32</sup> Glycosylation is also an efficient modulator of cell signaling and has been implicated in memory consolidation

pathways.<sup>33-36</sup> Specifically, glycans can mediate growth factor interactions with their associated receptors to control cell proliferation, regulate axon guidance and facilitate intercellular signaling.<sup>37-40</sup> Genetic ablation of glycosylation enzymes often leads to developmental defects and can influence various organismal behaviors, such as stress and cognition.<sup>41-44</sup> Thus, the complexity of glycan functions help to orchestrate proper neuronal development during embryogenesis, as well as influence behaviors in the adult organism.

Multiple studies have suggested a role for fucosylation in learning and memory. First, fucose has been reported to play a significant role in neural development.<sup>45-47</sup> Fucosylated glycoproteins are highly enriched at neuronal synapses,<sup>48,49</sup> where they are expressed as complex N-linked oligosaccharides.<sup>50</sup> Furthermore, the incorporation of fucose into glycoconjugates in the brain is significantly enhanced by task-dependent learning in both chicks and rats.<sup>51-54</sup> In particular, [<sup>3</sup>H]-fucose is highly incorporated into synaptic glycoconjugates in animals that are trained in a brightness discrimination task to avoid entering a dark chamber.<sup>53</sup> Moreover, fucosyltransferases activity is upregulated during synaptogenesis and upon passive-avoidance training in animals.<sup>55,56</sup> Finally, exogenous application of L-fucose or 2-Fucosyllactose (Fig 2.2) enhance long-term potentiation (LTP), an electrophysiological model for learning and memory, both in vivo and in hippocampal slices.<sup>57,58</sup> In contrast, fucose incorporation into hippocampal glycoproteins is found to be significantly reduced in trained rats when treated with 2-deoxy-D-galactose (2-dGal; Fig 2.2).<sup>59, 60</sup> Overall, these studies suggest that Fuc $\alpha$ (1-2)Gal glycans (Fig 2.2) are implicated in a variety of complex and critical neuronal communication processes.

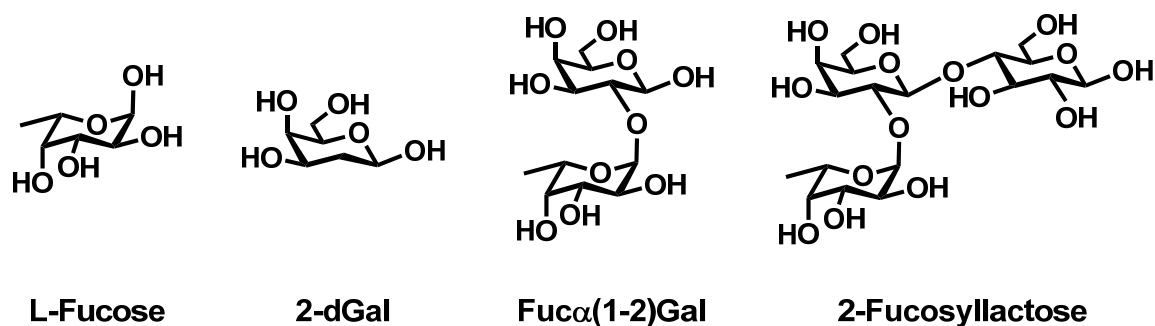


**Fig 2.2.** Chemical structures of L-fucose, 2-deoxy-D-galactose (2d-Gal), Fucose- $\alpha$ (1-2)-Galactose (Fuc $\alpha$ (1-2)Gal) and 2-Fucosyllactose (Fuc $\alpha$ (1-2)Gal $\beta$ (1-4)Glc).

The significance of Fuc $\alpha$ (1-2)Gal is supported by behavioral and electrophysiological studies using the unnatural 2-dGal sugar analogue. Specifically, 2-dGal, which competes with native galactose for incorporation into glycan chains, inhibits the formation of the specific  $\alpha$ (1-2) fucose linkage because it lacks a hydroxyl group at the C-2 position (Fig 2.3). As a result, administration of 2-dGal treatment on animals during passive-avoidance training, has resulted in reversible amnesia and reduced protein fucosylation, presumably due to inhibition of the  $\alpha$ (1-2) linkage formation.<sup>61-63</sup> Similarly, 2-dGal treatment suppresses LTP maintenance in the hippocampus both in vitro and in vivo.<sup>64</sup> In contrast, other small molecule sugars, such as galactose or glucose, had no effect on memory formation, suggesting a unique function for Fuc $\alpha$ (1-2)Gal disaccharides. Furthermore, application of a monoclonal antibody specific for Fuc $\alpha$ (1-2)Gal<sup>65</sup> significantly impaired memory formation in animals most likely by blocking the interaction with the Fuc $\alpha$ (1-2)Gal epitope.<sup>66</sup>

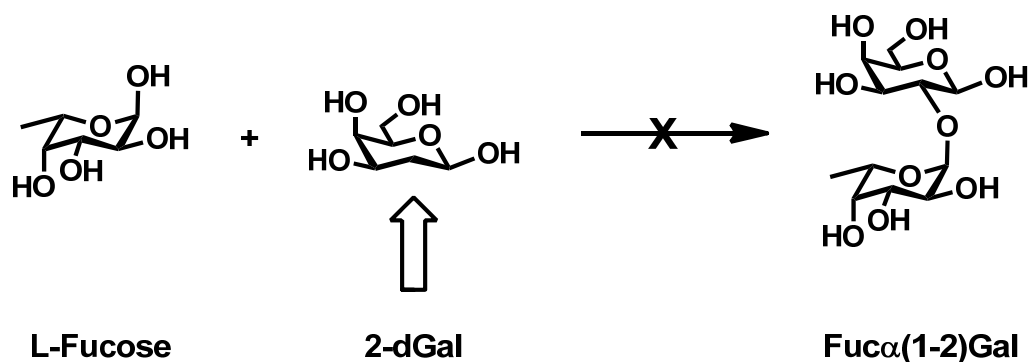


**Fig 2.3.** Incorporation of 2-dGal inhibits the formation of Fuc $\alpha$ (1-2)Gal linkages.

Despite these intriguing behavioral and electrophysiological results, the roles of Fuc $\alpha$ (1-2)Gal carbohydrates on synaptic remodeling and neuronal morphologies have been largely uncharacterized. An understanding of their precise functions has been hampered by a lack of information regarding Fuc $\alpha$ (1-2)Gal glycoproteins. Presently, synapsin I, a presynaptic phosphoprotein involved in neurotransmitter release and synaptogenesis,<sup>67</sup> is the only well-characterized Fuc $\alpha$ (1-2)Gal glycoprotein identified in the mammalian brain.<sup>68</sup> Fucosylation is shown to regulate the stability and turnover of synapsin I, protecting it from proteolytic degradation by the calcium-activated protease calpain. Inhibition of protein fucosylation with 2-dGal reduces synapsin expression and delays synapse formation in hippocampal cultures.<sup>68</sup> Efforts to identify additional Fuc $\alpha$ (1-2)Gal glycoproteins are currently underway to elucidate their functional roles in neuronal communications and memory consolidation. However, these studies are only partially effective because no Fuc $\alpha$ (1-2)Gal lectins have been identified from the mammalian nervous system.

### 2. 3. Fucose- $\alpha$ (1-2)-Galactose and Lectin Association in the Brain

Recent works from our lab has provided the first demonstration that Fuc $\alpha$ (1-2)Gal and its associated lectins induces hippocampal neuron outgrowth.<sup>69</sup> The presence of endogenous neuronal lectins specific to Fuc $\alpha$ (1-2)Gal carbohydrates are confirmed on several fronts. First, lectin receptors are labeled using chemical probes bearing the Fuc $\alpha$ (1-2)Gal recognition element. The interactions between Fuc $\alpha$ (1-2)Gal glycans and these ‘unidentified’ lectins promote neurite outgrowth and are only specific to Fuc $\alpha$ (1-2)Gal carbohydrates (Fig 2.4). As carbohydrates have weak binding affinities for lectins, their interactions are multivalent in nature. Indeed, the stimulatory effect of Fuc $\alpha$ (1-2)Gal polymers on hippocampal neurons is dependent on the concentration and valency of the disaccharide epitope. In particular, the growth-promoting activity of the Fuc $\alpha$ (1-2)Gal glycan increases with each polymer concentration, while the potency of the compounds is dramatically enhanced with increasing carbohydrate density (Fig 2.5) . In contrast, a monovalent ligand showed only modest activity even though it was capable of binding to neurons. These results suggest that the multivalent presentation of a glycan epitope on a polymeric scaffold (PAA) promotes the interaction of Fuc $\alpha$ (1-2)Gal with lectin receptors and facilitates their assembly into higher-order structures. The clustering of these lectin receptors presumably initiates receptor complex activation, which elicit downstream signaling events, leading to neuronal growth.

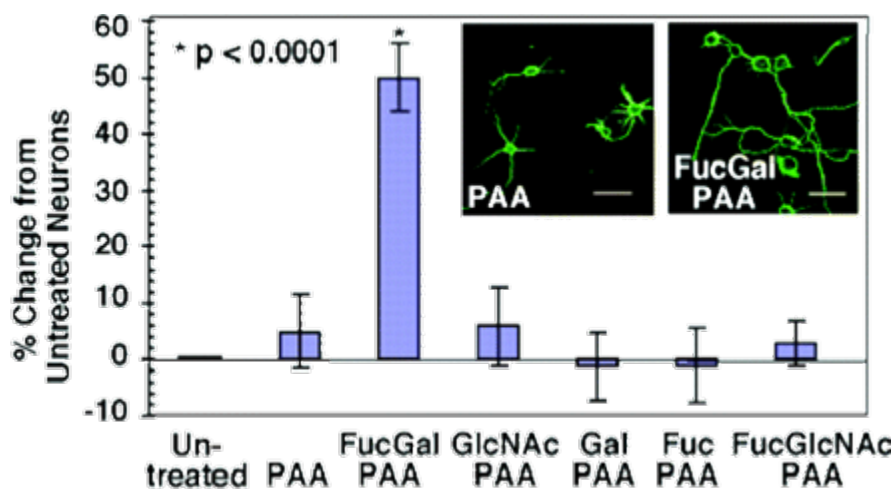


**Fig 2.4.** Neurite outgrowth activity is specific to Fuc $\alpha$ (1-2)Gal PAA treatment (130  $\mu$ M). PAA: polyacrylamide; GlcNAc: Acetylglucosamine; Gal: Galactose; Fuc: Fucose; FucGlcNAc: Fucose $\alpha$ (1-3)GlcNAc. Reprinted with permission from (69).

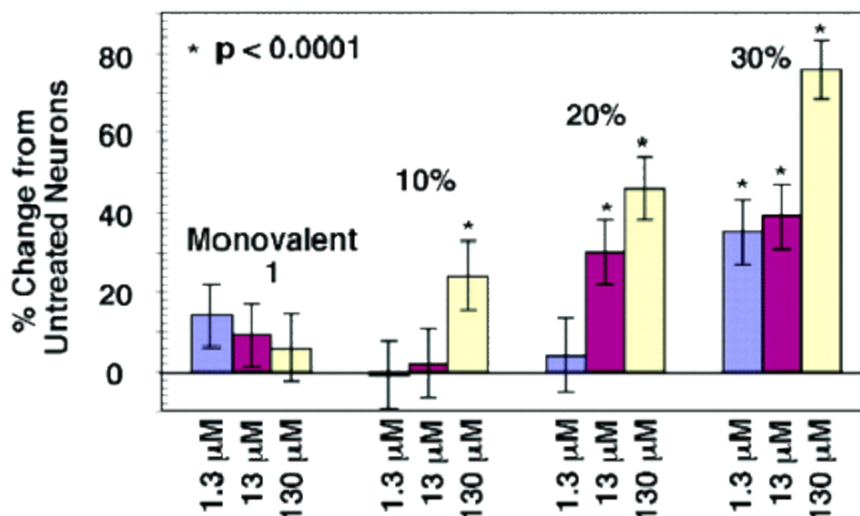


**Fig 2.5.** The multivalent interaction between Fuc $\alpha$ (1-2)Gal and its associated lectin. Neurite outgrowth activity increases with increasing Fuc $\alpha$ (1-2)Gal concentration and polymer valency. Reprinted with permission from (69).

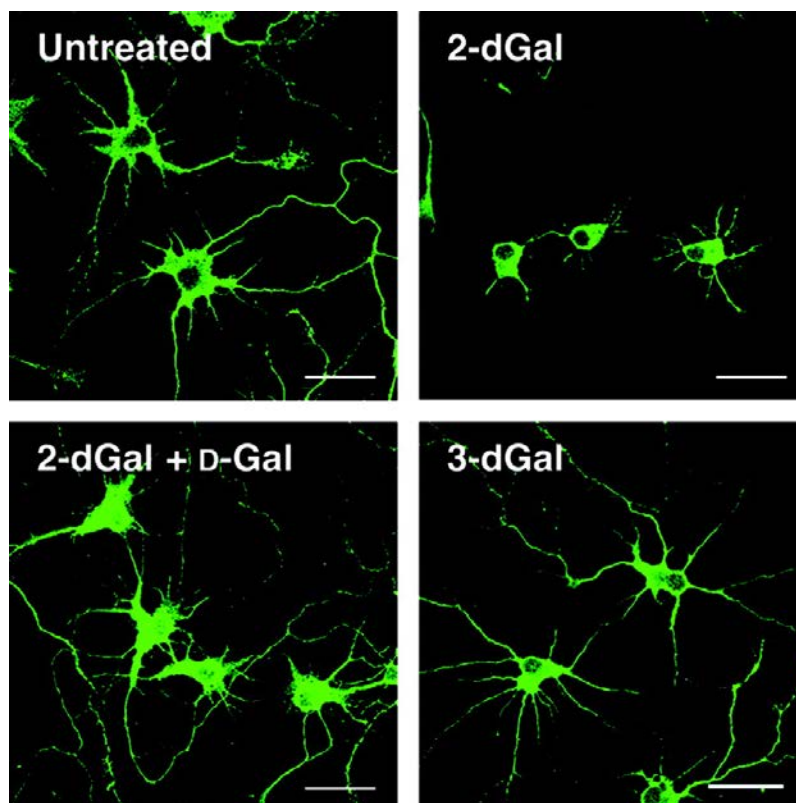


**Fig 2.6.** Inhibition of  $\text{Fuc}\alpha(1-2)\text{Gal}$  linkages with 2-dGal leads to stunted neurite outgrowth in hippocampal neurons. D-Gal is able to rescue the effects of 2-dGal. 3-dGal has no effect on neurite outgrowth. Scale bar = 45  $\mu\text{M}$ . Images courtesy of Cristal Gama.

The effects of 2-dGal on neuronal growth and morphology were also investigated in hippocampal neurons. Treatment of neurons with 2-dGal leads to a significant retraction of dendrites and the collapse of synapses, whereas 3-dGal had no effect on neurite outgrowth. Interestingly, the effect of 2-dGal is partially reversed by the subsequent addition of D-Gal, which stimulates the regeneration of neuronal processes (Fig 2.6). The partial rescue of D-Gal can be attributed to the decreased plasticity of older neurons. These results indicate that the growth-promoting activity of fucosyl glycans is mediated only by the specific  $\alpha(1-2)$ -linked fucose epitope. Therefore, disruption of fucosylated glycan synthesis, in particular,

Fuca(1–2)Gal glycoconjugates, alters neuronal morphology and modifies functional neuronal connections.

Collectively, these results highlight the importance of Fuca(1–2)Gal glycoconjugates and their associated lectins in synaptic remodeling and neuronal communication. These studies show that Fuca(1–2)Gal carbohydrates stimulate neurite outgrowth, while 2-dGal treatment perturbs its biosynthesis and abolishes its growth-promoting activity. Furthermore, this stimulatory effect is facilitated by the interactions with lectin receptors that are specific to Fuca(1–2)Gal disaccharides and are multivalent in nature. Understanding the molecular mechanisms by which Fuca(1–2)Gal sugars contribute to such processes has been challenging, at least in part, by the fact that no Fuca(1–2)Gal lectins have been identified from the mammalian nervous system. Therefore, we seek to identify these lectins and elucidate the specific mechanisms and pathways leading to neuronal growth.

Despite their importance, efforts to identify novel mammalian lectins that interact with specific glycan ligands of interest have been challenging. Many of the well-characterized lectins are derived from plants and were discovered through the slow process of isolating and purifying individual proteins.<sup>70</sup> Furthermore, lectin-like properties can only be inferred from their agglutinating activities and structural homology towards other existing lectins.<sup>71</sup> In fact, database searches for mammalian lectins that have structural homology towards known Fuca(1–2)Gal lectin of plants origin, *Ulex europaeus* agglutinin I (UEAI), have yet to provide great results. Moreover, the weak binding affinities for their carbohydrate ligands complicate efforts to capture and identify endogenous lectins. Indeed,

the development of general, systems-level approaches to identify glycan-binding proteins is important for understanding the biological roles of specific glycan structures. This thesis describes the development of chemical probes for the proteomic identification of novel mammalian lectins. We will focus on the synthesis of multivalent probes and their use in lectin enrichment. Captured lectins are identified with mass-spectrometry (MS)-based analyses and validated for their  $\text{Fuca}(1-2)\text{Gal}$  binding *in vitro*. Finally, the functional relevance of these binding events was examined by studying lectin activity in  $\text{Fuca}(1-2)\text{Gal}$ -deficient (FUT1 or FUT2 KO) mice.

## REFERENCES

1. Springer, T.A. *Cell*. **1994**, 76, 301
2. Lowe, J. B. *Kidney. Int*. **1997**, 51, 1418
3. Hooper, L.V. ; Gordon, J. I. *Glycobiology*, **2001**, 11, 1R
4. Guruge, J. L.; Falk, P. G.; Lorenz, R. G.; Dans, M.; Wirth, H. P.; Blaser, M. J.; Berg, D. E.; Gordon, J. I. *Proc. Natl. Acad. Sci. USA*. **1998**, 95, 3925
5. Lowe, J. B. *Baillieres. Clin. Haematol*. **1993**, 6, 465
6. Miyoshi, E.; Moriwaki, K.; Nakagawa, T. *J. Biochem*. **2008**, 143, 725
7. Thompson, S.; Dargan, E.; Turner, G. A. *Cancer. Lett*. **1992**, 66, 43
8. Brockhausen, I. *Biochim. Biophys. Acta*. **1999**, 1473, 67
9. Ma, B.; Simala-Grant, J. L.; Taylor, D. E. *Glycobiology*. **2006**, 16, 158R
10. Butcher, E. C.; Picker, L. J. *Science*. **1996**, 272, 60, 66
11. Lowe, J. B. *Curr. Opin. Cell. Biol*. **2003**, 15, 531
12. Staudacher, E.; Altmann, F.; Wilson, I. B. H.; Marz, L. *Biochim. Biophys. Acta*. **1999**, 1473, 216
13. Wang, J-E.; Ambros, R. A.; Weber, P. B.; Rosano, T. G. *Cancer. Res*. **1995**, 55, 3654
14. Artavanis-Tsakonas, S.; Rand, M. D.; Lake, R. J. *Science*. **1999**, 284, 770
15. Weinmaster, G.; Kintner, C. *Annu. Rev. Cell Dev. Biol*. **2003**, 19, 367
16. Stanley, P. *Curr. Opin. Struct. Biol*. **2007**, 17, 530
17. Joutel, A.; Tournier-Lasserre, E. *Semin. Cell Dev. Biol*. **1998**, 9, 619
18. Bulman, M. P.; Kusumi, K.; Frayling, T. M.; McKeown, C.; Garrett, C. et al. *Nat. Genet*. **2000**, 24, 438
19. Ellisen, L. W.; Bird, J.; West, D. C.; Soreng, A. L.; Reynolds, T. C. et al. *Cell*. **1991**, 66, 649
20. Artavanis-Tsakonas, S. *Nat. Genet*. **1997**, 16, 212
21. Becker, D. J.; Lowe, J. B. *Glycobiology*. **2003**, 13, 41R
22. Sarnesto, A.; Kohlin, T.; Thurin, J.; Blaszczyk-Thurin, M. *J. Biol. Chem*. **1990**, 265, 15067
23. Larse, R. D.; Ernst, L. K.; Nair, R. P.; Lowe, J. B. *Proc. Natl. Acad. Sci. USA*. **1990**, 87, 6674
24. Rouquier, R.; Lowe, J. B.; Kelly, R. J.; Fertitta, A. L.; Lennon, G. G.; Giorgi, D. *J. Biol. Chem*. **1995**, 270, 4632
25. Kelly, R. J.; Rouquier, S.; Giorgi, D.; Lennon, G. G.; Lowe, J. B. *J. Biol. Chem*. **1995**, 270, 4640
26. Morgan, W. T. *Proc. R. Soc. Lond. B. Biol. Sci*. **1960**, 151, 308
27. Domino, S. E.; Zhang, L.; Gillespie, P. J.; Saunders, T. L.; Lowe, J. B. *Mol. Cell. Biol*. **2001**, 21, 8336
28. Iwamori, M.; Domino, S. E. *Biochem. J*. **2004**, 380, 75
29. Murrey, H. E.; Ficarro, S. B.; Krishnamurthy, C.; Domino, S. E.; Peters, E. C.; Hsieh-Wilson, L. C. *Biochemistry*. **2009**, 48, 7261
30. Matani, P.; Sharrow, M.; Tiemeyer, M. *Front. Biosci*. **2007**, 12, 3852

31. Kleene, R.; Schachner, M. *Nat. Rev. Neurosci.* **2004**, 5, 195
32. Rutishauser, U. *Nat. Rev. Neurosci.* **2004**, 5, 195
33. Sandi, C.; Rose, S. P. R.; Mileusnic, R.; Lancashire, C. *Neuroscience.* **1995**, 69, 1087
34. Salinska, E.; Bourne, R. C.; Rose, S. P. R. *Eur. J. Neurosci.* **2004**, 19, 3042
35. Welzl, H.; Stork, O. *News Physio. Sci.* **2003**, 18, 147
36. Murphy, K. J.; Regan, C. M. *Neurobiol. Learn. Mem.* **1998**, 70, 73
37. Inatani, M.; Irie, F.; Plump, A. S.; Tessier-Lavigne, M.; Yamaguchi, Y. *Science.* **2003**, 302, 1044
38. Bulow, H. E.; Hobert, O. *Neuron.* **2004**, 41, 723
39. Huber, A. B.; Kolodkin, A. L.; Ginty, D. D.; Cloutier, J. F. *Ann. Rev. Neurosci.* **2003**, 26, 509
40. Brown, J. M.; Xia, J.; BinQuan, Z.; Cho, K-S.; Rogers, C. J. et al. *Proc. Natl. Acad. Sci. USA.* **2012**, 109, 4768
41. Jaeken, J.; Matthijs, G. *Annu. Rev. Genomics Hum. Genet.* **2007**, 8, 261
42. Ohtsubo, K.; Marth, J. D. *Cell.* **2006**, 126, 855
43. Best, T.; Kemps, E.; Bryan, J. *Nutr. Rev.* **2005**, 63, 409
44. Kudo, T.; Fujii, T.; Ikegami, S.; Inokuchi, K.; Takayama, Y. et al. *Glycobiology.* **2007**, 17, 1
45. Louvi, A.; Artavanis-Tsakonas, S. *Nat. Rev. Neurosci.* **2006**, 7, 93
46. Lu, L. C.; Stanley, P. In *Functional Glycomics*; Fukuda, M.; Ed: Methods in Enzymology; Elsevier: Amsterdam, **2006**, Vol 417
47. Shi, S.; Stanley, P. *Proc. Natl. Acad. Sci. USA.* **2003**, 100, 5234
48. Zanetta, J. P.; Reeber, A.; Vincendon, G.; Gombos, G. *Brain. Res.* **1977**, 138, 317
49. Krusius, T.; Finne, J. *Eur. J. Biochem.* **1977**, 78, 369
50. Taniguchi, T.; Adler, A. J.; Mizuochi, T.; Kochibe, N.; Kobata, A. *J. Biol. Chem.* **1986**, 261, 1730
51. Sukumar, R.; Rose, S. P. R.; Burgoyne, R. D. J. *J. Neurochem.* **1980**, 34, 1000
52. McCabe, N. R.; Rose, S. P. R. *Neurochem. Res.* **1985**, 10, 1083
53. Pohle, W.; Acosta, L.; Ruthrich, H.; Krug, M.; Matthies, H. *Brain. Res.* **1987**, 410, 245
54. Bullock, S.; Rose, S. P. R.; Zamani, R. *J. Neurochem.* **1992**, 58, 2145
55. Matsui, Y.; Lombard, D.; Massarelli, R.; Mandel, P.; Dreyfus, H. *J. Neurochem.* **1986**, 46, 144
56. Popov, N.; Schmidt, S.; Schulzeck, S.; Jork, R.; Lossner, B.; Matthies, H. *Pharmacol. Biochem. Behav.* **1983**, 19, 43
57. Krug, M.; Wagner, M.; Staak, S.; Smalla, K. H. *Brain. Res.* **1994**, 643, 130
58. Matthies, H.; Staak, S.; Krug, M. *Brain. Res.* **1996**, 725, 276
59. Jork, R.; Potter, J.; Bullock, S.; Grecksch, G.; Matthies, H. et al. *Neurosci. Res. Commun.* **1989**, 5, 105
60. Jork, R.; Schnurra, J.; Smalla, K-H.; Grecksch, G.; Popov, N. et al. *Neurosci. Res. Commun.* **1989**, 5, 3
61. Rose, S. P. R.; Jork, R. *Behav. Neural. Biol.* **1987**, 48, 246

62. Bullock, S.; Potter, J.; Rose, S. P. R. *J. Neurochem.* **1990**, 54, 135
63. Lorenzini, C. G. A.; Baldi, E.; Bucherelli, C.; Sacchetti, B.; Tassoni, G. *Neurobiol. Learn. Mem.* **1997**, 68, 317
64. Krug, M.; Jork, R.; Reymann, K.; Wagner, M.; Matthies, H. *Brain. Res.* **1991**, 540, 237
65. Karsten, U.; Pilgrim, G.; Hanisch, F. G.; Uhlenbruck, G.; Kasper, M. et al. *Br. J. Cancer.* **1988**, 58, 176
66. Jork, R.; Smalla, K. H.; Karsten, U.; Grecksch, G.; Ruthrich, H. L. et al. *Neurosci. Res. Commun.* **1991**, 8, 21
67. Ferreira, A.; Rapoport, M. *Cell. Mol. Life. Sci.* **2002**, 59, 589
68. Murrey, H. E.; Gama, C. I.; Kalovidouris, S. A.; Luo, W. I.; Driggers, E. M. et al. *Proc. Natl. Acad. Sci. USA.* **2006**, 103, 21
69. Kalovidouris, S. A.; Gama, C. I.; Lee, L. W.; Hsieh-Wilson, L. C. *J. Am. Chem. Soc.* **2005**, 127, 1340
70. Sharon, N.; Lis, H. *Glycobiology.* **2004**, 14, 53R
71. Taylor, M. E.; Drickamer, K. *Methods Enzymol.* **2003**, 362, 560

*Chapter 3*

## SYNTHESIS OF PHOTOACTIVATABLE GLYCOPOLYMERS

**3.1. Synthetic Probes for Lectin Isolation**

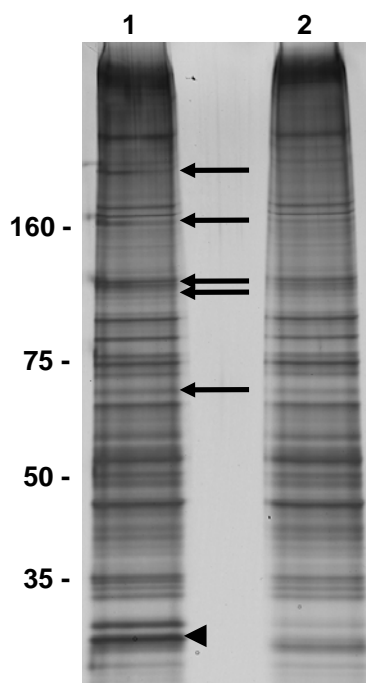
The low-affinity interactions between lectins and their glycan ligands generally require multivalency to accomplish their intended biological effect. Accordingly, many methods to assess lectin-glycan interactions depend upon multiple displays of one or both binding partners. Indeed, many glycomimetic designs are multivalent, in which the relevant groups are presented on a scaffold that is preorganized for binding.<sup>1,2</sup> Multivalent carbohydrate derivatives can exploit unique modes of recognition not available to their monovalent counterparts. Indeed, many lectins contain more than one saccharide-binding site or can oligomerize to form larger structures with multiple binding sites. Therefore, multivalent ligands that can interact with these clustered binding sites have an advantage over their monovalent counterparts. The designs of many synthetic ligands or glycan-based inhibitors have focused on multimeric structures.<sup>3-6</sup> Highly valent glycodendrimers and glycopolymers have been demonstrated as tools to study lectin biology and have been used to inhibit the binding of toxins<sup>7</sup> and viruses,<sup>8,9</sup> selectin-mediated inflammation<sup>10</sup> and leukocyte trafficking.<sup>11,12</sup>

Chemical synthesis provides architecturally diverse multivalent ligands, including low-molecular-weight displays (glycoclusters), dendrimers, polymers, liposomes, and neoglycoproteins.<sup>13,14</sup> Unlike naturally occurring multivalent glycan ligands, the valency of a synthetic ligand can be controlled by varying length or size of the scaffold. The flexibility

offered by chemical synthesis is illustrated by the different biological application of multivalent ligand architecture. For example, discrete polymers of defined lengths and spacing have been shown to elicit signaling events in neurons and the immune system.<sup>15,16</sup> In addition, many features of the scaffold such as shape, rigidity, ligand density and orientation can have significant effects on biological activity. Given these diverse variables, synthetic scaffold is an attractive tool for studying receptor-ligand interactions. Therefore, we will apply synthetic glycopolymers as glycoprotein mimetics to isolate novel lectins in the brain. These glycopolymers exploit multivalency by amplifying weak lectin-carbohydrate interactions and enabling affinity enrichment of the Fuc $\alpha$ (1-2)Gal lectins.

Early attempts by our laboratory to use monovalent Fuc $\alpha$ (1-2)Gal ligands conjugated to an agarose support or to photoactivatable cross-linking groups resulted in the detection of putative neuronal Fuc $\alpha$ (1-2)Gal lectins but were unsuccessful at isolating them in sufficient quantities for mass spectrometry (MS) analysis. In these experiments, monovalent-biotinylated probes containing photoactivatable trifluoromethyl phenyldiazirine were incubated with neuronal cells and cross-linked by UV irradiation (350 nm). Captured proteins were isolated by streptavidin affinity purification and resolved by SDS-PAGE for subsequent proteomic analysis. Efforts using multivalent biotinylated glycopolymers to isolate lectins from neuronal lysates were also tested. Cellular lysates from the hippocampi of rat pups were incubated with biotinylated polymers containing Fuc $\alpha$ (1-2)Gal epitope to probe for endogenous lectins. These lectins were isolated by streptavidin affinity purification while a parallel competitive experiment using L-fucose was performed to identify any non-specific binding. Lectins from both experiments were

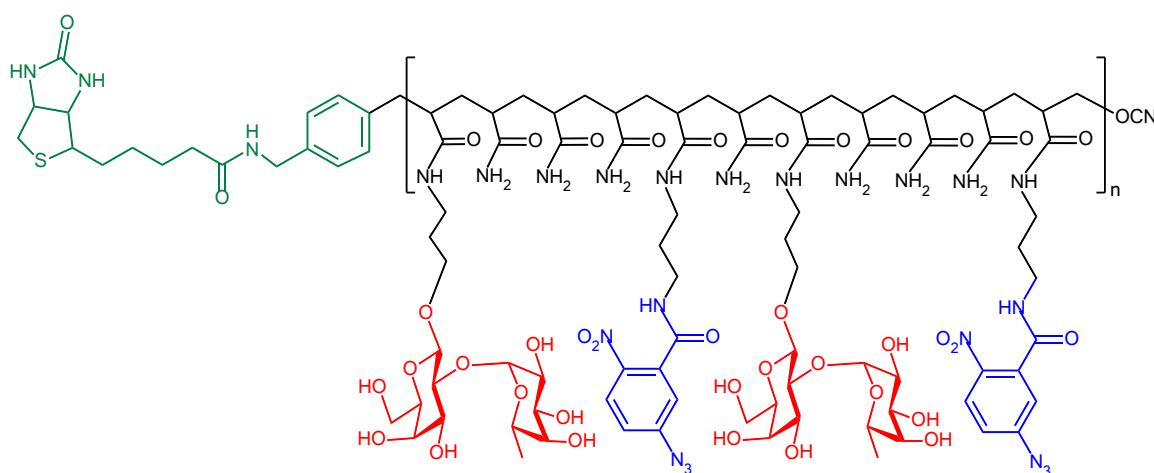
eluted from the affinity column and resolved by SDS-PAGE. Comparisons between these experiments showed no significant differences in their lectin enrichment profiles, presumably due to the high background signal (Fig 3.1). Distinct protein bands corresponding to putative lectin candidates were extracted from the gel and analyzed by MS. However, the low amount of protein capture rendered the analyses inconclusive. Therefore, better enrichment methods are required for isolating weak binding  $\text{Fuc}\alpha(1-2)\text{Gal}$  lectins in the presence of high, non-specific binding interactions.



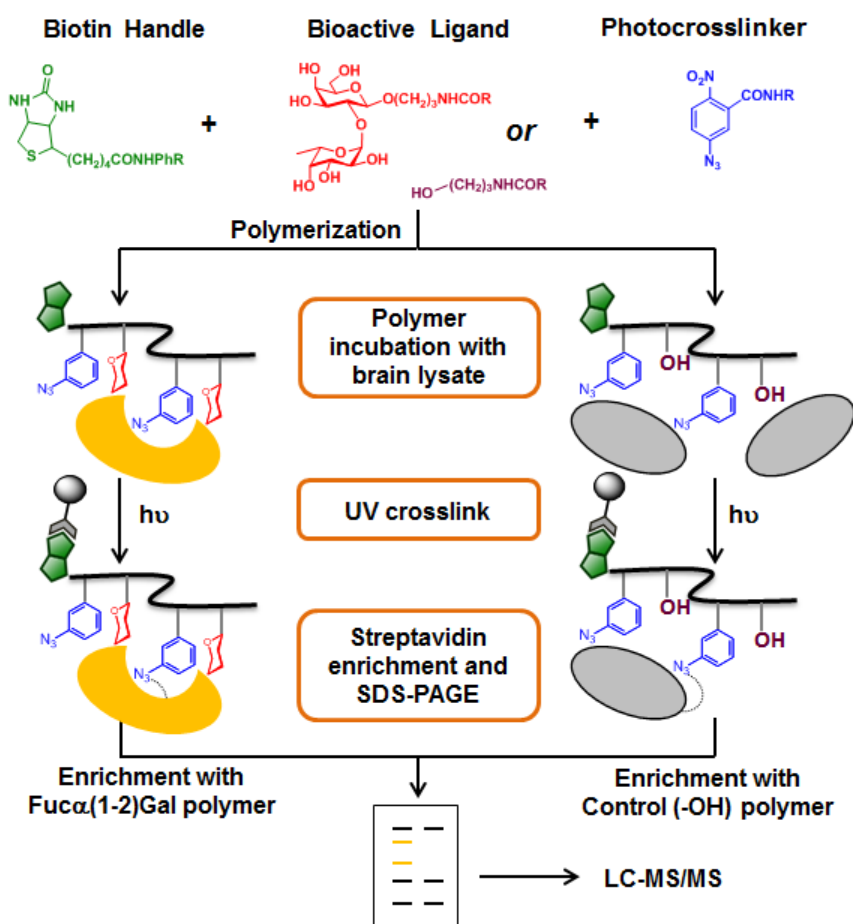
**Fig 3.1.** Lectin capture from rat pup lysates using  $\text{Fuc}\alpha(1-2)\text{Gal}$  affinity column. Lane 1: Eluent from the  $\text{Fuc}\alpha(1-2)\text{Gal}$  affinity column. Lane 2: Eluent from the L-fucose competition column to eliminate false positives. Proteins at  $\sim 65$ ,  $80$ ,  $140$ , and  $300$  kDa (bands indicated by arrows) were selectively captured by the  $\text{Fuc}\alpha(1-2)\text{Gal}$  affinity column (Lane 1). The UEAI lectin was also specifically captured (arrowhead, Lane 1). Image courtesy of Cristal Gama.

### 3.2. Design and Synthesis of Photoactivatable Glycovalent Probes

We sought to exploit synthetic glycopolymers containing multiple key elements (Fig 3.2). First, we used multivalent Fuc $\alpha$ (1-2)Gal units to augment weak carbohydrate-lectin interactions and facilitate affinity enrichment of the lectins. Second, we incorporated a photoreactive phenylazide group to enable covalent crosslinking of the glycopolymer to associated proteins. Lastly, we labeled the glycopolymers with a terminal biotin functionality to allow for facile purification and identification of the lectins (Fig 3.3). Although synthetic glycopolymers have been used extensively to study glycan-protein interactions,<sup>16-18</sup> to our knowledge, they have not been exploited for systems-level, proteomics-based profiling of lectins.



**Fig 3.2.** Multivalent Biotinylated Fuc $\alpha$ (1-2)Gal Glycopolymer. Biotin handle for affinity purification. Fuc $\alpha$ (1-2)Gal disaccharide for lectin binding. Phenyl azide photoactivatable crosslinker for protein capture.

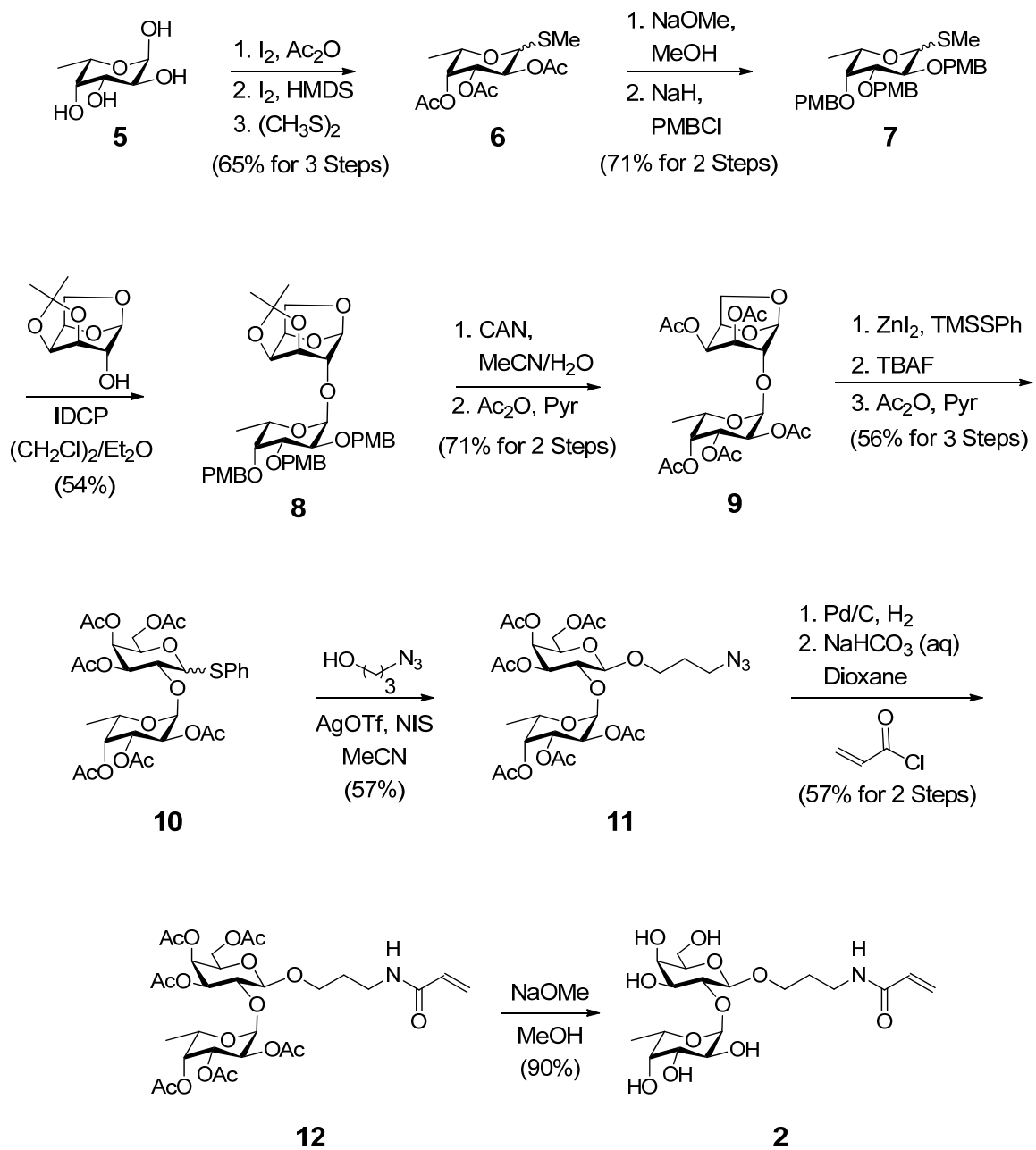


**Fig 3.3.** Lectin isolation with multivalent probes. Glycopolymers containing a biotin handle, multiple  $Fuc\alpha(1-2)Gal$  ligands and phenyl azide crosslinker units were used to covalently label potential lectins in mammalian brain. Captured proteins were isolated and identified by LC-MS/MS.

With these considerations in mind, we explored a cyanoxyl (OCN)-mediated radical polymerization strategy for glycopolymer synthesis due in part to its broad functional group tolerance and water compatibility. To incorporate a biotin handle in the glycopolymers, we adopted a straightforward approach using a biotin-derivatized initiator system that has been developed by Chaikoff and coworkers.<sup>19</sup> We envisioned that the use of a simple biotin-arylamine initiator ensured complete installation of the biotin handle in our glycopolymers. A phenylazide group was chosen as the photoactivatable crosslinking

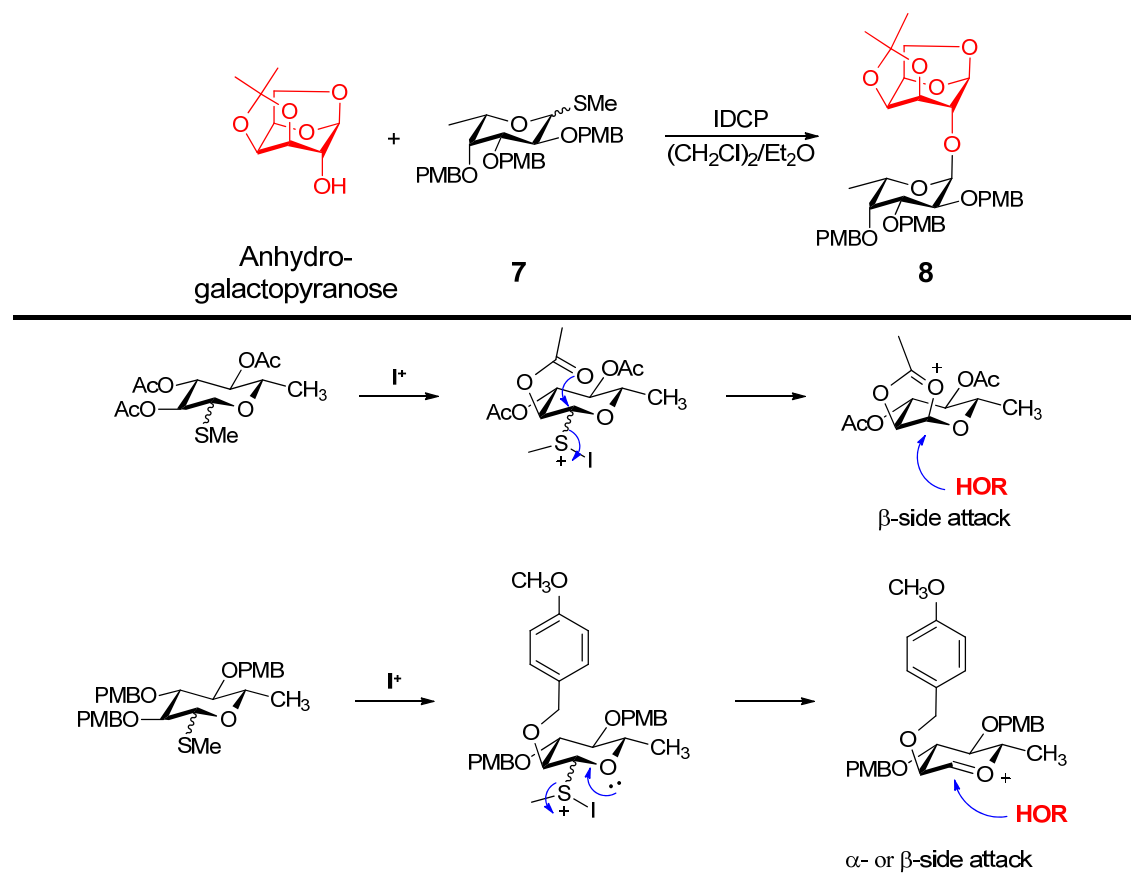
agent due to its successful application to proteins at membrane interfaces.<sup>20</sup> In addition, OCN-mediated polymerizations exhibit qualities of a controlled/living process due to the persistent, stabilized cyanoxyl radicals.<sup>21,22</sup> Using this process, we were able to readily synthesize well-characterized, biotin end-functionalized glycopolymers with varying ratios of Fuc $\alpha$ (1-2)Gal to phenylazide moieties in order to optimize glycan-lectin interactions. We also synthesized a control polymer with each starting disaccharide monomer unit replaced by two equivalents of N-(3-hydroxypropyl)acrylamide. By analyzing lectin enrichment with the control polymer, we identify lectins that specifically interact with Fuc $\alpha$ (1-2) carbohydrates and eliminate proteins that were captured non-specifically.

Traditional synthesis of oligosaccharides is often a tedious task, owing to time-consuming work-up and purification steps. A main characteristic of many glycan syntheses is their orthogonal protecting group manipulations. Indeed, traditional Fuc $\alpha$ (1-2)Gal synthesis required more than ten steps to afford the disaccharide in a mixture of  $\alpha/\beta$  isomers.<sup>23</sup> This preparation of Fuc $\alpha$ (1-2)Gal monomer was reported to proceed via Lewis acid-catalyzed reaction with an activated fucosyl imidate donor. Given this synthetic challenge, we sought to develop a new route that is shorter, modular and scalable. We envisioned using a single protecting group to minimize the need for selective protection and deprotection of the sugar hydroxyl groups. Indeed, Fuc $\alpha$ (1-2)Gal monomer was exclusively prepared in eight steps, from L-fucose, using several multi-step, one-pot reactions with minimal protecting group manipulations (Scheme 3.1)

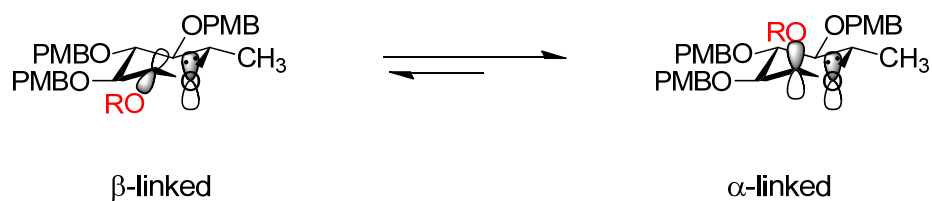
Scheme 3.1. Synthesis of Fuc $\alpha$ (1-2)Gal glycomonomer **2**

Fuca(1-2)Gal monomer **2** was prepared on a large-scale from L-fucose monosaccharide **5**. Solvent-free per-*O*-acetylation of **5** with stoichiometric acetic anhydride and catalytic iodine proceeded to give the pyranose products as anomeric mixtures. Peracetylation of L-fucose was followed by the subsequent anomeric substitution using TMSI, which was generated *in situ* from iodine and hexamethyldisilane,<sup>24</sup> to give the corresponding fucosyl iodides. Further treatment with dimethyl disulfide yielded thiofucoside **6** in 65% yield over a one-pot, three steps reaction.<sup>25</sup> Thioglycoside **6** was deacetylated under Zemplén conditions, neutralized and concentrated before being re-introduced into a solution of *p*-methoxybenzyl chloride under basic condition. The subsequent introduction of a single *p*-methoxybenzyl (PMB) protecting group afforded fucosyl donor **7** in 71% overall yield. Direct reaction of the 1,6 anhydro-3,4 O-Isopropylidene- $\beta$ -D-galactopyranose acceptor with an anomeric mixture of donor **7** in the presence of iodonium di(*sym*-collidine) perchlorate (IDCP), gave the  $\alpha$ -linked disaccharide **8** exclusively<sup>26</sup> in 55% yield. Glycosylation of **7** was mediated presumably by an oxocarbenium intermediate that was susceptible to nucleophilic attack from either the axial or equatorial position. Consequently, installation of the PMB protecting group precluded acetyl coordination at the anomeric position, which would have favored the undesired  $\beta$ -linked disaccharides formation (Scheme 3.2). Without a participating group, the observed stereochemistry of **8** could be attributed to the kinetic preference of the  $\alpha$ -linkages due to the anomeric effects. (Scheme 3.3)

Scheme 3.2. Directing Stereoselectivity by Protecting Group Manipulation



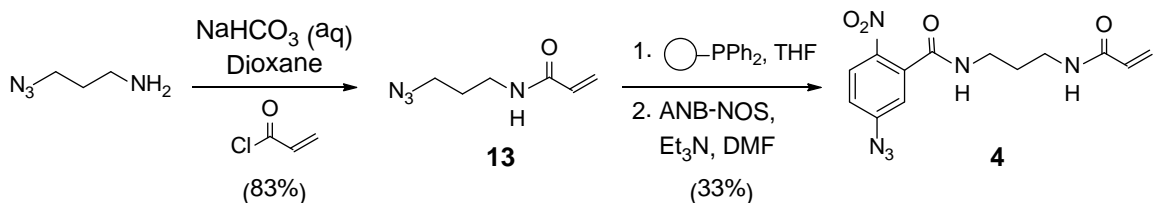
Scheme 3.3. Anomeric Effect on Glycan Linkage



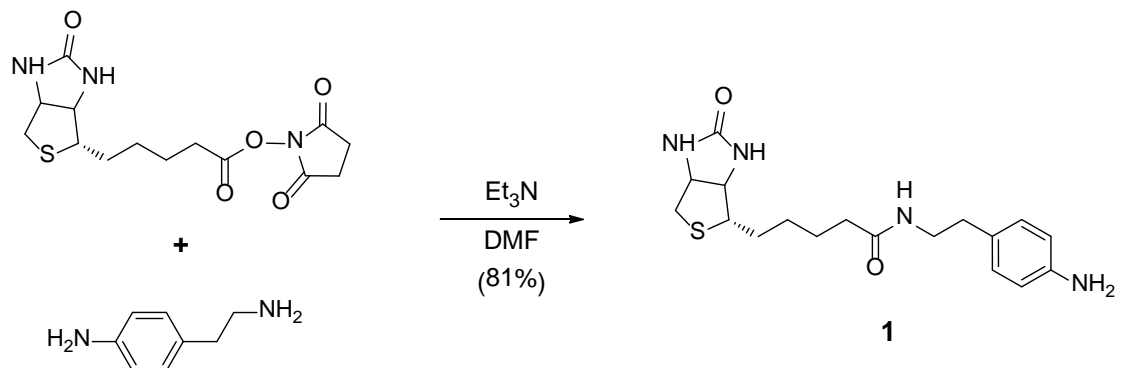
Disaccharide **8** was treated with ceric ammonium nitrate (CAN) for the simultaneous removal of the *p*-methoxybenzyl and isopropylidene groups, and the intermediate was then acetylated in the same pot to give **9** in 68% yield. The 1,6-anhydro ring of disaccharide **9** was subsequently hydrolyzed for thiophenylation using (phenylthio)trimethylsilane and zinc iodide. Following hydrolysis, the reaction mixture was deprotected without further purification using tetrabutylammonium fluoride (TBAF), and the resulting free hydroxyl group was acetylated to form thioglycoside **10**.<sup>27</sup> Next, the latent amino propyl spacer was installed to facilitate expedient presentation of the disaccharide away from the polymer backbone. Initial coupling of 3-azidopropanol with thioglycoside donor **10** in the presence of thiophilic promoter NIS/AgOTf in CH<sub>2</sub>Cl<sub>2</sub> yielded an anomeric  $\alpha/\beta$  mixture. However, the use of MeCN promoted formation of the  $\beta$ -linked glycoside **11** as the major product in 64% yield. By coordinating to the anomeric carbon in the axial position, the nitrilium ion could presumably be displaced by the attack of an incoming azidopropanol from the equatorial position.<sup>28</sup> Catalytic hydrogenation of **11** over Pd/C led to the amine intermediate, which was directly transformed without further purification into **12** using acryloyl chloride. Finally, facile deacetylation of the N-acryloyl glycoside **12** under Zemplén conditions afforded glycomonomer **2** in 90% yield.

Phenylazide monomer **4** was readily synthesized from the commercially available compounds, 3-azidopropylamine and *N*-azido-nitrobenzoyloxysuccinimide (ANB-NOS) (Scheme 3.4). First, 3-azidopropylamine was end-functionalized with acryloyl chloride to give azidopropylacrylamide **13** in 83% yield. Staudinger reaction of **13** with resin-bound diphenylphosphine reduced the azide selectively. This reaction was then followed by the coupling of the amine intermediate to ANB-NOS to afford capture monomer **4**. Biotin-derivatized arylamine initiator **1** was conveniently prepared in a single step by reacting 2-(4-aminophenyl)ethylamine with *N*-biotin succinimide (Scheme 3.5).<sup>29</sup>

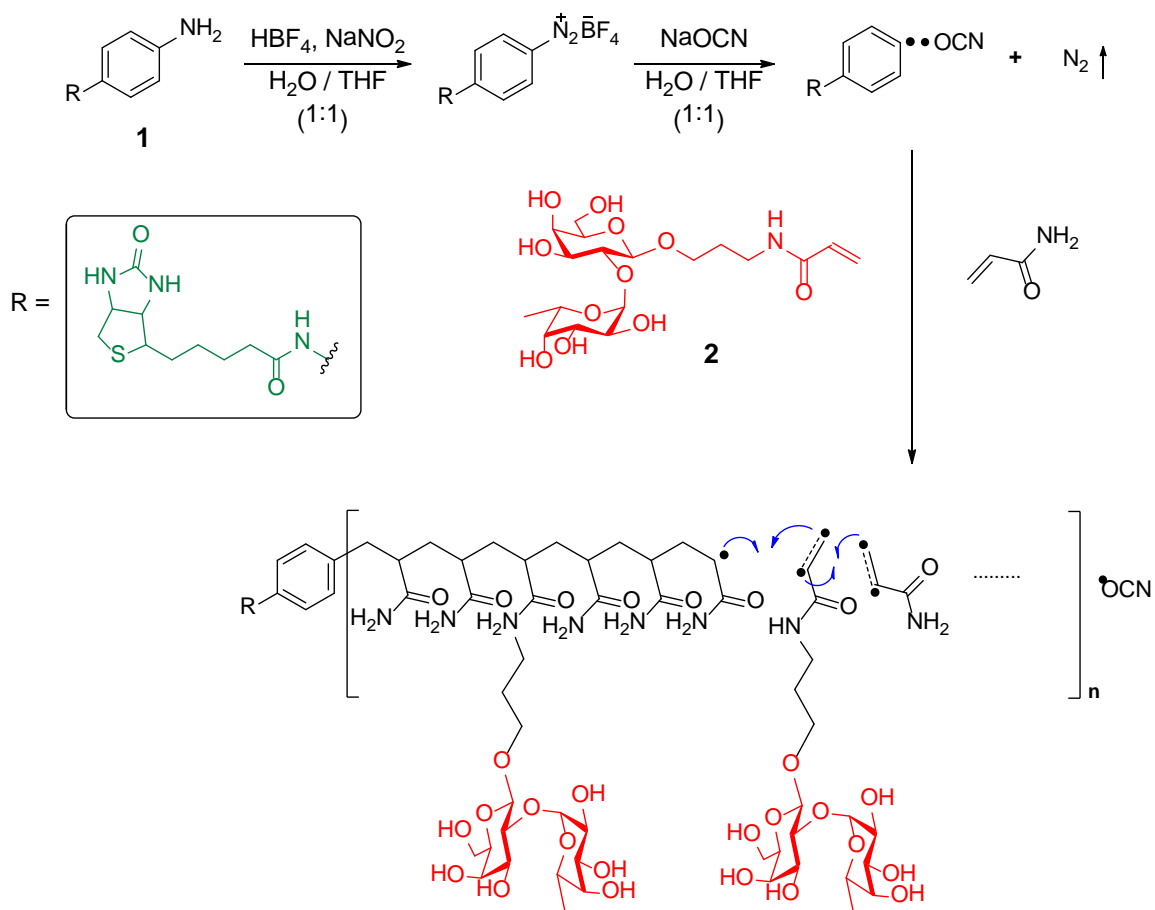
**Scheme 3.4.** Synthesis of Phenylazide cross-linker monomer **4**



**Scheme 3.5.** Synthesis of Biotin-Arylamine Initiator **1**



**Scheme 3.6.** Synthesis of Biotin-Chain-Terminated Glycopolymer



With the monomers in hand, we first generated glycopolymers **I** containing monomer **2** while using an acrylamide comonomer as the polymer backbone to test for ligand density. A spacer arm between the biotin and polymer backbone was used for further optimization of polymer-streptavidin interaction during affinity purification. Treatment of **1** with  $\text{HBF}_4$  and  $\text{NaNO}_2$  in degassed  $\text{H}_2\text{O}/\text{THF}$  (1:1) gave the arenediazonium cation, which upon reaction with  $\text{NaOCN}$  at  $60^\circ\text{C}$  generated the biotinyl aryl radical and the cyanoxyl ( $\bullet\text{OCN}$ ) free radical *in situ*. This initiator system triggered acrylamide and glycomonomer **2** addition to form a growing polymer chain that was terminated by the addition of  $\text{OCN}$

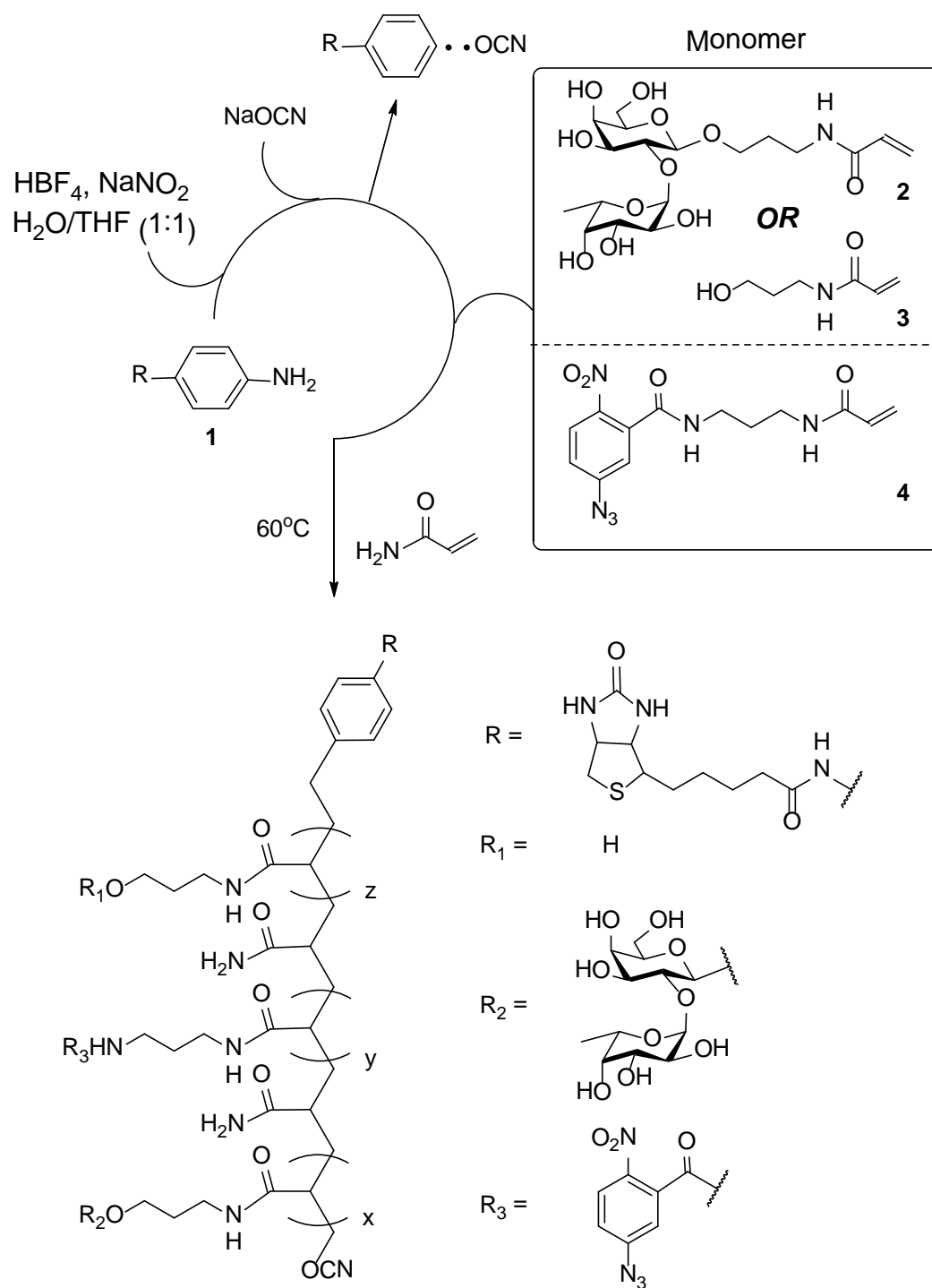
radical species (Scheme 3.6). Next, we synthesized glycopolymers **II** containing **2** and **4** in a 3:1 monomer ratio to afford polymers with optimal density and solubility (Scheme 3.7). By varying the glycan to phenylazide content of the polymer, we sought to maximize multivalent glycan-lectin interactions while still maintaining the polymer's covalent capture functionality. Similarly, we generated control polymers **III** containing **3** and **4** in a 6:1 monomer ratio where each starting disaccharide monomer unit replaced by two equivalents of *N*-(3-hydroxypropyl)-acrylamide **3** (Scheme 3.7). Characterization of the glycopolymers by <sup>1</sup>H-NMR and size- exclusion chromatography multi-angle laser light scattering (SEC-MALLS) revealed narrow polydispersity index (PDI) values (~ 1.2) with number average molecular weight ( $M_n$ ) of 24 – 26 kDa, which corresponds to up to 30 disaccharide units per polymer (Table 1). Importantly, the ligand-to-crosslinker ratio in the glycopolymer was readily tunable as shown by the close agreement to the initial monomer ratio in the polymerization reaction (Table 3.1).

**Table 3.1.** Biotin End-Functionalized Glycopolymer

Pol	Monomer	$[C]_o/[L]_o^a$	$x^b$	$y^b$	$z^b$	$M_n^c$	PDI <sup>c</sup>
<b>I</b>	<b>2</b>	-	19	-	-	26300	1.17
<b>II</b>	<b>2 and 4</b>	1/3	30	9	-	23900	1.22
<b>III</b>	<b>3 and 4</b>	1/6	-	7	43	23000	1.17

a) Initial ratio of crosslinker (4) to ligand (2 or 3). b) Crosslinker and ligand content in the resulting polymer (Scheme 3.7) are estimated by <sup>1</sup>H NMR. c) Number average molecular weight ( $M_n$ ) in (g/mol) and polydispersity index (PDI) were determined by SEC-RI/MALLS.

Scheme 3.7. Synthesis of Biotin End-Functionalized Photoactivatable Glycopolymer



Information on the structure and spatial distribution of many soluble lectins and membrane-bound receptors were largely unknown. With the synthesis of these multivalent glycopolymer probes, we sought to capture Fuc $\alpha$ (1-2)Gal lectins by covalent cross-linking. Based on our earlier attempts, lectins enrichment requires extensive washing to remove the many non-specific interactions. Thus, the UV-light cross-linking ensured the capture of weak glycan-receptor interactions that might otherwise be disrupted during affinity purification. In addition to the design of the glycopolymers, the linear scaffold endowed greater flexibility for lectin binding, unlike other rigid glycovalent structures (e.g., dendrimers). The linear scaffolds facilitate optimal glycan-lectins interactions because they can accommodate many types of binding sites and are therefore suitable for lectin isolation. Given the complexity of the lectin profile of the brain, we would first evaluate the capture of a known Fuc $\alpha$ (1-2)Gal, UEA I, in vitro using our multivalent capture probe. These efforts and their subsequent applications in neuronal lysates are discussed in the next chapter.

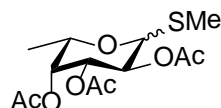
### 3.3.1. Methods and Materials

Unless otherwise stated, reactions were performed in flame-dried glassware under an argon atmosphere, using dry solvents. Solvents were dried by passage through an activated alumina column under argon. All other commercially obtained reagents were used as received unless otherwise noted. Thin-layer chromatography (TLC) was performed using E. Merck silica gel 60 F254 precoated plates (0.25 mm). Visualization of the developed chromatogram was performed by UV, p-anisaldehyde and ninhydrin stain as necessary. ICN silica gel (particle size 0.032 - 0.063 mm) was used for flash chromatography. Gel filtration chromatography (Sephadex LH-20, and G-25 ultrafine) was used in order to achieve purification of the final products.  $^1\text{H}$  NMR was recorded on Varian Inova 500 (500 MHz) and Varian Inova 600 (600 MHz) spectrometers and are reported in parts per million ( $\delta$ ) relative to  $\text{CDCl}_3$  (7.26 ppm),  $\text{CD}_3\text{OD}$  (4.87 ppm) and  $\text{D}_2\text{O}$  (4.80 ppm). Data for  $^1\text{H}$  are reported as follows: chemical shift ( $\delta$  ppm), multiplicity (s = singlet, d = doublet, t = triplet, q = quartet, m = multiplet), coupling constant in Hz, and integration.  $^{13}\text{C}$  NMR was recorded on Varian Inova 500 (125 MHz) spectrometers and are reported in terms of chemical shift. High-resolution mass spectra were obtained from the Caltech Mass Spectral Facility.

GPC was carried out in 100 mM  $\text{NaNO}_3$  and 200 ppm  $\text{NaN}_3$  in water on an OHpak SB – 804 HQ column (Shodex), which was connected in series with a miniDAWN TREOS MALLS detector and Optilab rEX differential refractometer (both from Wyatt Technology). The  $\text{dn/dc}$  values were obtained for each injection assuming 100% mass

elution from the column using dextran (40K) as a calibration standard to confirm complete mass recovery.

### 3.3.2. Synthetic Procedure



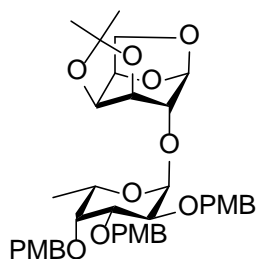
**Methyl 2,3,4-tri-O-acetyl-1-thio-L-fucopyranoside (6).** Compound **6** was prepared following a procedure by *Mukhopadhyay et al.*<sup>30</sup> To a suspension of L-fucose **5** (5.00 g, 30.46 mmol) in acetic anhydride (11.8 ml, 124.3 mmol) was added solid iodine (0.542 g, 2.13 mmol) and the mixture was allowed to stir at room temperature. After acetylation was completed as monitored by TLC (2:1 Hex:EtOAc), CH<sub>2</sub>Cl<sub>2</sub> (30.0 ml) was added into the reaction mixture followed by addition of solid iodine (4.648 g, 18.28 mmol) and Hexamethyldisilane (3.95 ml, 18.28 mmol). The mixture was allowed to stir for 2 hours at room temperature to allow full conversion to fucosyl iodide as monitored by TLC (19:1 CH<sub>2</sub>Cl<sub>2</sub>:Acetone). After complete conversion to fucosyl iodide, dimethyl sulfide (1.62 ml, 18.28 mmol) was added to the mixture and allowed to stir overnight. TLC showed complete conversion of the iodide to a slightly lower spot before the reaction mixture was diluted with CH<sub>2</sub>Cl<sub>2</sub> and washed successively with 10% aq Na<sub>2</sub>S<sub>2</sub>O<sub>3</sub>, saturated aq NaHCO<sub>3</sub> and water. The organic extract was dried (Na<sub>2</sub>SO<sub>4</sub>) and concentrated *in vacuo* before the crude product was purified by column chromatography (2:1 Hex:EtOAc) to afford white solid **6** (6.38 g, 65.4%).

$^1\text{H}$  NMR ( $\text{CDCl}_3$ ): [ $\alpha$ ]:  $\delta$  5.56 (d,  $J = 5.6$  Hz, 1H), 5.29 (dd,  $J = 10.4, 4.4$  Hz, 2H), 5.23 (dd,  $J = 10.7, 3.3$  Hz, 1H), 4.45 (q,  $J = 6.5$  Hz, 1H), 2.17 (s, 3H), 2.07 (s, 3H), 2.05 (s, 3H), 1.99 (s, 3H), 1.17 (d,  $J = 6.5$  Hz, 3H). [ $\beta$ ]:  $\delta$  5.30 (d,  $J = 1.0$  Hz, 1H), 5.25 (t,  $J = 9.9$  Hz, 1H), 5.05 (dd,  $J = 10.0, 3.4$  Hz, 1H), 4.36 (d,  $J = 9.8$  Hz, 1H), 3.85 (dd,  $J = 12.8, 6.4$  Hz, 1H), 2.20 (s, 3H), 2.18 (s, 3H), 2.08 (s, 3H), 1.99 (s, 3H), 1.22 (d,  $J = 6.4$  Hz, 3H). ESI-MS  $m/z$  calculated for  $\text{C}_{13}\text{H}_{20}\text{O}_7\text{S}$  [ $\text{M}+\text{Na}$ ] $^+$  343.1; Found : 343.1



**Methyl 2,3,4-Tri-O-(p-methoxybenzyl)-1-thio-L-fucopyranoside (7).** Compound **7** is prepared following a procedure by *Izumi et al.*<sup>26</sup> To a solution of **6** (6.38 g, 19.92 mmol) in MeOH (39.8 ml) was added 0.5M NaOMe (20.0 ml, 9.96 mmol), and the mixture was left to stir for 1.5 hours at room temperature. After deacetylation was completed as monitored by TLC, the reaction mixture was neutralized to pH  $\sim 7$  by the addition of Dowex 50W-X4-200 ( $\text{H}^+$ ) and the resin was filtered off. The filtrate was concentrated *in vacuo* and dried under high vacuum before it was re-dissolved in DMF (79.0 ml). NaH (4.16 g, 173.26 mmol) was added at  $0^\circ\text{C}$  to the solution and the mixture was stirred for 30 minutes before PMBCl (13.8 ml, 99.60 mmol) was added. The reaction mixture was allowed to stir overnight at room temperature. Methanol was added to the solution before the reaction mixture was diluted with EtOAc and washed extensively with aq NaCl. The organic extract was dried ( $\text{Na}_2\text{SO}_4$ ) and concentrated *in vacuo* before the crude product was purified by column chromatography (3:1 Hex:EtOAc) to afford white solid **7** (9.70 g, 70.9%).

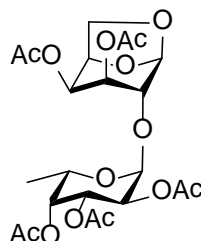
$^1\text{H NMR}$  (500 MHz,  $\text{CDCl}_3$ ) [ $\alpha$ ]:  $\delta$  7.35 – 7.23 (m, 6H), 6.90 – 6.81 (m, 6H), 5.30 (d,  $J = 5.5$  Hz, 1H), 4.89 (d,  $J = 11.3$  Hz, 1H), 4.76 (d,  $J = 11.4$  Hz, 1H), 4.68 (d,  $J = 11.6$  Hz, 1H), 4.65 – 4.56 (m, 2H), 4.24 (dd,  $J = 9.9, 5.5$  Hz, 1H), 4.14 – 4.05 (m, 1H), 3.81 (d,  $J = 2.4$  Hz, 3H), 3.81 – 3.79 (m, 6H), 3.75 (dd,  $J = 9.9, 2.7$  Hz, 1H), 2.00 (s, 3H), 1.08 (d,  $J = 6.4$  Hz, 3H). [ $\beta$ ]:  $\delta$  7.36 – 7.26 (m, 6H), 6.90 – 6.83 (m, 6H), 4.90 (d,  $J = 11.5$  Hz, 1H), 4.77 (dd,  $J = 22.1, 9.8$  Hz, 2H), 4.68 (q,  $J = 11.4$  Hz, 2H), 4.62 (d,  $J = 11.6$  Hz, 1H), 4.26 (d,  $J = 9.6$  Hz, 1H), 3.82 (s, 3H), 3.80 (s, 3H), 3.80 (s, 3H), 3.77 (d,  $J = 9.4$  Hz, 1H), 3.55 (d,  $J = 2.8$  Hz, 1H), 3.53 (d,  $J = 2.8$  Hz, 1H), 3.47 – 3.42 (m, 1H), 2.19 (d,  $J = 1.1$  Hz, 3H), 1.15 (d,  $J = 6.4$  Hz, 3H). ESI-MS  $m/z$  calculated for  $\text{C}_{31}\text{H}_{38}\text{NaO}_7\text{S}$  [ $\text{M}+\text{Na}$ ] $^+$  557.2; Found = 577.2



**1,6 Anhydro-3,4-O-Isopropylidene 2-O-(Methyl 2,3,4-Tri-O-p-methoxybenzyl-L-fucopyranosyl)- $\beta$ -D-galactopyranoside (8).** A mixture of 1,6 anhydro-3,4 O-Isopropylidene- $\beta$ -D-galactopyranose (5.00 g, 24.73 mmol, Toronto Research Chemical) and IDCP (10.02 g, 21.17 mmol)<sup>31</sup> in  $(\text{CH}_2\text{Cl}_2)_2$  -  $\text{Et}_2\text{O}$  (1:5) (110.0 ml) with 4Å molecular sieves was stirred for 1 hr at 0°C under Ar atmosphere. To the mixture was added a solution of **7** (9.70 g, 14.12 mmol, 40 ml) and the reaction mixture was stirred for 2.5 hrs while it warmed up to room temperature. After complete consumption of donor **7** as monitored by TLC (3:2 Hex:EtOAc), reaction mixture was diluted with chloroform, and washed with 2 M aq  $\text{Na}_2\text{S}_2\text{O}_3$ . The organic extract was dried ( $\text{Na}_2\text{SO}_4$ ) and concentrated *in*

*vacuo* before the crude product was purified by column chromatography (3:2 Hex:EtOAc) to afford yellowish-white solid **3** (5.39 g, 53.9 %).

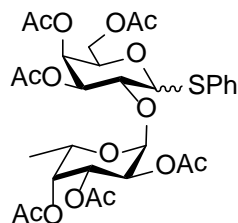
$^1\text{H}$  NMR (500 MHz,  $\text{CDCl}_3$ )  $\delta$  7.47 – 7.14 (m, 6H), 6.89 (d,  $J = 8.6$  Hz, 3H), 6.83 (dd,  $J = 8.7, 2.4$  Hz, 3H), 5.41 (s, 1H), 4.87 (dd,  $J = 12.4, 7.6$  Hz, 2H), 4.76 (dd,  $J = 11.3, 3.2$  Hz, 2H), 4.65 (d,  $J = 11.1$  Hz, 1H), 4.56 (dd,  $J = 11.4, 1.9$  Hz, 2H), 4.45 (dt,  $J = 13.1, 6.0$  Hz, 2H), 4.22 (d,  $J = 7.2$  Hz, 1H), 4.08 (d,  $J = 7.5$  Hz, 1H), 4.01 – 3.92 (m, 2H), 3.87 (dd,  $J = 10.2, 2.9$  Hz, 1H), 3.82 (s, 3H), 3.80 (s, 3H), 3.79 (s, 3H), 3.68 (s, 1H), 3.64 (d,  $J = 1.8$  Hz, 1H), 3.55 (dd,  $J = 7.3, 5.4$  Hz, 1H), 1.53 (s, 3H), 1.32 (s, 3H), 1.06 (d,  $J = 6.5$  Hz, 3H). ESI-MS  $m/z$  calculated for  $\text{C}_{39}\text{H}_{48}\text{NaO}_{12}$   $[\text{M}+\text{Na}]^+$  731.3; Found = 731.3



**3,4-Di-O-acetyl-1,6-anhydro-2-O-(Methyl 2,3,4-Tri-O-acetyl- $\alpha$ -L-fucopyranosyl)- $\beta$ -D-galactopyranoside (9).** A solution of disaccharide **8** (5.39 g, 7.61 mmol) and Ceric Ammonium Nitrate (CAN) in MeCN/ $\text{H}_2\text{O}$  (9:1) was stirred at rt for 2.5 h. After complete deprotection of p-methoxy benzyl and isopropylidene group as monitored by TLC, pyridine, acetic anhydride and catalytic amount of DMAP were added to the reaction mixture at  $0^\circ\text{C}$  before the reaction mixture was allowed to stir at rt. After the reaction was completed as monitored by TLC, the mixture was diluted with chloroform and washed successively with aq  $\text{CuSO}_4$ ,  $\text{H}_2\text{O}$  and aq  $\text{NaHCO}_3$ . The organic extract was dried

(MgSO<sub>4</sub>) and concentrated in vacuo before the crude product was purified by column chromatography (3:2 Hex:EtOAc) to afford white solid **8** (2.69 g, 68.2%).

<sup>1</sup>H NMR (500 MHz, CDCl<sub>3</sub>) δ 5.43 (s, 1H), 5.35 – 5.30 (m, 2H), 5.24 (d, J = 3.8 Hz, 1H), 5.19 (t, J = 4.7 Hz, 1H), 5.13 (dd, J = 10.8, 3.6 Hz, 1H), 5.08 (d, J = 5.4 Hz, 1H), 4.47 (t, J = 4.4 Hz, 1H), 4.34 – 4.26 (m, 2H), 3.72 (dd, J = 7.2, 5.1 Hz, 1H), 3.61 (s, 1H), 2.16 (s, 3H), 2.14 (s, 3H), 2.09 (s, 3H), 2.05 (s, 3H), 1.99 (s, 3H), 1.13 (d, J = 6.6 Hz, 3H). <sup>13</sup>C NMR (125 MHz, CDCl<sub>3</sub>) δ 170.87, 170.76, 170.23, 169.92, 169.34, 100.52, 97.23, 72.22, 71.01, 68.23, 68.09, 67.62, 65.31, 65.27, 64.58, 62.44, 21.02, 20.89, 20.84, 20.83, 20.77, 16.07. HRMS m/z Calculated for C<sub>22</sub>H<sub>31</sub>O<sub>14</sub> [M+H]<sup>+</sup> 519.1714. Found : 519.1731.

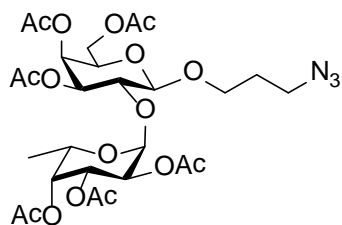


**Phenyl 3,4,6-Tri-O-acetyl-2-O-(Methyl 2,3,4-Tri-O-acetyl- $\alpha$ -L-fucopyranosyl)-1-thio-D-galactopyranoside (10).** A mixture of **9** (510 mg, 0.98 mmol), (phenylthio)-trimethylsilane (0.77 ml, 3.94 mmol) and zinc iodide (1.29 g, 3.94 mmol) in CH<sub>2</sub>Cl<sub>2</sub> (1.0 ml) was stirred overnight at rt.<sup>32</sup> After complete consumption of the starting material as monitored by TLC, the mixture was diluted with EtOAc and washed successfully with aq NaHCO<sub>3</sub>, H<sub>2</sub>O and aq NaCl. The organic extract was dried with Na<sub>2</sub>SO<sub>4</sub> and concentrated in vacuo before it was re-dissolved in dry THF (2.80 ml) and 1M tetrabutylammonium fluoride in THF (1.97 ml) was added into the solution. After one hour, solvent was removed in vacuo and the residue was re-dissolved in EtOAc, washed with H<sub>2</sub>O, aq

NaHCO<sub>3</sub>, and aq NaCl, dried over with Na<sub>2</sub>SO<sub>4</sub> and concentrated to afford thioglycoside.

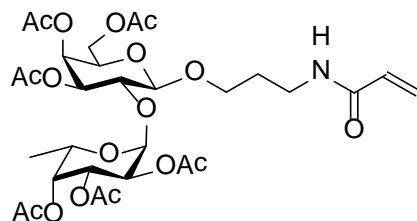
To a solution of thioglycoside in dry pyridine (9.55 ml, 118.08 mmol) was added catalytic amount of DMAP and acetic anhydride (6.05 ml, 63.96 mmol) before the mixture was allowed to stir at rt. After complete protection of free hydroxyl group, the reaction mixture was diluted with EtOAc, washed successively with aq CuSO<sub>4</sub>, aq NaHCO<sub>3</sub>, H<sub>2</sub>O and aq NaCl. The organic extract was dried with Na<sub>2</sub>SO<sub>4</sub> and concentrated in vacuo before the crude product was purified by column chromatography (3:2 Hex:EtOAc) to afford white solid 9 (363 mg, 55%).

<sup>1</sup>H NMR (500 MHz, CDCl<sub>3</sub>) δ 7.48 (d, J = 7.3 Hz, 2H), 7.36 – 7.27 (m, 3H), 5.69 (d, J = 5.7 Hz, 1H), 5.45 (d, J = 3.1 Hz, 1H), 5.34 (d, J = 3.2 Hz, 1H), 5.30 (d, J = 3.7 Hz, 2H), 5.21 (dd, J = 10.6, 3.4 Hz, 1H), 5.03 (dd, J = 10.7, 3.9 Hz, 1H), 4.73 (t, J = 6.5 Hz, 1H), 4.36 (q, J = 6.5 Hz, 1H), 4.29 (dd, J = 10.6, 5.7 Hz, 1H), 4.07 (t, J = 6.4 Hz, 2H), 2.15 (s, 3H), 2.14 (s, 3H), 2.04 (s, 3H), 1.99 (s, 6H), 1.96 (s, 3H), 1.00 (d, J = 6.5 Hz, 3H). <sup>13</sup>C NMR (125 MHz, CDCl<sub>3</sub>) δ 170.69, 170.65, 170.56, 170.27, 170.03, 169.97, 133.22, 131.70 (2C), 129.32 (2C), 127.78, 98.21, 87.81, 73.15, 70.99, 70.09, 68.16 (2C), 67.89, 67.35, 65.87, 61.83, 20.92, 20.88, 20.84 (2C), 20.81, 20.80, 16.03. HRMS m/z Calculated for C<sub>30</sub>H<sub>38</sub>O<sub>15</sub>S [M]<sup>+</sup> 670.1931. Found : 670.1941.



**3-azidopropyl 3,4,6-Tri-O-acetyl-2-O-(Methyl 2,3,4-Tri-O-acetyl- $\alpha$ -L-fucopyranosyl)-D-galactopyranoside (11).** The following is modified procedure from Kanie et al.<sup>33</sup> Compound **10** (363 mg, 0.54 mmol) and 3-azidopropanol (75  $\mu$ l, 0.81 mmol) was azeotroped with toluene, dissolved in acetonitrile with 4Å molecular sieves and cooled to  $-20^{\circ}\text{C}$ . To the mixture, *N*-Iodosuccinimide (192 mg, 0.81 mmol) was added and it was allowed to stir for 15 minutes. Next, silver triflate (209 mg, 0.81 mmol) was added and the mixture was allowed to warm up to room temperature and stirred for 1 h. After the reaction was completed as monitored by TLC, the reaction mixture was diluted with EtOAc and washed successively with sat aq  $\text{Na}_2\text{SO}_3$ , aq  $\text{NaHCO}_3$ , and aq  $\text{NaCl}$ . The organic extract was dried with  $\text{MgSO}_4$  and concentrated *in vacuo* before the crude product was purified by column chromatography (3:2 Hex:EtOAc) to afford pale-yellow solid **10** (228 mg, 64%,  $\alpha:\beta = 1:3$ ).

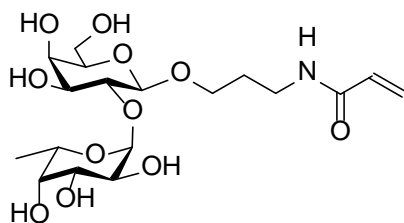
$^1\text{H}$  NMR (500 MHz,  $\text{CDCl}_3$ ) [ $\beta$ ]:  $\delta$  5.39 (d,  $J = 3.9$  Hz, 1H), 5.35 – 5.25 (m, 3H), 5.05 – 4.98 (m, 2H), 4.54 – 4.44 (m, 2H), 4.18 (dd,  $J = 11.2, 6.5$  Hz, 1H), 4.10 (dd,  $J = 11.3, 6.9$  Hz, 1H), 4.01 – 3.85 (m, 3H), 3.68 (dt,  $J = 9.9, 6.3$  Hz, 1H), 3.43 (t,  $J = 6.6$  Hz, 2H), 2.16 (s, 3H), 2.13 (s, 3H), 2.05 (s, 3H), 2.01 (s, 3H), 1.99 (d,  $J = 3.4$  Hz, 6H), 1.93 – 1.86 (m, 2H), 1.13 (d,  $J = 6.5$  Hz, 3H).  $^{13}\text{C}$  NMR (125 MHz,  $\text{CDCl}_3$ )  $\delta$  170.78, 170.73, 170.54, 170.41 (2C), 170.20, 101.75, 95.85, 73.83, 71.91, 71.25, 70.63, 68.33, 67.73, 67.31, 67.02, 64.77, 61.38, 48.28, 29.44, 20.88, 20.84 (3C), 20.80, 20.77, 15.90. HRMS  $m/z$ . Calculated for  $\text{C}_{27}\text{H}_{39}\text{O}_{16}\text{Na}$  [ $\text{M}+\text{Na}$ ] $^+$  684.2228. Found : 684.2228.



**3-N-Acryoyl-aminopropyl-3,4,6-Tri-O-acetyl-2-O-(Methyl 2,3,4-Tri-O-acetyl- $\alpha$ -L-fucopyra-nosyl)-D-galactopyranoside (12).** A suspension of **11** (204 mg, 0.31 mmol) and Pd/C (20% by wt) in dry EtOAc (3.1 ml) was charged with H<sub>2</sub> gas for 3.5 h in the presence of catalytic amount of triethyl amine. After reduction of azido group was completed, reaction mixture was diluted with EtOAc and was filtered off packed celite. The filtrate was concentrated *in vacuo* and the crude material was dissolved in dioxane (3.0 ml) before the addition of aq NaHCO<sub>3</sub> (32.8 mg in 2.9 ml H<sub>2</sub>O, 0.39 mmol). The mixture was cooled to 0°C, stirred for 15 mins before acryloyl chloride (37.2  $\mu$ l, 0.45 mmol) was added dropwise and allowed to warm up overnight while minimizing exposure to light. Once reaction was completed, the mixture was diluted with EtOAc and washed with H<sub>2</sub>O. The organic layer was concentrated *in vacuo* and the crude product was purified by column chromatography (1:9 MeOH:CH<sub>2</sub>Cl<sub>2</sub>) to afford **11** as colorless oil (119 mg, 57%).

<sup>1</sup>H NMR (500 MHz, CDCl<sub>3</sub>)  $\delta$  6.30 (dd,  $J$  = 17.0, 1.4 Hz, 1H), 6.14 (dd,  $J$  = 17.0, 10.3 Hz, 1H), 5.64 (dd,  $J$  = 10.3, 1.4 Hz, 1H), 5.40 (d,  $J$  = 3.8 Hz, 1H), 5.32 – 5.27 (m, 3H), 5.04 – 4.97 (m, 2H), 4.54 (q,  $J$  = 6.6 Hz, 1H), 4.47 (d,  $J$  = 7.8 Hz, 1H), 4.18 (dd,  $J$  = 11.3, 6.7 Hz, 1H), 4.11 (dd,  $J$  = 12.4, 6.9 Hz, 1H), 3.97 – 3.86 (m, 3H), 3.76 – 3.69 (m, 1H), 3.44 (q,  $J$  = 6.6 Hz, 2H), 2.16 (s, 3H), 2.14 (s, 3H), 2.05 (d,  $J$  = 2.1 Hz, 3H), 2.01 (s, 3H), 2.00 (s, 3H), 1.99 (s, 3H), 1.89 (td,  $J$  = 13.1, 6.6 Hz, 2H), 1.13 (d,  $J$  = 6.5 Hz, 3H). <sup>13</sup>C NMR (125 MHz,

CDCl<sub>3</sub>)  $\delta$  170.71, 170.70, 170.53, 170.47, 170.32, 170.30, 165.86, 131.02, 126.35, 101.74, 95.67, 73.72, 71.62, 71.15, 70.77, 68.24, 67.98, 67.83, 67.40, 64.79, 61.44, 37.03, 29.69, 20.88, 20.81, 20.78 (2C), 20.73 (2C), 15.83. HRMS  $m/z$  Calculated for C<sub>30</sub>H<sub>44</sub>NO<sub>17</sub> [M+H]<sup>+</sup> 690.2609. Found : 690.2629.



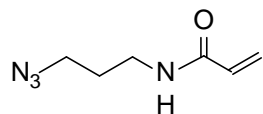
**3-N-Acryloyl-aminopropyl-2-O-( $\alpha$ -L-fucopyranosyl)-D-galactopyranoside (2).**

To a solution of **12** (119 mg, 0.17 mmol) in MeOH (1.1 ml) was added 0.5M NaOMe (0.10 ml, 0.052 mmol), and the mixture was left to stir at rt for 1 h. After deacetylation was completed as monitored by TLC, the reaction mixture was neutralized to pH  $\sim$  7 by the addition of Dowex 50W-X4-200 (H<sup>+</sup>) and the resin was filtered off. The filtrate is concentrated *in vacuo* and purified with gel filtration chromatography (Sephadex LH-20) to obtain glycomonomer **2** (68 mg, 89.7%).

<sup>1</sup>H NMR (500 MHz, D<sub>2</sub>O)  $\delta$  6.25 (dd,  $J$  = 17.1, 10.2 Hz, 1H), 6.17 (dd,  $J$  = 17.1, 1.3 Hz, 1H), 5.74 (dd,  $J$  = 10.2, 1.3 Hz, 1H), 5.23 (d,  $J$  = 3.9 Hz, 1H), 4.48 (d,  $J$  = 7.9 Hz, 1H), 4.29 (q,  $J$  = 6.5 Hz, 1H), 3.95 (dt,  $J$  = 10.2, 6.8 Hz, 1H), 3.89 (d,  $J$  = 3.3 Hz, 1H), 3.84 (dt,  $J$  = 9.5, 2.7 Hz, 2H), 3.81 – 3.71 (m, 5H), 3.67 (dd,  $J$  = 7.7, 4.5 Hz, 1H), 3.58 (dd,  $J$  = 9.5, 7.9 Hz, 1H), 3.35 (dd,  $J$  = 11.3, 6.7 Hz, 2H), 1.91 – 1.84 (m, 2H), 1.19 (d,  $J$  = 6.6 Hz, 3H). <sup>13</sup>C NMR (125 MHz, D<sub>2</sub>O)  $\delta$  168.68, 130.08, 127.30, 101.68, 99.67, 77.09, 75.14, 73.83,

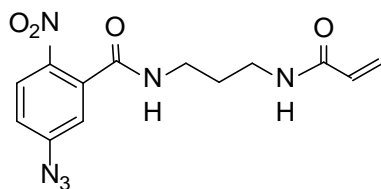
72.01, 69.64, 69.09, 68.48, 67.87, 66.98, 61.12, 36.57, 28.70, 15.51. HRMS  $m/z$

Calculated for  $C_{18}H_{31}NO_{11}Na$   $[M+Na]^+$  460.1795. Found : 460.1781.



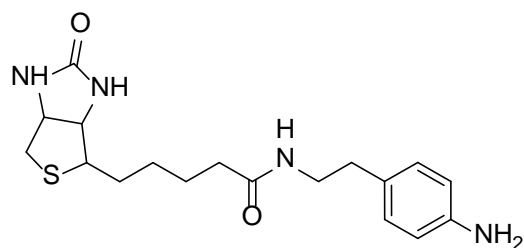
**3-N-Acryloyl- aminopropyl azide (13).** A solution of 3-azidopropylamine (873 mg, 8.721 mmol) in dioxane (20 ml) was added with aq  $NHCO_3$  (953 mg in 12 ml  $H_2O$ , 11.34 mmol) and was stirred and cooled to  $0^\circ C$ . After 15 mins, acryloyl chloride (1.08 ml, 13.08 mmol) was added dropwise to the reaction mixture and allowed to warm up to room temperature while minimizing exposure to light. After 2 h, the mixture was diluted with EtOAc, washed with  $H_2O$ , and the organic layer was concentrated *in vacuo*. Crude product was purified with column chromatography (1:1 Hex:EtOAc) to afford colorless oil **13** (1.12 g, 83%).

$^1H$  NMR (500 MHz,  $CDCl_3$ )  $\delta$  6.29 (dd,  $J = 17.0, 1.3$  Hz, 1H), 6.08 (dd,  $J = 17.0, 10.3$  Hz, 1H), 5.66 (dd,  $J = 10.3, 1.3$  Hz, 1H), 3.44 (dd,  $J = 13.0, 6.5$  Hz, 2H), 3.40 (t,  $J = 6.6$  Hz, 2H), 1.88 – 1.80 (m, 2H).  $^{13}C$  NMR (125 MHz,  $CDCl_3$ )  $\delta$  165.84, 130.77, 126.80, 49.52, 37.36, 28.87. HRMS  $m/z$  Calculated for  $C_6H_{10}N_4O$   $[M]^+$  154.0855. Found : 154.0842.



**3-N-Acryloyl-aminopropyl-2-Nitro-phenylazide (4).** The following is modified procedure from Lindsley et al.<sup>34</sup> and Hemming et al.<sup>35</sup> Triphenylphosphine polystyrene resin (Novabiochem) was first equilibrated by washing successively with THF, CH<sub>2</sub>Cl<sub>2</sub> and MeOH. After drying in vacuo, A suspension of the resin (3.40 g, 3.40 mmol) and **13** (526 mg, 3.39 mmol) in THF (21 ml) was gently shaken at 37°C for 24 h. The mixture was filtered off and the residual beads were washed successively with THF, CH<sub>2</sub>Cl<sub>2</sub> and MeOH. After drying in vacuo, the resin was resuspended in THF/H<sub>2</sub>O (10:1) (15 ml), and gently shaken at 37°C for 48 h before the reaction mixture was filtered off. The filtrate was collected, and the resins were washed off with CH<sub>2</sub>Cl<sub>2</sub> and MeOH. The filtrate and the washes were combined and concentrated in vacuo to afford the amine intermediate (185 mg, 42.6 %). To a solution of the amine in dry DMF (7.5 ml) was added Et<sub>3</sub>N (0.110 ml, 0.786) and ANB-NOS (Pierce) (200 mg, 0.655 mmol). The reaction was allowed to stir overnight in dark and concentrated *in vacuo* before the crude product was purified by column chromatography (10:1 EtOAc: MeOH) to afford crosslinker **6** (69 mg, 33%).

<sup>1</sup>H NMR (500 MHz, CDCl<sub>3</sub>) δ 8.13 (d, *J* = 8.7 Hz, 1H), 7.15-7.11 (m, 2H), 6.23 (dd, *J* = 17.0, 1.3 Hz, 1H), 6.10 (dd, *J* = 16.9, 10.2 Hz, 1H), 5.66 (dd, *J* = 10.2, 1.3 Hz, 1H), 3.54 – 3.45 (m, 4H), 1.89 – 1.81 (m, 2H). <sup>13</sup>C NMR (125 MHz, CDCl<sub>3</sub>) δ 166.93, 166.33, 146.52, 142.34, 135.78, 130.58, 127.16, 127.07, 120.13, 119.13, 36.51, 36.25, 29.41. HRMS *m/z* Calculated for C<sub>13</sub>H<sub>15</sub>N<sub>6</sub>O<sub>4</sub> [M+H]<sup>+</sup> 319.1155. Found : 319.1154.



**2-(4-Aminophenyl) Ethyl-Biotinylamide (1).** Compound **1** was synthesized according following previous work by Tseng et al.<sup>29</sup> To a solution of 4, 2-aminoethyl aniline (47  $\mu$ l, 0.35 mmol) in DMF (1.0 ml), was added triethyl amine (51  $\mu$ l, 0.37 mmol) and stirred for 30 min. Next, NHS-biotin dissolved in DMF (100 mg in 2.5 ml, 0.29 mmol) was transferred into the reaction mixture and stirred overnight. After all NHS-biotin was reacted, as monitored by TLC, reaction mixture was concentrated *in vacuo* before the crude product was purified by column chromatography (CHCl<sub>3</sub>:MeOH = 8:1) to obtain pale yellow solid **12** (88.2 mg, 84%).

<sup>1</sup>H NMR (500 MHz, CD<sub>3</sub>OD)  $\delta$  6.97 (d,  $J$  = 8.2 Hz, 2H), 6.68 (d,  $J$  = 8.2 Hz, 2H), 4.50 (dd,  $J$  = 7.8, 4.9 Hz, 1H), 4.30 (dd,  $J$  = 7.8, 4.5 Hz, 1H), 3.35 (ddd,  $J$  = 10.2, 7.6, 4.6 Hz, 2H), 3.23 – 3.16 (m, 1H), 2.94 (dd,  $J$  = 12.7, 5.0 Hz, 1H), 2.74 – 2.64 (m, 3H), 2.17 (t,  $J$  = 7.3 Hz, 2H), 1.75 – 1.53 (m, 4H), 1.44 – 1.35 (m, 2H). <sup>13</sup>C NMR (126 MHz, CD<sub>3</sub>OD)  $\delta$  175.95, 166.13, 146.81, 130.41 (2C), 130.09, 116.89 (2C), 63.37, 61.64, 56.97, 42.17, 41.04, 36.81, 35.71, 29.68, 29.48, 26.93. ESI-MS  $m/z$  Calculated for C<sub>18</sub>H<sub>27</sub>N<sub>4</sub>O<sub>2</sub>S [M+H]<sup>+</sup> 363.2. Found : 363.2

**Copolymerization reaction with a biotin-derivatized initiator.** Copolymerization reaction was set up according to procedure modified from Hou et al.<sup>36</sup> In a typical polymerization experiment, 4-aminobenzyl-biotinylamide **1** (16.6 mg, 45.9  $\mu$ mol) was

dissolved in degassed H<sub>2</sub>O/THF (1:1) (0.8 ml) and reacted with HBF<sub>4</sub> (8.7 μl, 50 wt % aqueous solution, 68.8 μmol) at 0°C under an Ar atmosphere. The diazonium salt was generated by the addition of NaNO<sub>2</sub> (3.92 mg, 55.1 μmol) into the reaction mixture. After 30 min, a degassed mixture of glycomonomer **2** (75.25 mg, 172.1 μmol), crosslinker monomer **4** (18.26 mg, 57.4 μmol), acrylamide (48.9 mg, 688 μmol), and NaOCN (15.15 mg, 224 μmol) in H<sub>2</sub>O/THF (1:1) (1.2 ml) were introduced to the diazonium salt and the reaction mixture was heated to 60°C for 16 h. Copolymers formed are dialyzed (3000 MW Cutoff) at 4°C against H<sub>2</sub>O for 48 h and purified by gel filtration chromatography (G-25). The resulting polymer was lyophilized to afford biotin-polymer as fluffy powder.

Conversion of the glycosyl monomer was calculated by comparing the integrals of the methyl peaks of fucose (1.24 ppm, 3H) and those of the phenyl group of the biotin handle (7.18 ppm, 4H). Conversion of the crosslinker was calculated by comparing the integrals of the phenyl azide proton peaks (8.27 ppm, 3H) and those of the phenyl group of the biotin handle.

**FucGal polymer (I).** Polymer I was prepared using the above procedure without the crosslinker monomer to yield an orange fluffy powder (41.8%). M<sub>n</sub> (SEC) = 26300. PDI (SEC) = 1.17. <sup>1</sup>H NMR (500 MHz, D<sub>2</sub>O) δ 7.18 (d, *J* = 15.5 Hz, 5H), 5.24 (s, 11H), 5.11 – 5.01 (m, 5H), 4.55 – 4.26 (m, 32H), 4.13 – 3.51 (m, 186H), 3.48 – 3.12 (m, 38H), 2.43 – 2.04 (m, 229H), 1.91 – 1.44 (m, 500H), 1.30 – 1.15 (m, 58H).

**FucGal crosslinker polymer (II).** Polymer **II** was prepared using the above procedure to yield a light yellow fluffy powder (19.5% yield).  $M_n$  (SEC) = 23900. PDI (SEC) = 1.22.  $^1\text{H}$  NMR (500 MHz,  $\text{D}_2\text{O}$ )  $\delta$  8.27 – 7.95 (m, 28H), 7.18 (d,  $J$  = 16.3 Hz, 6H), 5.24 (s, 25H), 5.12 – 4.99 (m, 18H), 4.55 – 4.25 (m, 58H), 4.12 – 3.49 (m, 374H), 3.42 – 3.12 (m, 80H), 2.44 – 2.00 (m, 159H), 1.89 – 1.46 (m, 338H), 1.24 – 1.14 (m, 91H).

**Control crosslinker polymer (III).** Polymer **III** was prepared using the above procedure, substituting **2** with **3**, to yield a white fluffy powder (20.8% yield).  $M_n$  (SEC) = 23000. PDI (SEC) = 1.17.  $^1\text{H}$  NMR (500 MHz,  $\text{D}_2\text{O}$ )  $\delta$  8.29 – 7.90 (m, 20H), 7.18 (d,  $J$  = 16.1 Hz, 5H), 3.63 (s, 85H), 3.24 (s, 98H), 2.46 – 1.94 (m, 213H), 1.70 (d,  $J$  = 54.2 Hz, 477H).

## REFERENCES

1. Ernst, B.; Magnani, J. L. *Nat. Rev. Drug. Discov.* **2009**, 8, 661
2. Kiessling, L. L.; Splain, R. A. *Annu. Rev. Biochem.* **2010**, 79, 619
3. Brewer, C. F.; Miceli, M. C.; Baum, L. G. *Curr. Opin. Struct. Biol.* **2002**, 12, 616
4. Collins, B. E.; Paulson, J. C. *Curr. Opin. Chem. Biol.* **2004**, 8, 617
5. Gestwicki, J. E.; Cairo, C. W.; Strong, L. E.; Oetjen, K. A.; Kiessling, L. L. *J. Am. Chem. Soc.* **2002**, 124, 14922
6. Lundquist, J. J.; Toone, E. J. *Chem. Rev.* **2002**, 102, 555
7. Nishikawa, K.; Matsuoka, K.; Kita, E.; Okabe, N.; Mizuguchi, M. et al. *Proc. Natl. Acad. Sci. USA.* **2002**, 99, 7669
8. Kensinger, R. D.; Catalone, B. J.; Krebs, F. C.; Wigdahl, B.; Schengrund, C. L. *Antimicrob. Agents. Chemother.* **2004**, 48, 1614
9. Gambaryan, A. S.; Boravleva, E. Y.; Matrosovich, T. Y.; Matrosovich, M. N.; Klenk, H-D. et al. *Antiviral Res.* **2005**, 68, 116
10. Rele, S. M.; Cui, W.; Wang, L.; Hou, S.; Barr-Zarse, G. *J. Am. Chem. Soc.* **2007**, 127, 10132
11. Ali, M.; Hicks, A. E.; Hellewel, P. G.; Thoma, G.; Norman, K. E. *FASEB. J.* **2004**, 18, 152
12. Mowery, P.; Yang, Z-Q.; Gordon, E. J.; Dwir, O.; Spencer, A. G. *Chem. Biol.* **2004**, 11, 725
13. Kiessling, L. L.; Gestwicki, J. E.; Strong, L. E. *Angew. Chem. Int. Ed.* **2006**, 45, 2348
14. Pieters, R. J. *Org. Biomol. Chem.* **2009**, 7, 2013
15. Courtney, A. H.; Puffer, E. B.; Pontrello, J. K.; Yang, Z-Q.; Kiessling, L. L. *Proc. Natl. Acad. Sci. USA.* **2009**, 106, 2500
16. Rawat, M.; Gama, C. I.; Matson, J. B.; Hsieh-Wilson, L. C. *J. Am. Chem. Soc.* **2008**, 130, 2959
17. Belardi, B.; O'Donoghue, G. P.; Smith, A. W.; Groves, J. T.; Bertozzi, C. R. *J. Am. Chem. Soc.* **2012**, 134, 9549.
18. Sigal, G. B.; Mammen, M.; Dahman, G.; Whitesides, G. M. *J. Am. Chem. Soc.* **1996**, 118, 3789.
19. Sun, X. L.; Faucher, K. M.; Grande, D.; Chaikof, E. L. *J. Am. Chem. Soc.* **2002**, 124, 7258.
20. Gubbens, J.; Ruijter, E.; de Fays, L. E. V.; Damen, J. M. A.; de Kruijff, B. et al. *Chem. Biol.* **2009**, 16, 3.
21. Druliner, J. D. *Macromolecules.* **1991**, 24, 6079
22. Grande, D.; Guerrero, R.; Gnanou, Y. *J. Polym. Sci. Part A, Polym. Chem.* **2005**, 43, 519.
23. Wegmann, B.; Schidmt, R. *Carbohydr. Res.* **1988**, 184, 254
24. Olah, G. A.; Narang, S. C.; Gupta, B. G. B.; Malhotra, R. *Angew. Chem. Int. Ed.* **1979**, 18, 612

25. Mukhopadhyay, B.; Kartha, K. P. R.; Russel, D. A.; Field, R. A. *J. Org. Chem.* **2004**, 69, 7758
26. Izumi, M.; Tsuruta, O.; Harayama, S.; Hashimoto, H. *J. Org. Chem.* **1997**, 62, 992
27. Motawia, M. S.; Olsen, C. E.; Moller, B. L.; Marcussen, J. *Carbohydr. Res.* **1994**, 252, 69, 84
28. Braccini, I.; Derouet, C.; Esnault, J.; Dupenhoat, C. H.; Mallet, J. M. et al. *Carbohydr. Res.* **1993**, 246, 23
29. Tseng, P. Y.; Rele, S. M.; Sun, X. L.; Chaikof, E. L. *Biomaterials.* **2006**, 27, 2627
30. Mukhopadhyay, B.; Kartha, K. P. R.; Russel, D. A.; Field, R. A. *J. Org. Chem.* **2004**, 69, 7758
31. Lemieux, R. U.; Morgan, A. R. *Can. J. Chem.* **1965**, 43, 2190
32. Damager, I.; Olsen, C. E.; Moller, B. L.; Motawia, M. S. *Synthesis.* **2002**, 3, 418
33. Kanie, O.; Ito, Y.; Ogawa, T. *Tet. Lett.* **1996**, 37, 4551
34. Lindsley, C.W.; Zhao, Z.; Newton, R. C.; Leister, W. H.; Strauss, K. A. *Tet. Lett.* **2002**, 43, 4467.
35. Hemming, K.; Bevan, M. J.; Loukou, C.; Patel, S. D.; Renaudeau, D. *Synlett.* **2000**, 11, 1565.
36. Hou, S.; Sun, X-L.; Dong, C-M.; Chaikof, E.L. *Bioconjugate. Chem.* **2004**, 15, 954

PROTEOMIC IDENTIFICATION OF FUC $\alpha$ (1-2)GAL LECTINS**4.1. Lectin Discovery by Mass Spectrometry**

Mass-spectrometry (MS)-based strategies have been highly successful in identifying and profiling proteins in complex mixtures. Key insights into composition, regulation and function of molecular complexes and pathways have been characterized using MS-based technologies. Indeed, new MS-based method for rapid analysis of protein structures and function, are responsible for generating large data sets, which ultimately are translated into novel discoveries. These large-scale approaches to protein science are collectively termed proteomics.

The goal of proteomics is to investigate the protein spectrum and its biological functions, and consequently to extract meaningful information for disease prognosis and drug targeting.<sup>1</sup> Large-scale proteomic analysis is supported by the advances in MS technology, computer and software sciences and the enormous amount of genomic information, which is now available for many organisms. A proteomic analysis comprises two steps: (i) separation of protein mixtures and (ii) identification of the separated proteins by various analytical methods, mainly by mass spectrometry.<sup>2-6</sup> MS has become the dominant technique for several reasons, mainly because of its unparalleled ability to acquire high-content quantitative information about complex biological samples from many different tissue samples including the brain.<sup>7-9</sup> Furthermore, MS can be used for *de*

*novo* sequencing to determine structural information (in particular post-translational modifications) as well as to quantify relative and absolute amounts of proteins through isotopic or chemical labeling methods.<sup>10-12</sup>

The challenge of studying glycosylation in cellular environment is attributed to the heterogeneity of the glycans, the complex biosynthesis of the epitopes, the multivalent nature of glycan recognition and the subtle phenotypes of glycan manipulation that often require multicellular environments to manifest.<sup>13</sup> The development of large-scale systematic MS methods is critical for advancing the frontiers of functional glycomics and for understanding the biological roles of specific glycan structures.<sup>14</sup> Identification of glycoproteins typically requires the combination of affinity purification using lectin enrichment or chemical tagging and MS-based analysis of the glycan structures. On the other hand, general, systems-level approaches for the proteome-wide identification of glycan-binding proteins have been lacking. As a result, we seek to address these challenges by employing our multivalent crosslinking probes for the discovery of novel mammalian lectins.

#### **4.2. Lectin Capture with Biotinylated Multivalent Probes**

To show the application of our capture probes, we first targeted the known Fuc $\alpha$ (1-2)Gal plant lectin *Ulex europaeus* agglutinin I (UEAI), which binds  $\alpha$ -L-Fucose-OMe with weak affinity ( $K_a = 6.4 \times 10^3 \text{ M}^{-1}$ ).<sup>15</sup> UEAI was also found to agglutinate human red cells due to its strong affinity for the H-type 2 determinant (Fuc $\alpha$ (1-2)Gal $\beta$ (1-4)GlcNAc).<sup>16,17</sup> The UEAI-H-type 2 glycan complex consisted of a single UEAI dimer,

two  $\text{Ca}^{2+}$  and  $\text{Mn}^{2+}$  ions (one  $\text{Ca}^{2+}$  and  $\text{Mn}^{2+}$  per subunit) and a single H-type 2-OMe glycan epitope.<sup>18</sup> The increased hydrogen bonding of Gal and GlcNAc epitopes towards the respective R102 and R222 residues of UEAI binding site, resulted in affinity enhancement ( $K_a = 1.8 \times 10^6 \text{ M}^{-1}$ ) and stabilization of the UEAI-H-type2 carbohydrate complex.<sup>17-19</sup> Consequently, these studies confirmed the multivalent interactions between UEAI and  $\text{Fuc}\alpha(1-2)\text{Gal}$  carbohydrates. As a result, we sought to demonstrate that the glycopolymer capture probes would be suitable for lectin enrichment. In addition, we will further evaluate the UV crosslink enrichment to assess the potential for lectin isolation and identification from more complex samples.

Fluorescein-conjugated UEAI was incubated with polymer **II** for 3 h at 37°C, exposed to 365 nm light, and the crosslinked proteins were isolated by affinity purification using immobilized streptavidin resin conjugate. Captured UEAI was eluted, resolved with SDS-PAGE and quantified by in-gel fluorescence imaging. As a control, we used polymer **III** to determine the specificity of UEAI enrichment to the carbohydrate ligand. Only glycopolymer **II** was capable of capturing UEAI, indicating the selective binding to  $\text{Fuc}\alpha(1-2)\text{Gal}$  glycan (Fig 4.1). Moreover, incorporation of the photoactivatable crosslinking group in the polymer led to a twofold increase in UEAI capture. These results validate the polymer design and show that synthetic glycopolymers can be used for efficient affinity capture of lectins with weak carbohydrate-binding affinity.

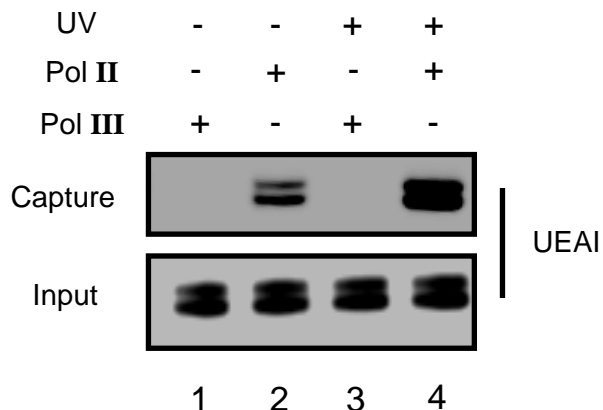


**Fig 4.1.** UEAI Capture with Glycopolymer probes. UEAI isolation is specific to Fuc $\alpha$ (1-2)Gal (lane 2 vs 1) and UV irradiation increases captured protein enrichment (lane 4 vs 2).

### 4.3. Identification of Fuc $\alpha$ (1-2)Gal Lectins in the Brain

We next investigated the use of polymer **II** to target Fuc $\alpha$ (1-2)Gal lectins from neurons. To ensure that the multivalent probes were non-toxic to neuronal cells, we examined the effects of polymer treatment on neuronal morphology. Hippocampal neurons were isolated from E18 rats, cultured for 24 h *in vitro* and treated with polymer **II** for 20 h. Following fixation and staining with tubulin antibody, neurons were imaged with fluorescence microscopy and analyzed for neurite outgrowth. Treatment of hippocampal neurons with the glycopolymer probes elicited no visible sign of cellular toxicity after 20 h incubation (Fig 4.2). Furthermore, neurons exposed to the Fuc $\alpha$ (1-2)Gal glycopolymer exhibited a 22% increase in neurite outgrowth relative to the untreated control (Fig 4.3), indicating that the multivalent probes were suitable for our biological study even at high concentration treatment (60  $\mu$ M).

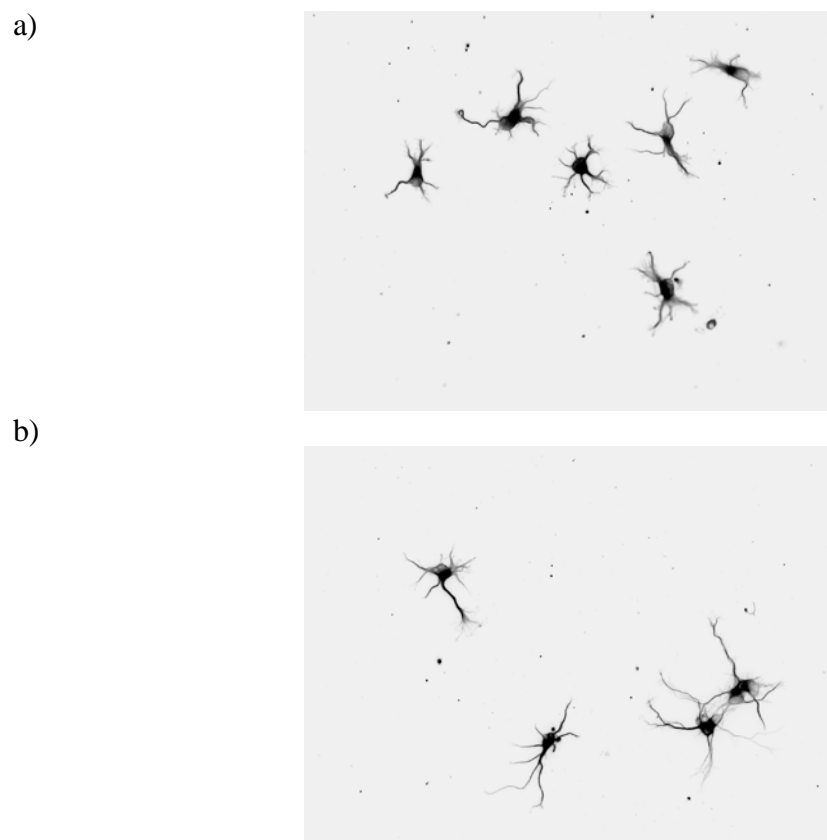


**Fig 4.2.** Synthetic Fuc $\alpha$ (1-2)Gal Multivalent Probes are non-toxic to hippocampal neurons a) untreated neurons b) treatment with 60  $\mu$ M Pol II.

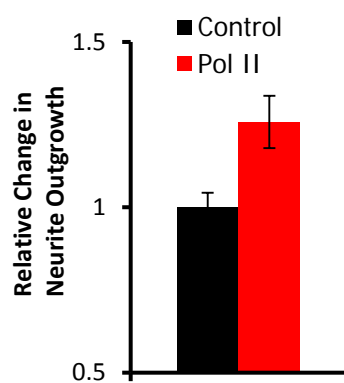


**Fig 4.3.** Fuc $\alpha$ (1-2)Gal stimulates neuronal growth. Neurite Outgrowth was quantified from 70-80 neurons in three separate experiments. p values are relative to the untreated control neurons ( $p < 0.01$ ).

Having tested these polymers on neuronal cells, we next investigated the use of polymer **II** to identify Fuc $\alpha$ (1-2)Gal lectins from the brain . While recent works by Cisar et al.<sup>20</sup> and Li et al.<sup>21</sup> highlight the elegant applications of SILAC-based quantitative proteomic technologies to identify weak-binding interactions, such approaches cannot be applied to post-mitotic neuronal cells. As a result, we performed a series of proteomic experiments on different brain lysate fractions to identify protein subsets that bind to Fuc $\alpha$ (1-2)Gal carbohydrates. Using these strategies, we sought to characterize lectin distribution across different cellular compartments and isolate lectin candidates from the membrane interface. By profiling lectin distribution across various lysate fractions, we sought to develop functional understanding of the Fuc $\alpha$ (1-2)Gal interactions in different cellular localization.

Subcellular fractions from rat brain were incubated with polymer **II** or **III** for 3 h at 37°C, exposed to 365 nm light, and the crosslinked proteins were isolated by streptavidin affinity chromatography. Captured proteins were eluted, resolved with SDS-PAGE, proteolytically digested and subjected to LC-MS/MS analysis (Fig 4.4). Lectin enrichment profiles were analyzed by silver staining to screen for distinct protein bands that were captured by Fuc $\alpha$ (1-2)Gal polymer **II** but were absent from control polymer **III**. We observed limited specificity towards Fuc $\alpha$ (1-2)Gal binding in whole lysates as well as the cytosolic, nuclear and cytoskeletal fractions (Fig 4.5). In contrast, we discovered enhanced protein capture specificity from both synapse-enriched (synaptosome) and neuronal membrane fractions, indicating that Fuc $\alpha$ (1-2)Gal interactions could be concentrated around the synaptic region (Fig 4.6).



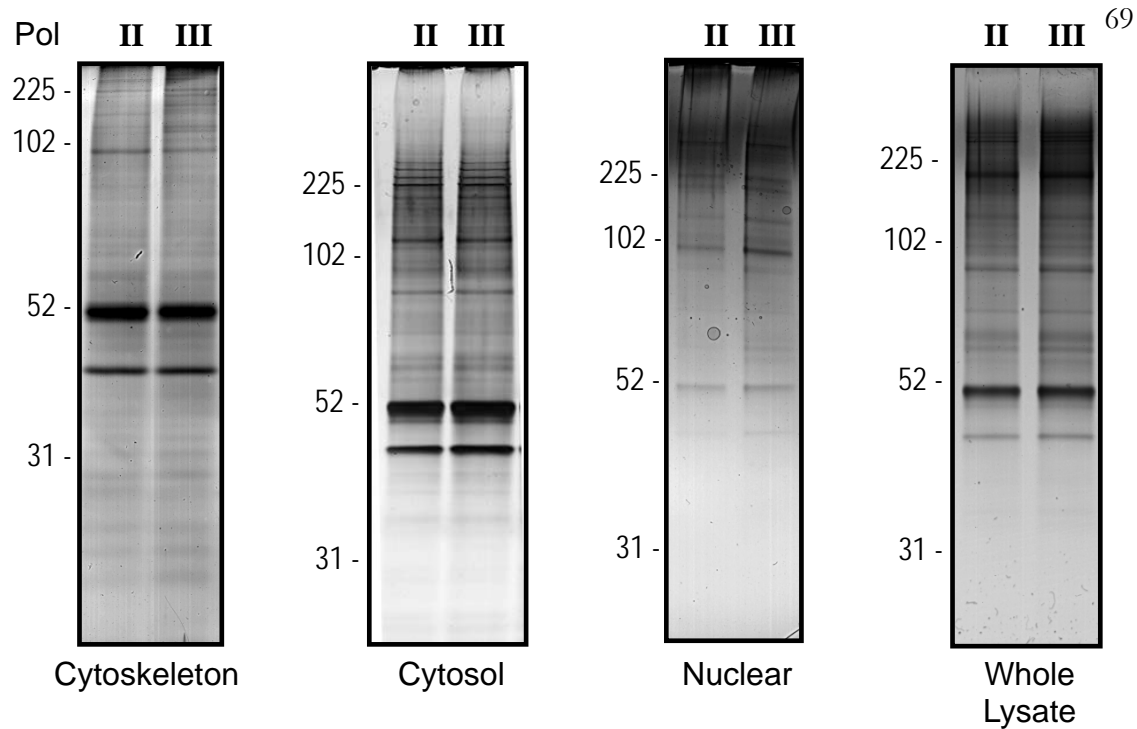


**Fig 4.5.** Representative gel profiling captured lectins from the whole lysates, cytoskeleton, cytosol and membrane fractions.

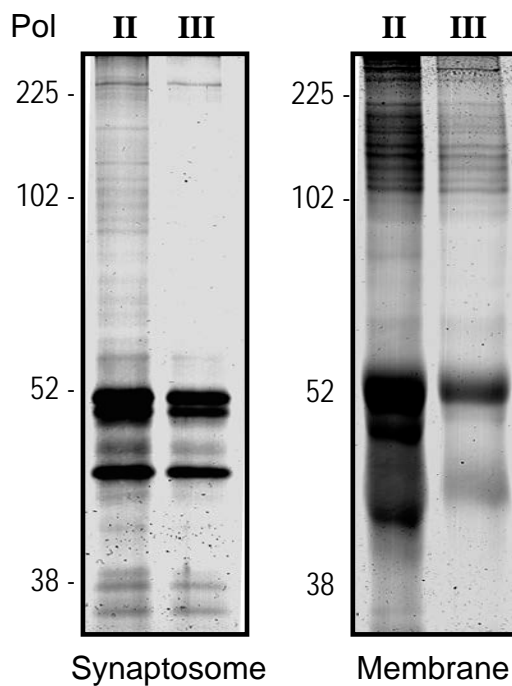


**Fig 4.6.** Representative gel profiling captured lectins from the synaptosome and membrane fractions (n=3 each).

In total, we identified 44 candidate Fuc $\alpha$ (1-2)Gal lectins and/or receptors from six total experiments (three each using synaptosome or neural membrane fractions) with highly stringent identification criteria. Lectin candidates were selected when: 1) the proteins contained at least 3 unique peptides and are absent in the negative control, 2) the proteins are identified at least twice out of the three sample runs and 3) the total number of unique peptides for each protein is  $\geq 6$ . Bioinformatics analyses were performed on candidate lectins using NCBI-Pubmed and EMBL-EBI database search, and each protein was inspected in 3 categories: spectral abundance, protein structures and molecular function. Interestingly, the candidate lectins fall into a broad range of functional classes, including those involved in cellular signaling, protein trafficking, protein scaffolding and cellular metabolism (Fig 4.7). In addition, sequence coverage and unique peptide assignments that were specific to the protein candidate were listed in Table 4.1.

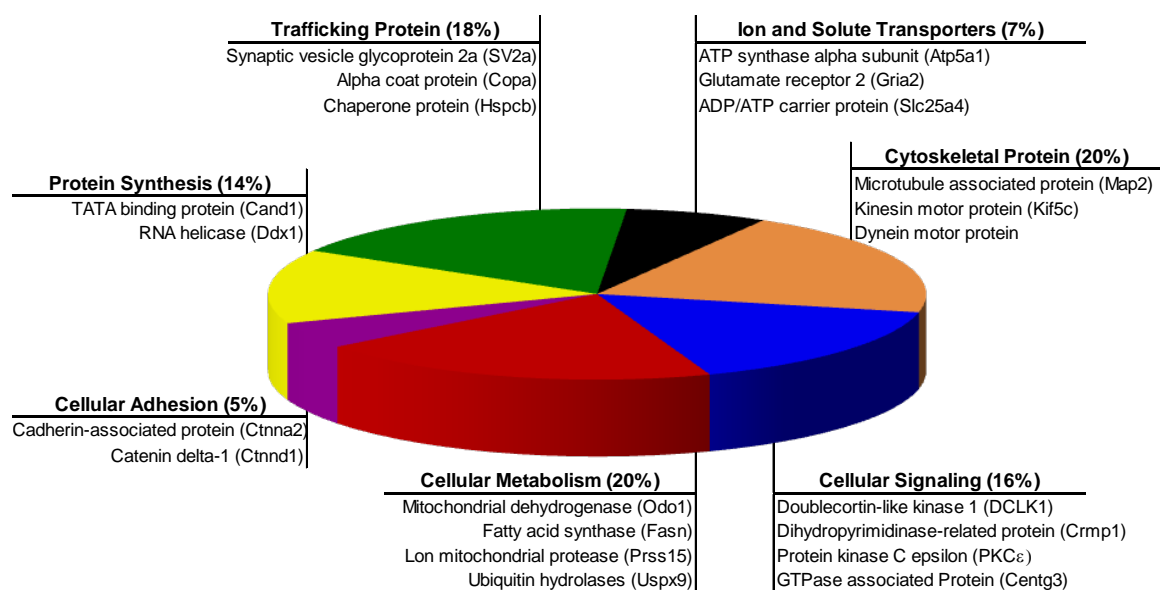


**Fig 4.7.** Functional classifications of Fuc $\alpha$ (1-2)Gal lectins in the brain.

**Table 4.1.** Fuc $\alpha$ (1-2)Gal lectins from rat synaptosome and membrane fractions.<sup>a</sup>

Protein	Ascension Number	Unique Peptide <sup>b</sup>	Coverage (%) <sup>b</sup>	MW (Da)	Function
<i>Cellular Adhesion</i>					
Ctnna2	IPI00364916.2	8	13.6	100000	Cellular differentiation
Ctnnd1	IPI00359491.3	6	10	105000	Cellular recognition
<i>Cellular Signalling</i>					
Dclk1 (Ania 4)	IPI00778626.1	13	23.8	84000	Neuronal migration
Centg3	IPI00358128.3	6	9	102000	Signal transduction
Crrmp1 (DRP-1; Ulip3; Dpysl1)	IPI00561065.2	9	16	74000	Axonal guidance
Crimp4 (Dpysl3; TUC-4b)	IPI00203250.1	7	13.6	74000	Neurite outgrowth
G $\alpha$ o	IPI00231505.5	7	22.3	40000	Signal transduction
Gnaq	IPI00230868.4	6	20.1	42000	Signal transduction
Pkc $\epsilon$	IPI00551781.4	10	17.8	83000	Phosphorylation
<i>Cytoskeletal Associated Protein</i>					
Ckap5	IPI00764313.1	9	5.9	197000	Microtubule elongation
Cyln2 (Clip2)	IPI00195929.1	10	12.3	111000	Microtubule associated transport
Dync1h1 (dyhc1, map1c)	IPI00327630.1	54	13.5	532000	Dynein motor protein
Kif5b	IPI00364904.2	10	15.1	110000	Kinesin motor protein
Kif5c	IPI00193402.4	16	21.2	109000	Kinesin motor protein
Macf1 (LOC362587)	IPI00359003.4	6	1	831000	Actin regulation
Map4 (LOC367171 )	IPI00393975.2	8	10.4	110000	Microtubule assembly
Mtap2 (Map2)	IPI00206171.1	10	7.1	202000	Cytoskeletal organization
Tbcd (LOC363309)	IPI00765967.1	6	5.6	134000	Microtubule regulation
<i>Cellular Metabolism</i>					
Aco2	IPI00421539.3	8	13.1	85000	Mitochondrial metabolism
Cad	IPI00365582.3	6	3.1	243000	Enzymatic biosynthesis
Fasn	IPI00200661.1	21	11.1	273000	Lipid biosynthesis
Hk1	IPI00202543.1	10	13	102000	Mitochondrial metabolism
Immt	IPI00364895.4	7	12.4	82000	Mitochondrial homeostasis
Odo1 (LOC360975)	IPI00215093.1	13	17.9	116000	Mitochondrial metabolism
Phgdh	IPI00475835.3	7	16.9	56000	Enzymatic biosynthesis
Prss15	IPI00205076.1	10	12.9	106000	Mitochondrial proteases
Uspx9	IPI00204923.4	11	5.4	291000	Ubiquitin Hydrolases
<i>Protein Synthesis</i>					
Aars	IPI00363563.3	8	11.5	107000	Translation
Cand1	IPI00205466.1	8	7.1	136000	Transcription
Ddx1	IPI00555314.1	8	12.8	82000	Transcription
Lrpprc Leucine rich protein 157	IPI00360075.2	12	10.7	157000	Transcription
Nars	IPI00565217.3	7	15.2	64000	Translation
Tufm	IPI00371236.3	7	19.7	50000	Translation
<i>Transporters</i>					
Atp5a1	IPI00396910.1	10	24.6	60000	ADP/ATP biosynthesis
Gria2	IPI00780113.1	6	7.5	103000	Glutamate Receptor
Slc25a4	IPI00231927.11	8	29.9	33000	ADP/ATP Translocase
<i>Trafficking Protein</i>					
Dctn1	IPI00196703.1	8	7.2	142000	Retrograde vesicle transport
Dmx-like 2 (LOC315676)	IPI00369671.3	7	3.1	344000	Synaptic vesicle scaffolding
Hspcb	IPI00471584.7	13	18.9	83000	Chaperone for protein folding
Hspd1 (CH60)	IPI00339148.2	12	33	61000	Chaperone for mitochondrial protein
Sv2a	IPI00208115.4	6	10.8	83000	Neurotransmitter release
Syn2	IPI00210036.1	6	17.1	63000	Neurotransmitter release
Vac14	IPI00230981.1	7	11.6	88000	Endosome regulation
Vps35 (Mem3)	IPI00363493.2	6	9.6	92000	Retrograde protein transport

- a) Proteins from Sprague Dawley Rat were captured using the Biotinylated Glycopolymer probe. Proteins are tabulated by function, accession id, number of unique sequence peptides and unique peptide coverage
- b) The number of full tryptic unique peptides and their coverage were identified from a reversed database searching strategy. See Materials and Methods for procedures and analysis criteria.

In summary, we reported the first successful capture of Fuc $\alpha$ (1-2)Gal binding proteins using synthetic multivalent probes. We identified novel lectin candidates from the brain and discovered that Fuc $\alpha$ (1-2)Gal binding proteins were highly enriched in the membrane and synaptic region. The functional diversity represented by this set of proteins implicates novel and important roles for Fuc $\alpha$ (1-2)Gal glycans. Projecting forward, we seek to validate binding interactions between Fuc $\alpha$ (1-2)Gal carbohydrates and these lectin candidates. Importantly, we are interested in understanding functional significance of these binding events. We hope to perform specific functional assays to confirm and elucidate Fuc $\alpha$ (1-2)Gal role in mediating neuronal communication. Efforts towards validating lectin interaction with Fuc $\alpha$ (1-2)Gal will be discussed in the next chapter.

#### 4.4. Experimental Methods

**Animals, Tissue Isolation and Synaptosome Preparation.** Sprague Dawley rats, C57BL/6 wild type, FUT1<sup>-/-</sup> and FUT2<sup>-/-</sup> mice were maintained in accordance with proper Institute of Animal Care and Use Committee (IACUC) procedures. Adult mice (3-4 months of age) and postnatal day 3 (P3) pups were anesthetized with CO<sub>2</sub> and dissected to remove the cortex and hippocampus. Synaptosomes (P2') were prepared from P3 rat pups by using a sucrose density gradient as previously described<sup>22</sup> and were dissolved in lectin binding buffer [100 mM Tris (pH 7.5), 150 mM NaCl, 1 mM CaCl<sub>2</sub>, 1 mM MgCl<sub>2</sub>, 0.5% NP-40, and 0.2% sodium deoxycholate supplemented with EDTA-free Complete protease inhibitors (Roche)]. To prepare neuronal lysate fractions, cortices from P3 rat pups were extracted and fractionated using the Qproteome Cell Compartment Kit (Qiagen) to give a final protein concentration of 5 mg/ml.

**Immunocytochemistry of Hippocampal Neuronal Cultures.** After 48 h in culture, the hippocampal neurons on coverslips were rinsed one time with PBS, fixed in 4% paraformaldehyde for 20 min at rt, washed thrice with PBS, permeabilized in 0.3% Triton X-100 for 5 min at rt, and washed twice with PBST (PBS + 0.05% Tween 20). Non-specific binding was blocked by incubating with 5% goat serum for 1 h at 4°C and then rinsing twice with PBST. Cells were then incubated with anti-tubulin antibodies (rabbit polyclonal, 1:500; Sigma) in 5% goat serum overnight at 4 °C. Excess antibody was rinsed away 5 times with PBST. Secondary antibody, anti-rabbit IgG AlexaFluor 488 (1:500; Molecular Probes), was added for 1 h at 37 °C in 5% goat serum. Excess secondary antibody was washed off 5 times with PBST. The coverslips were mounted onto glass

slides using Vectashield mounting medium (Vector Labs) and sealed with clear nail polish. Cells were imaged on a Nikon Eclipse TE2000-S inverted microscope. The images were captured with MetaMorph 6.1 software using a 40x plan fluor oil objective.

**Morphometric Analysis.** All experiments were performed in triplicate and 70-80 randomly selected cells were analyzed for each experiment. To ensure accurate measurements, only neurites longer than  $\sim 10 \mu\text{m}$  and not in contact with other cells were quantified with NIH software ImageJ using the NeuronJ plugin.<sup>23</sup> Neurite outgrowth was expressed as mean neurite lengths and statistical analysis was performed using the student's unpaired t-test.

**UEA I Lectin Enrichment and Photocrosslinking Capture.** Fluorescein-conjugated UEA1 (100  $\mu\text{g}$ , Vector Laboratories) was treated with 50 $\mu\text{M}$  polymer **II** or **III** in lectin binding buffer and was incubated with gentle end-over-end mixing at 37°C for 3 h in dark. The samples were irradiated with UV light using Blak-Ray B100 AP (Upland) for 15 mins at 4°C and allowed to mix further at rt for 45 mins in dark. The samples were diluted with binding buffer to a final concentration of 1 mg/ml and were incubated with pre-treated (blocked with 0.1% fish gelatin) streptavidin agarose resin (Pierce) at 4°C for 2h. The resin was washed twice with 10 column volumes each of low salt buffer (0.1 M Na<sub>2</sub>HPO<sub>4</sub> pH 7.5, 0.15 M NaCl, 1% Triton X-100, 0.5% sodium deoxycholate, 0.1% SDS), twice with 10 column volumes each of high salt buffer (0.1 M Na<sub>2</sub>HPO<sub>4</sub> pH 7.5, 0.5 M NaCl, 0.2% Triton X-100), and once with 10 column volumes of 50 mM Tris•HCl pH 7.4. Captured protein was eluted in boiling sample buffer (50 mM Tris pH 6.8, 2.5% SDS, 2mM DTT, 10% Glycerol and 2 mM Biotin) for 5 min. The sample was resolved on a

NuPAGE 4-12% Bis-Tris gel (Invitrogen), transferred to polyvinylidene difluoride (PVDF) membrane (Millipore) and visualized using a Typhoon Scanner (GE Healthcare).

**Fuco(1-2)Gal Lectin Enrichment and Photocrosslinking Capture.** Brain lysates from synaptosome and membrane fractions (1.2 mg) obtained as described above, were pre-treated with 35 $\mu$ M polymer **III** in lectin binding buffer and were precleared with high capacity streptavidin agarose resin (Pierce) with gentle end-over-end mixing for 2 h in dark. After centrifugation, the supernatant was treated with 75 $\mu$ M polymer **II** or **III** in lectin binding buffer and was incubated with gentle end-over-end mixing at 37°C for 3 h in dark. The samples were irradiated with UV light using Blak-Ray B100 AP for 15 mins at 4°C and allowed to mix further at rt for 45 mins in dark. After diluting with binding buffer to a final concentration of 1 mg/ml, samples were incubated with pre-treated (blocked with 0.1% fish gelatin) high capacity streptavidin agarose resin at 4°C for 4 h. The resin was washed twice with 10 column volumes each of low salt buffer, twice with 10 column volumes each of high salt buffer, once with 20 column volumes of 4 M urea + 1% SDS and once with 10 column volumes of 50 mM Tris•HCl pH 7.4. Captured protein was eluted in boiling sample buffer for 5 min and subsequently resolved by 10% SDS-PAGE for LC-MS analysis.

**Silver Staining, In-Gel Digestion, and LC-MS Analysis.** All silver staining reagents were prepared fresh before they were used. The staining and destaining, in-gel tryptic digests, and peptide extractions were performed as described previously.<sup>24</sup> NanoLC-MS of in-gel tryptic digests was performed on a Thermo Fisher LTQ XL linear ion trap mass spectrometer using a modified vented column setup and data-dependent scanning.<sup>25</sup>

Samples were loaded onto a 360  $\mu\text{m}$  x 100  $\mu\text{m}$  precolumn (2 cm, 5  $\mu\text{m}$  Monitor C18) and desalted before the precolumn was placed in-line with the analytical column. Peptides were then eluted with a linear gradient from 0 to 40% B over 30min (A, 0.1M aqueous HOAc; B, 0.1MHOAc in CH<sub>3</sub>CN), with a flow rate of approximately 250 nL/min, and using a 360  $\mu\text{m}$  x 75  $\mu\text{m}$  self-packed column with an integrated electrospray emitter (10 cm, 5  $\mu\text{m}$  Monitor C18). For data-dependent experiments, the mass spectrometer was programmed to record a full-scan ESI mass spectrum (m/z 400-2000), followed by five data-dependent MS/MS scans in the ion trap (relative collision energy of 35%, 3.5 Da isolation window). Dynamic exclusion parameters were set as follows: repeat count=1, repeat duration=15 s, and exclusion duration=30 s.

MS/MS spectra were searched against a rat subset of the European Bioinformatics Institute-International Protein Index (EBI-IPI) database (downloaded August 1, 2007), with an appended reversed database using Sequest 3.0. A fixed modification of Cys (+57), a variable modification of Met (+16), and trypsin cleavage were specified. Mass tolerances of 3.0 Da for the parent and 0.8 Da for the fragment ions were employed. Search results were compiled and filtered in Scaffold 2.0 (Proteome Software, Inc., Portland, OR). Peptide identifications were accepted if they could be established at  $\geq 95.0\%$  probability as specified by the Peptide Prophet algorithm.<sup>26</sup> Protein identifications were accepted if they could be established at  $\geq 99.0\%$  probability and contained at least three unique identified peptides. Protein probabilities were assigned by the Protein Prophet algorithm.<sup>27</sup> For a protein to be listed in Table 4.1, the protein had to be identified as described above in at least two of the three synaptosome and/or neural membrane fractions.

## REFERENCES

1. Cravatt, B. F.; Wright, A. T.; Kozarich, J. W. *Annu. Rev. Biochem.* **2008**, *77*, 383
2. Fountoulakis, M. Two-dimensional electrophoresis. *In : Encyclopedia of separation science, II/electrophoresis.* **2000**, London: Academic Press. 1356
3. Griffin, T. J.; Aebersold, R. *J. Biol. Chem.* **2001**, *276*, 45497
4. Aebersold, R.; Mann, M. *Nature.* **2003**, *422*, 198
5. Gingras, A-C.; Gstaiger, M.; Raught, B.; Aebersold, R. *Nat. Rev. Mol. Cell Biol.* **2007**, *8*, 645
6. Ahn, N. G.; Shabb, J. B.; Old, W. M.; Resing, K. A. *ACS. Chem. Biol.* **2007**, *2*, 39
7. Fountoulakis, M. *Mass. Spectrom. Rev.* **2004**, *23*, 231
8. Choudhary, J.; Grant, S. G. N. *Nat. Neurosci.* **2004**, *7*, 440
9. Bayes, A.; Grant, S. G. N. *Nat. Rev. Neurosci.* **2009**, *10*, 635
10. Cravatt, B. F.; Simon, G. M.; Yates, J. R. III. *Nature.* **2007**, *450*, 991
11. Witze, E. S.; Old, W. M.; Resing, K. A.; Ahn, N. G. *Nat. Methods.* **2007**, *4*, 798
12. Ong, S. E.; Mann, M. *Nat. Chem. Biol.* **2005**, *1*, 252
13. Pilobello, K. T.; Mahal, L. K. *Curr. Opin. Chem. Biol.* **2007**, *11*, 300
14. Raman, R.; Raguram, S.; Venkataraman, G.; Paulson, J. ; Sasisekharan, R. *Nat. Methods.* **2005**, *2*, 817
15. Hindsgaul, O.; Khare, D. P.; Bach, M.; Lemieux, R. U. *Can. J. Chem.* **1985**, *63*, 2653.
16. Cazal, P.; Lalaurie, M. *Acta. Haematol.* **1952**, *8*, 73
17. Lemieux, R. U.; Baker, D. A.; Weinstein, W. M.; Switzer, C. M. *Biochemistry.* **1981**, *20*, 199
18. Audette, G. F.; Olson, D. J.; Ross, A. R.; Quail, J. W.; Delbaere, L. T. *Can. J. Chem.* **2002**, *80*, 1010
19. Audette, G. F.; Delbaere, L. T.; Xiang, J. *Curr. Protein Pept. Sci.* **2003**, *4*, 1
20. Cisar, J. S.; Cravatt, B. F. *J. Am. Chem. Soc.* **2012**, *134*, 10385
21. Li, X.; Foley, E. A.; Molloy, K. R.; Li, Y.; Chait, B. T.; Kapoor, T. M. *J. Am. Chem. Soc.* **2012**, *134*, 1982
22. Huttner, W. B.; Schiebler, W.; Greengard, P.; De Camilli, P. *J. Cell Biol.* **1983**, *96*, 1374
23. Meijering, E.; Jacob, M.; Sarria, J. C. F.; Steiner, P.; Hirling, H.; Unser, M. *Cytometry. Part A.* **2004**, *58*, 167
24. Clark, P.M.; Dweck, J.F.; Mason, D.E.; Hart, C.R.; Buck, S.B.; Peters, E.C.; Agnew, B.J.; Hsieh-Wilson, L.C. *J. Am. Chem. Soc.* **2008**, *130*, 11576
25. Murrey, H.E.; Ficarro, S.B.; Krishnamurthy, C.; Domino, S.E.; Peters, E.C.; Hsieh-Wilson, L.C. *Biochemistry.* **2009**, *48*, 7261
26. Keller, A.; Nesvizhskii, A.I.; Kolker, E.; Aebersold, R. *Anal. Chem.* **2002**, *75*, 5383

27. Nesvizhskii, A.I.; Keller, A.; Kolker, E.; Aebersold, R. *Anal. Chem.* 2003, 75, 4646

VALIDATION OF FUC $\alpha$ (1-2)GAL LECTIN CANDIDATES**5.1. Biological Impact of MS-Based Proteomics**

Glycomics is an integrated approach to study structure–function relationships of complex carbohydrates. Glycomic studies have been challenged by the sheer diversity and functional information encoded in the glycan structures. These challenges arise from two fundamental aspects of the glycan structure–function relationships. First, the biosynthesis of glycans is a non–template-driven process involving the coordinated expression of multiple glycosyltransferases. Second, understanding the biochemical basis of glycan–protein interactions in the context of a biological pathway is complicated by the multivalency and the graded affinity towards different glycan structures.<sup>1</sup> Therefore, the study of glycans requires a systems-level approach involving multiple components as well as integration of information at molecular, cellular, tissue and higher levels.

Global analyses of the Fuc $\alpha$ (1-2)Gal lectin proteome identified diverse roles for our candidate lectins. However, the discovery of ‘true’ lectins is confounded by the fact that although receptor-glycan interactions are governed by carbohydrate recognition specificity, other factors, such as the protein domain contribution of the glycoconjugates and subcellular localization of the lectin and its ligand, must also be considered. As such, only specific lectin-glycoprotein pair interactions are functional *in situ*. As Fuc $\alpha$ (1-2)Gal carbohydrates have been implicated in synaptic regulation and neuronal plasticity,<sup>2,3</sup> we focused our attention on lectins associated with similar functions. Candidate lectins were

additionally prioritized based on their reported expression and functional profiles. As a result, we sought to pursue the validation of four candidate lectins; double cortin-like kinase 1 (DCLK1), protein kinase C epsilon subunit (PKC $\epsilon$ ), synaptic vesicle glycoprotein 2a (SV2a) and guanine nucleotide-binding protein G(o) alpha subunit (G $\alpha$ O).

DCLK1 is a brain-associated, membrane-bound protein that is closely related to doublecortin (DCX), a protein that is critical for neuronal migration and adult neurogenesis.<sup>4,5</sup> In addition to the N-terminal DCX-domain-like that binds to microtubules, DCLK1 also has a C-terminal serine/threonine kinase domain (CPG 16) that has been shown to be upregulated during LTP.<sup>6</sup> PKC $\epsilon$  has been shown to regulate neurotransmission through GABA<sub>A</sub> receptor trafficking and modulate Na<sup>+</sup> channels in hippocampal neurons.<sup>7,8</sup> Furthermore, PKC $\epsilon$  has also been reported to mediate neurite outgrowth through its actin-binding activity.<sup>9</sup> G $\alpha$ O is a member of the heterotrimeric G protein family that has been implicated as modulator of calcium channels and reported to promote neurite outgrowth in neuronal cells.<sup>10,11</sup> SV2a is a synaptic vesicle transmembrane protein that mediates neurotransmitter release by enhancing the Ca<sup>2+</sup> responsiveness of each synaptic vesicle.<sup>12</sup> Indeed, SV2a has been implicated in the regulation of presynaptic Ca<sup>2+</sup> through its interaction with synaptotagmin 1 (syt1).<sup>13</sup> With functions that are complementary to the role of Fuc $\alpha$ (1-2)Gal glycoproteins, these lectin candidates would be ideal for our initial target validation.

## 5.2. Validating Lectin Binding towards $\text{Fuca}(1-2)\text{Gal}$ Carbohydrates

We first sought to validate the binding interactions of these lectins with  $\text{Fuca}(1-2)\text{Gal}$  glycans *in vitro*. Two candidate lectins (SV2a and PKC $\epsilon$ ) were expressed and purified and their binding specificities for  $\text{Fuca}(1-2)\text{Gal}$  were assessed using carbohydrate microarrays from the Consortium of Functional Glycomics. Lectin candidates were incubated with printed microarray slides containing 511 different mammalian glycans, and the bound lectins were detected and visualized with fluorescently-labeled antibodies. Both SV2a and PKC $\epsilon$  bound to the glycan arrays with weak affinity and exhibited binding specificities that were not limited to  $\text{Fuca}(1-2)\text{Gal}$  carbohydrates (Fig 5.1). The observed low affinities were consistent with monovalent interaction and were mediated presumably by imposing a one-to-one association between the lectin and its immobilized glycan substrate. Furthermore, lectins typically suffer from limited binding specificity as they exhibit cross-reactivity towards multiple glycan epitopes.<sup>14,15</sup> Therefore, we sought to characterize these weak interactions by measuring the affinity enhancement contributed by the  $\text{Fuca}(1-2)\text{Gal}$  epitopes.

Further analysis of these binding data revealed that the top 10% of all glycan structures recognized by PKC $\epsilon$  and SV2a were decorated with terminal  $\text{Fuca}(1-2)\text{Gal}$  or NeuAc epitopes. These fucose and/or sialic acid residues are commonly added to the non-reducing end of an oligosaccharide chain and are often important for lectin recognition. To establish their roles in lectin binding, we assessed several top binders containing  $\text{Fuca}(1-2)\text{Gal}$ -terminated saccharides and measured their relative change in binding affinities when

the terminal  $\text{Fuc}\alpha(1-2)\text{Gal}$  epitopes were removed. Significant affinity enhancement towards  $\text{Fuc}\alpha(1-2)\text{Gal}$  sugars was reported for PKC $\epsilon$  and SV2a (up to 24- and 45-fold, respectively), while a similar comparison for the terminal NeuAc showed more modest results with up to fourfold and sixfold increase for PKC $\epsilon$  and SV2a, respectively (Fig 5.2).

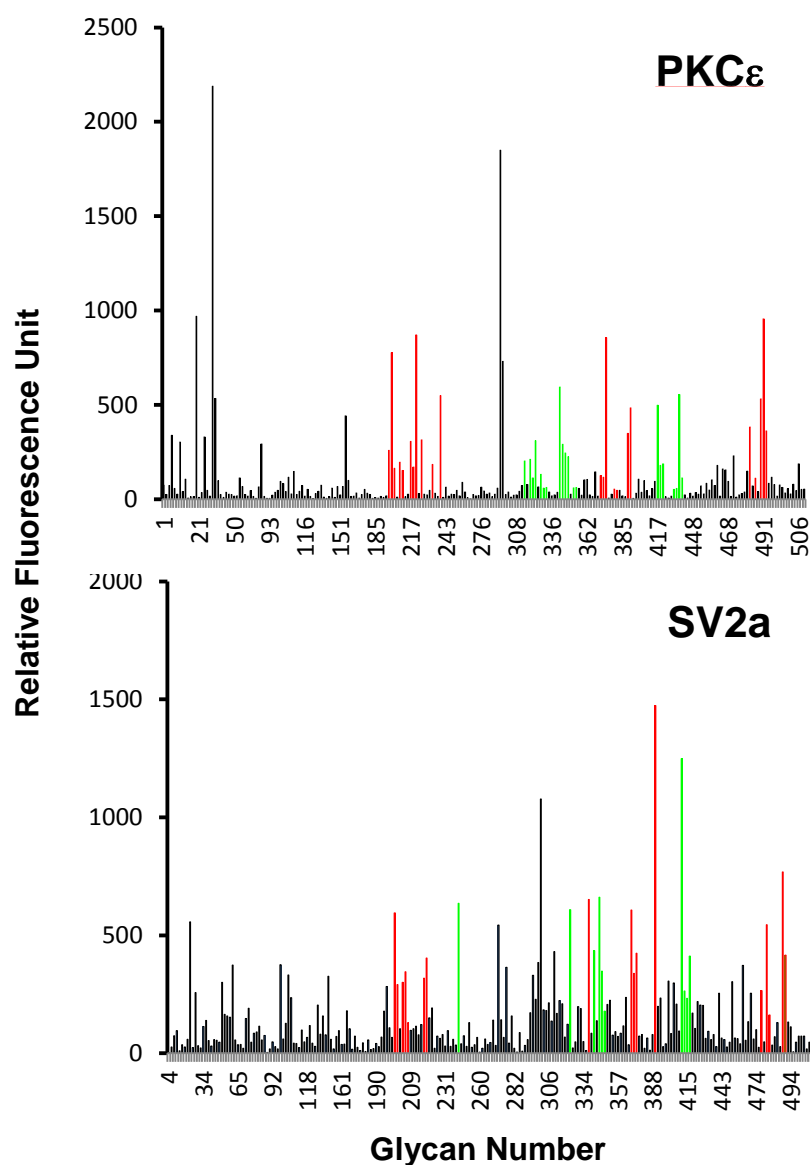


**Fig 5.1.** Binding profiles of PKC $\epsilon$  and SV2a. Lectin candidates were incubated with mammalian glycoarrays in replicates of 6. Top glycan chains recognized by the lectin candidates contain terminal fucose (red) or terminal sialic acid (green) epitopes. Other top binders are made up of charged glycan epitopes

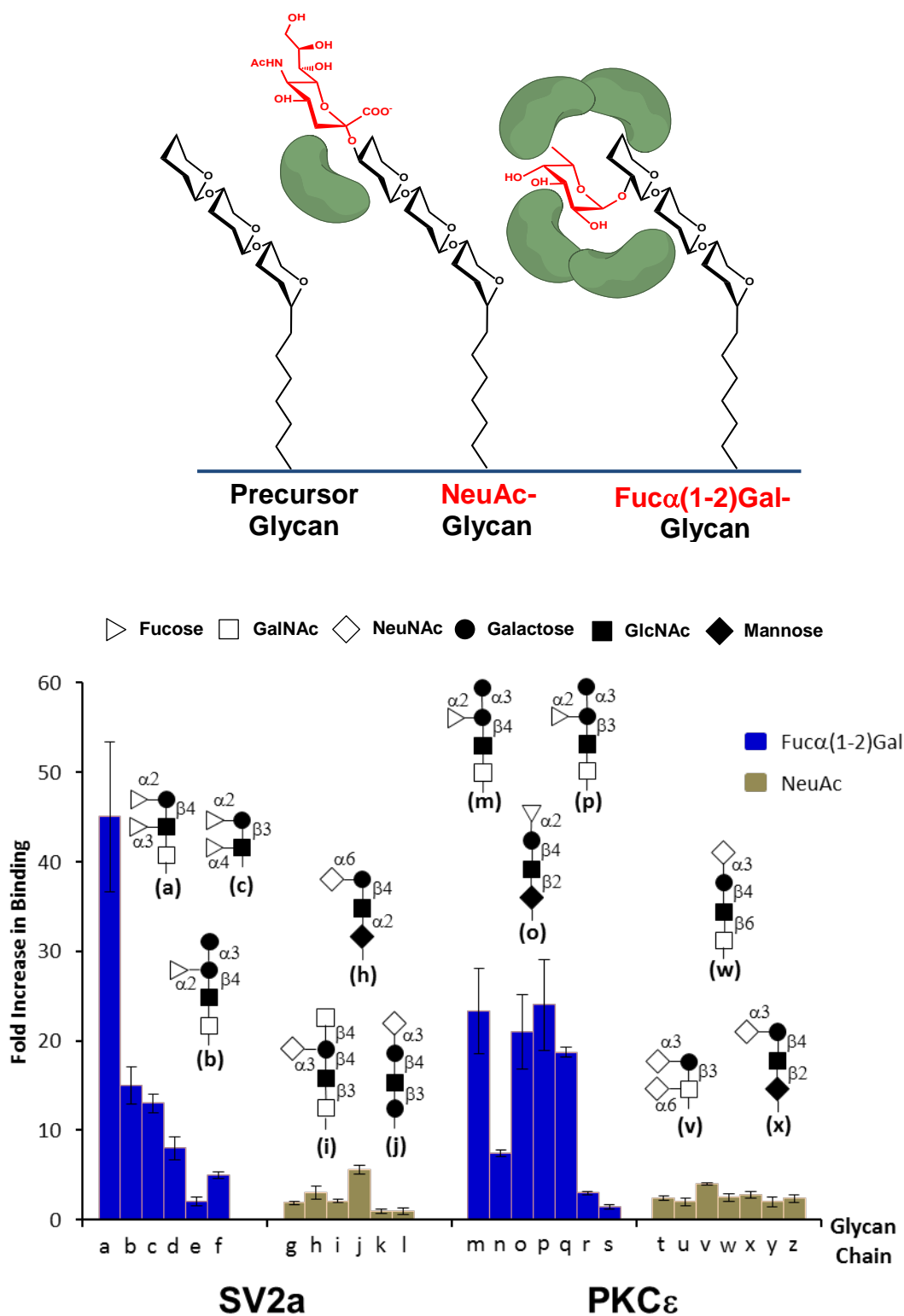


**Fig 5.2.** Binding affinity is measured on Fuca(1-2)Gal-terminated glycan and its precursor glycan chain. Fuca(1-2)Gal carbohydrates promote significant affinity enhancement of up to 45-fold for SV2a (glycan **a**) and 25-fold for PKCε (glycan **p**) in vitro.

Next, we sought to verify the multivalent interactions between Fuc $\alpha$ (1-2)Gal carbohydrates and the four candidate lectins (DCLK1, PKC $\epsilon$ , SV2a and G $\alpha$ O). The putative lectins were expressed and purified, and their binding affinity for Fuc $\alpha$ (1-2)Gal was assessed using enzyme-linked lectin assays (ELLA). Briefly, biotinylated glycopolymers containing Fuc $\alpha$ (1-2)Gal ( $10^{-3}$ – $10^2$   $\mu$ M) were incubated with the lectins immobilized on microtiter plates, and bound polymer was detected using streptavidin conjugated to horseradish peroxidase (-HRP). For comparison, we also examined the binding of biotinylated glycopolymers bearing Gal $\alpha$ (1-2)Gal sugar epitopes to the candidate lectins. We found that all four lectins interacted with the Fuc $\alpha$ (1-2)Gal glycopolymer in a dose-dependent manner, albeit with different affinities (Fig 5.3;  $K_{d,app} = \sim 1$ – $3$   $\mu$ M). Furthermore, three of the four lectins (DCLK1, PKC $\epsilon$  and SV2a) showed significantly greater binding to the Fuc $\alpha$ (1-2)Gal glycopolymers compared to the Gal $\alpha$ (1-2)Gal glycopolymers, suggesting the importance of the terminal fucose residue for lectin recognition. In contrast, G $\alpha$ O exhibited greater binding affinity towards Gal $\alpha$ (1-2)Gal glycopolymers, suggesting it may not be a true lectin with Fuc $\alpha$ (1-2)Gal specificity (Fig 5.3). Together, our results show that all four candidate lectins bind to Fuc $\alpha$ (1-2)Gal sugars *in vitro* and highlight the importance of multivalency for enhancing low-affinity glycan-receptor interaction.

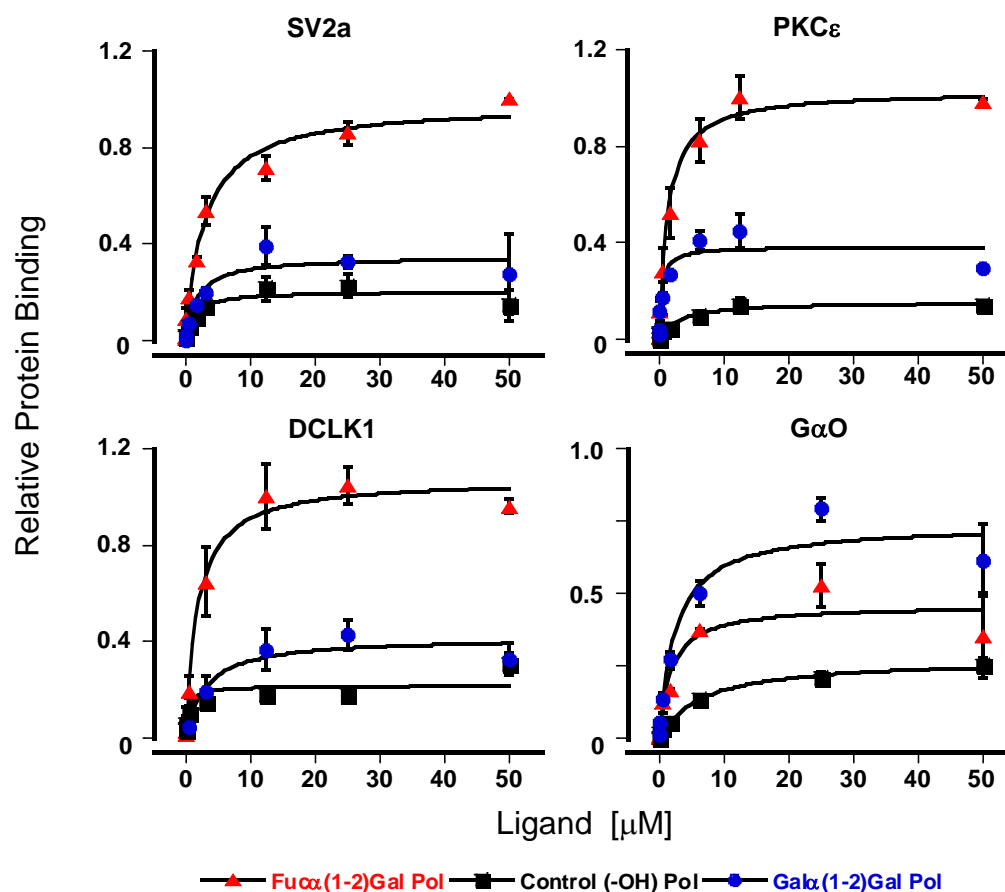


**Fig 5.3.** Binding profiles of lectin candidates using ELLA (n=3). DCLK1, PKC $\epsilon$  and SV2a bind Fu $\alpha$ (1-2)Gal carbohydrates with moderate affinities ( $K_{d,app}$  = 1.77  $\mu$ M, 1.26  $\mu$ M and 2.86  $\mu$ M, respectively).

### 5.3. Structural Analysis of Lectin Candidate SV2a

Consequently, we were interested in understanding the functional implications of such binding events. Specifically, we focused on SV2a to elucidate the physiological relevance of this glycan-lectin interaction in the brain. SV2 is a conserved integral membrane protein that is present on all vertebrate synaptic vesicles.<sup>16</sup> All SV2 proteins contain 12 putative transmembrane regions (TMRs) with N- and C-terminal cytoplasmic sequences and a large intravesicular loop that is N-glycosylated (Fig 5.4).<sup>17</sup> In mammals,

there are three SV2 isoforms, designated SV2A, SV2B, and SV2C.<sup>18</sup> SV2a is the most widely distributed isoform, being nearly ubiquitous in the central nervous system, as well as being present in endocrine cells.<sup>16,19</sup> Interestingly, SV2A and SV2A/B knock-out (KO) mice exhibit a severe seizure phenotype whereas the SV2B KOs do not.<sup>20,21</sup> Furthermore, SV2a was shown to be the target of the anti-epileptic drug levetiracetam, implicating its role in neural transmission.<sup>22</sup> Studies of the SV2 KOs indicate that SV2 has a crucial role in the regulation of vesicle function, although not in vesicle biogenesis or synaptic morphology.<sup>22</sup>

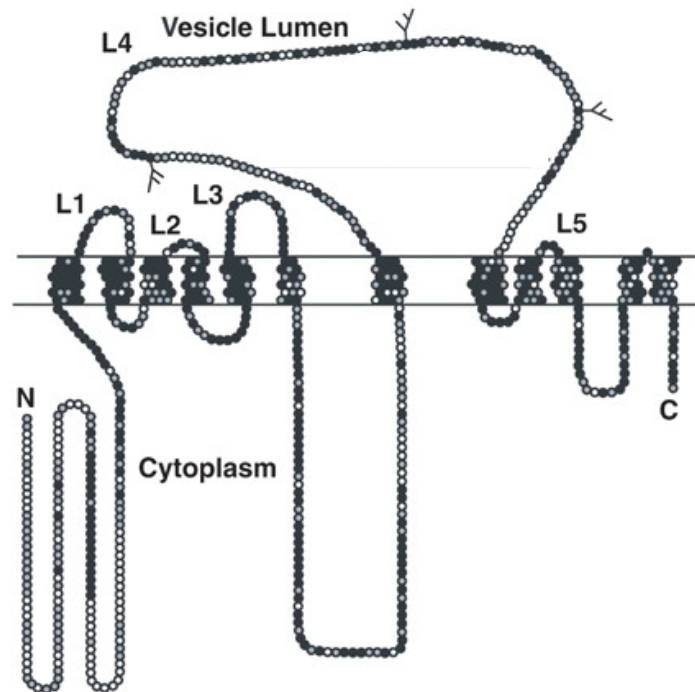


**Fig 5.4.** Model of SV2 topology. Black circles indicate conserved residues in all SV2 isoforms, gray circles are residues conserved in two SV2 isoforms, and open circles represent non-conserved residues. Adapted with permission from (17).

Like UEAI, SV2a exhibited a  $\text{Ca}^{2+}$ -dependent binding towards  $\text{Fuc}\alpha(1-2)\text{Gal}$  sugars. This characteristic is mostly observed in the C-type mammalian lectin superfamily. As a result, we assessed the existence of a lectin-like domain in SV2a by performing an extensive structural analysis against other known C-type animal lectins. Specifically, we sought to identify SV2a sequence homology with three well-studied C-type lectins: dendritic cell-specific ICAM-3 grabbing nonintegrin (DC-SIGN), asialoglycoprotein receptor 1 (ASGR1) and rattle snake lectin (RSL). DC-SIGN is a C-type lectin receptor that binds to the terminal mannose and fucose-containing oligosaccharide of a virus envelope glycoprotein.<sup>23-25</sup> ASGR1 is a hepatic endocytic receptor protein that plays a critical role in scavenging desialylated glycoproteins with exposed terminal galactose (Gal) or *N*-acetylgalactosamine (GalNAc) residues for lysosomal degradation.<sup>26</sup> RSL is a readily-prepared decameric C-type lectin that binds to terminal Gal and GalNAc sugars.<sup>27</sup> Given their specific glycan preferences, we performed multiple sequence alignment on SV2a and observed regions of significant sequence homologies (50–60%) around the putative L3–L4 intravesicular loop domain. Furthermore, sequence alignment analysis of SV2a with DC-SIGN, ASGR1 and RSL identified many conserved residues in the C-type lectin domain (CTLD) (Fig 5.5). In particular, high conservation of the consensus cysteine residues and WIGL motif were consistent with formation of the characteristic disulfide bridges in CTLD, implicating the existence of a lectin-like domain in SV2a.<sup>28,29</sup>

```

0 ----- RSL
8 FQHLDN---- --GPPPAPR- CSG--F--RL -FLLSLGLSI LLLVVVCVIT ASGR1
12 LRPLDEELL- SQVPL----- -----AL -QVLFLLAVCS VLLVVILVK- DCSIGN-1
31 VKGLDRV--- GEGPPGGRGE CGHGRFQWTL YFVLGLALMA DG-VEVFFV- SV2a

1 -----NNCP
120 SRLLLHVKQL VSDVRSLSQC MAALRG---- -----NG- SER---ICCP
95 TQLK----- -----AG- VDRLC-RSCP
207 LGLI----- -----VYLG M VVGAFWLGGL ADRLGRRCCL

          L3
5 ----- -LDWLPMNG LCYKIFNQLK TWEDAEMFCR KYKPG-----
155 ----- -INWVEYEG SCYWFSSSVK PWTEADKYCQ --LEN-----
110 ----- -WDWTHFQG SCYFFSVAQK SWNDSATAACH --NVG-----
286 QEKRGHLS- -HYGWSFQMG SAYQF---H SWRVFVLVCA FPSVFAIGA-

38 ----- -CHLASFH RYGESLEIAE YIS-----
186 ----- -AHLVVVT SW---EEQR FVQ-----
141 ----- -AQLVVIK SD---EEQN FLQ-----
382 ----GHPERV FSVTHIKTIH QEDELIEIQS DTGTWYQRWG VRALSLGGQV

          L4
58 ----- -DYHKGQ-- -ENVWIGLRD KKKDF-----
202 ----- -Q-HMGP-- -LNTWIGLTD QN--G-----
157 ----- -QTSKKR-- -GYTWMGLID MSKES-----
481 ARTKVFPGER VEHVTFNFTL ENQIHRGGQY FNDKFI GLRL KSVSFEDSLF

78 ----- -SWEWTD RSC --TDY-LTWD
219 ----- -PWKWVDGTD YETGF-KNWR
177 ----- -TWYWVDGSP LTL SFMKYWS
532 EECYFEDVTS SNTFFRNCTF INTVFYNTDL FEYKFN SRL VNSTF-LHNK

94 KNQPDHYQ-- ---NKEFCVE LVSLTGY---
237 PGQPDDWYGH GLGGGEDCAH FTT---D---
196 KGEPNNL-GE -----EDCAE FRD---D---
581 EGCPLDVTGT GEG--AYMVY FVS---FLGT LAVLPGNIVS ALLMDKIGRL

116 -----RL WND-----
261 -----GH WND-----
214 -----G WND-----
626 RMLAGSSVLS CVSCFFLSFG NSESAMIALL CLFGGVSIA S WNALDVLTV E

121 -----QVCES K-----D--
266 -----DVCRR P-----Y--
218 -----TKCTN K-----K--
676 LYPSDKRRTA FGFLNALCKL AAVLGISIFT SFVGITKAAP ILFASAALAL

127 -----AFLCQ -----CKF
272 -----RWVCE TEL--GKAN
225 -----FWICK KLSTSCPSK
726 GSSLALKLPE TR--QVLQ

```

**Fig 5.5.** Sequence alignment of SV2a with the C-type lectin superfamily. Residues that match the sequence motif characteristic of the canonical CTLD are highlighted in yellow. Other highly conserved residues in the C-type lectin proteins are highlighted in blue. Significance homologies are observed around the L3-L4 region.

#### 5.4. Characterization of SV2a Function in FUT KO Mice

A major challenge associated with the study of glycan-binding proteins has been elucidating their functional roles in vivo. The mere presence of a carbohydrate interaction in vitro is not sufficient to infer biological function. Therefore, we sought to elucidate the physiological relevance of this glycan-lectin interaction by focusing on the well-established role of SV2a in neurotransmitter release.<sup>30</sup> Trafficking of SV2a to synaptic vesicles is implicated during activity-dependent neurotransmission<sup>20</sup> because SV2a contributes to the priming of synaptic vesicle during Ca<sup>2+</sup>-dependent exocytosis. To investigate the role of Fuc $\alpha$ (1-2)Gal sugars in mediating SV2a trafficking, we utilized genetically altered mice lacking the  $\alpha$ (1-2) fucosyltransferase enzymes (FUT1 and FUT2) responsible for Fuc $\alpha$ (1-2)Gal biosynthesis. FUT1 and FUT2 -deficient mice have been shown to differentially regulate Fuc $\alpha$ (1-2)Gal expression in the olfactory bulb, gastrointestinal tract and reproductive organ.<sup>3,31,32</sup> As a result, we examined whether Fuc $\alpha$ (1-2)Gal expression in the mouse cortex was regulated by FUT1 or FUT2 using a chemoenzymatic labeling strategy.<sup>33</sup> This approach utilizes the substrate tolerance of bacterial glycosyl transferase A (BgtA) to rapidly label the specific glycan of interest with a non-natural sugar analogue. This analogue can then be detected and labeled with fluorescent-conjugated reporter using click chemistry (Fig 5.6).

A significant reduction in Fuc $\alpha$ (1-2)Gal expression was observed in glycoproteins from the cortex of *FUT2*(-/-) mice compared to WT littermate controls. In contrast, *FUT1*(-/-) mice showed a lower reduction in the extent of protein fucosylation with Fuc $\alpha$ (1-2)Gal (Fig 5.7a). Importantly, we observed a twofold increase in membrane-associated SV2a in

*FUT2*(-/-) cortical neurons compared to WT or *FUT1*(-/-) cortical neurons (Fig 5.7b).

Furthermore, we corroborated our finding through the cell-surface biotinylation of SV2a and identified a 1.9-fold increase in SV2a labeling on the plasma membrane of *FUT2*(-/-) cortical neurons (Fig 5.7c). As SV2a regulates the expression and sorting of the calcium sensor protein synaptotagmin (syt1),<sup>34</sup> the interaction between SV2a and Fuc $\alpha$ (1-2)Gal sugars could have important functional implications for syt1 localization. Indeed, we found that colocalization of SV2a and syt1 puncta at the neuronal synapse, expressed as the relative puncta density along the neuronal processes, increased by 1.6-fold compared to WT neurons (Fig 5.7d). This suggests that SV2a-mediated endocytosis of syt1 had been altered. We hypothesize that the increase in membrane-associated SV2a as caused by an attenuation of SV2a trafficking, is mediated by the loss in glycan-assisted interaction in *FUT2*(-/-) neuron, which resulted in the subsequent impairment of syt1 endocytosis. Thus, we provide evidence that the association of Fuc $\alpha$ (1-2)Gal sugars with SV2a may play important roles in the regulation of SV2a trafficking and syt1 endocytosis. Together, these results provide compelling support for a functional interaction between SV2 and Fuc $\alpha$ (1-2)Gal sugars.

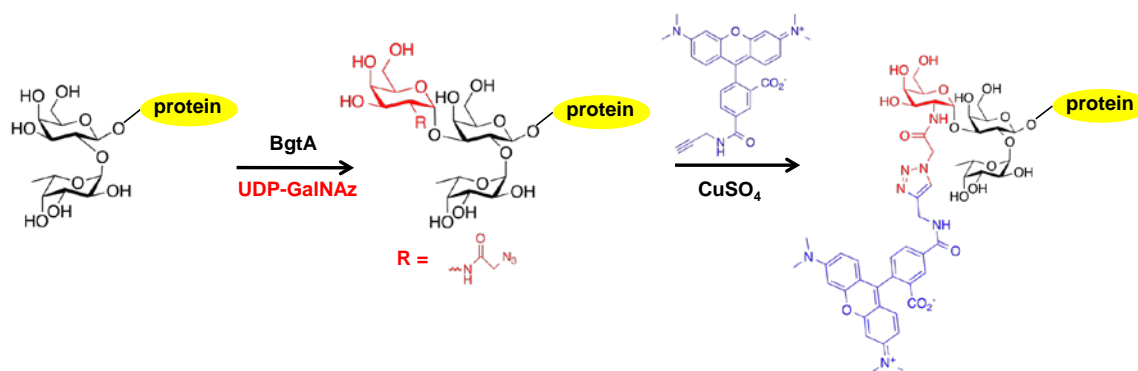


**Fig 5.6.** Chemoenzymatic strategy for the detection of Fuc $\alpha$ (1-2)Gal glycan

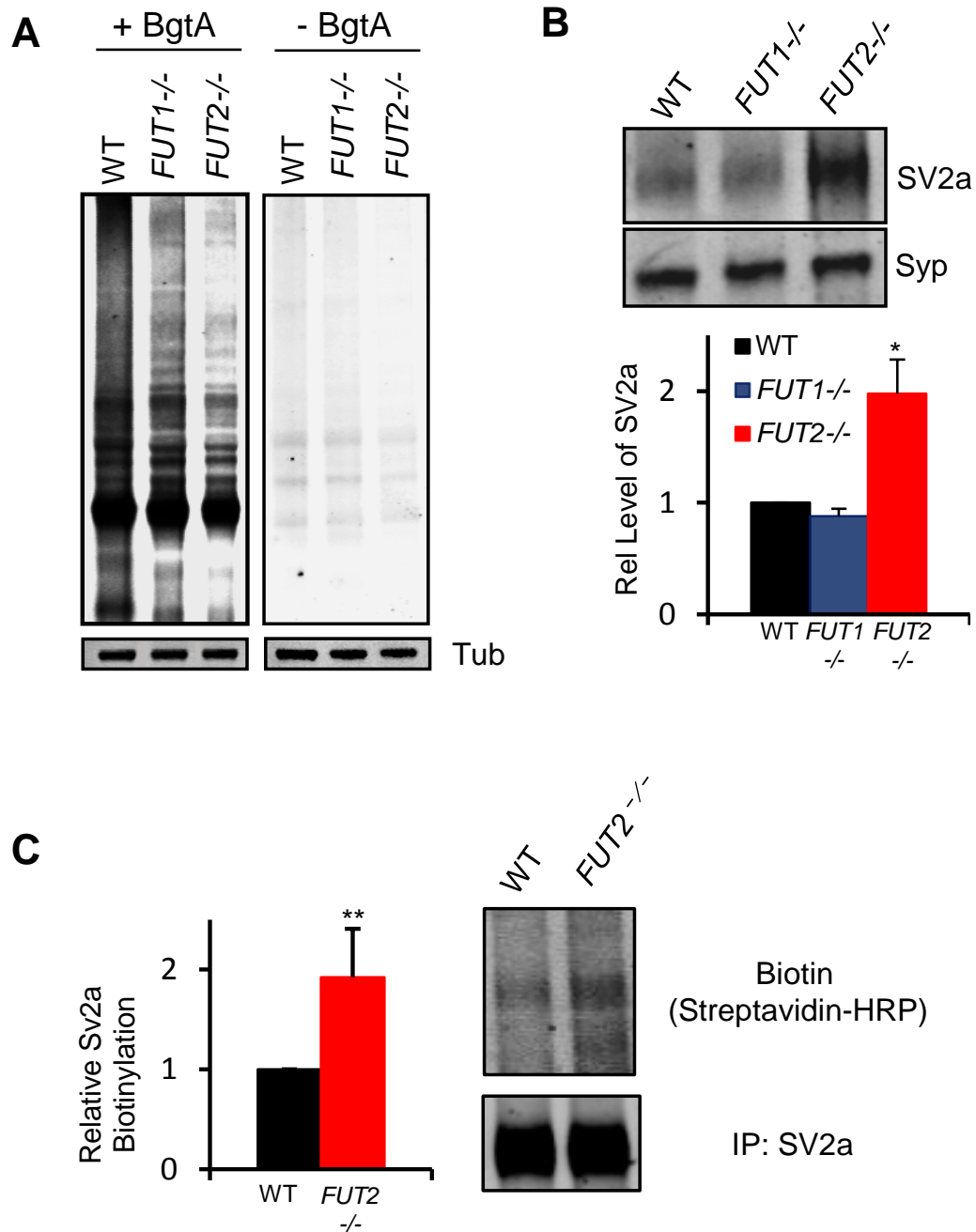


**Fig 5.7.** Functional analysis of Fuc $\alpha$ (1-2)Gal interaction with SV2a. (A) Fuc $\alpha$ (1-2)Gal expression is reduced on *FUT2*<sup>-/-</sup> cortical neurons as detected by chemoenzymatic labeling; (B) Relative level of SV2a in the membrane. SV2a is enriched in the membrane fractions of *FUT2*<sup>-/-</sup> mice (n= 3, p < 0.02); (C) Cell-surface biotinylation of SV2a. Increased surface biotinylation of SV2a on *FUT2*<sup>-/-</sup> cortical neurons (n=4, p < 0.05);

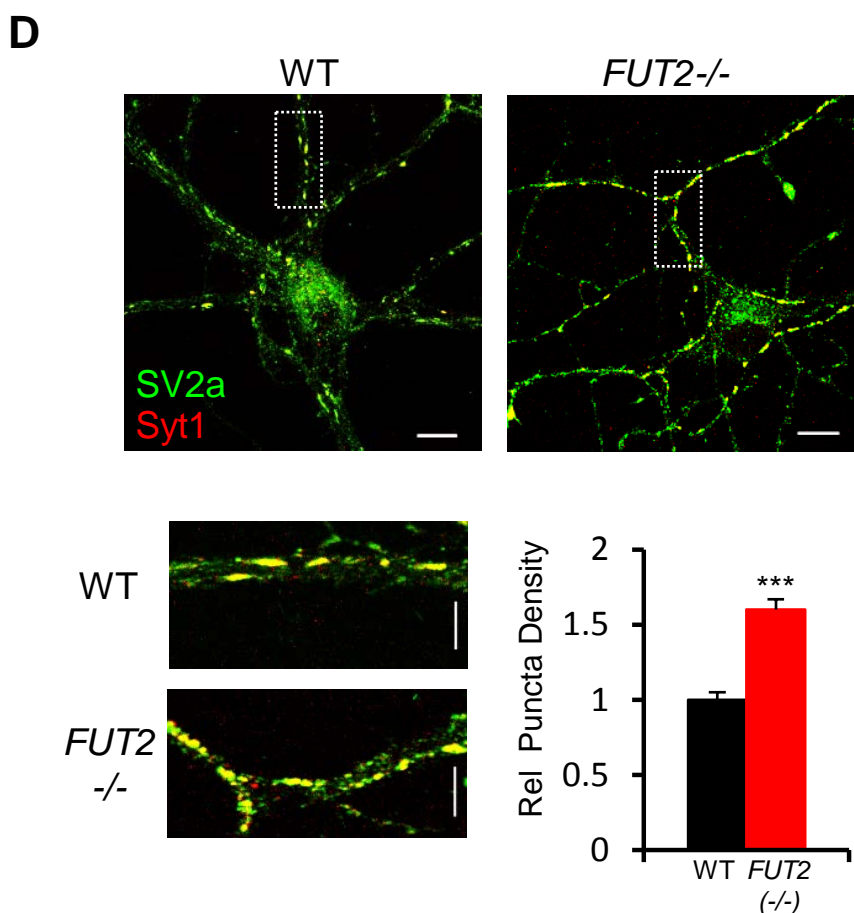


**Fig 5.7.** (D) Colocalization studies of SV2a and Syt1 in neuronal processes. Distinct puncta positively stained with SV2a and Syt1 are quantified per unit area of measurement ( $n=70-80$ ,  $p < 0.005$ ). Scale bar = 10  $\mu$ M

In summary, we demonstrate the design and synthesis of multivalent, photoaffinity capture glycopolymers as chemical tools for the identification of novel lectins. Our studies identify several new candidate lectins for Fuc $\alpha$ (1-2)Gal sugars in the brain and suggest that the interaction of these sugars with SV2a may have important functional consequences for protein trafficking. This work illustrates the potential use of glycopolymer mimetics as general tool to identify important low-affinity interactions that are characterized by multivalency in vivo. Continued investigations into Fuc $\alpha$ (1-2)Gal-lectin interactions will

provide further insights into the importance of these novel lectins and molecular mechanisms underlying neuronal communication in the brain. More importantly, we are excited about identifying specific glycan-lectin interaction pairs in neuron to understand how Fuc $\alpha$ (1-2)Gal- mediates learning and memory consolidation process.

## 5.5. Experimental Methods

**Protein Expression and Purification.** DCLK1 (DCAMKL1) was expressed and purified from *E. coli* BL21 (DE3) harboring the recombinant plasmid vector pET28a-DCLK1-His as previously described.<sup>35</sup> SV2a was expressed and purified from HEK293 cells transfected with plasmid vector SV2a-FLAG-pIRES2 as previously described.<sup>36</sup> G $\alpha$ O protein was kindly provided by Dr Tohru Kozasa (University of Illinois, Chicago). PKC $\epsilon$  protein was commercially purchased (ProspecBio).

### **Binding Validation of Lectin Candidate to Fuca(1-2)Gal by Microarray.**

Binding assays were performed following a known procedure.<sup>37</sup> Protein binding was carried out on mammalian glycan array by the core H of Consortium Functional Glycomics. Briefly, 200  $\mu$ g/ml of proteins (PKC $\epsilon$  and SV2a) in PBS (pH 7.4 with 1 mM CaCl<sub>2</sub> and 4 mM MgCl<sub>2</sub>) were incubated in a sandwich procedure with their labeled antibody on the glycan array. The samples (50–100  $\mu$ l) were applied either directly onto the surface of a single slide and covered with a microscope cover slip and then incubated in a humidified chamber for 30–60 min. Slides were subsequently washed by successive rinses in (i) Tris-HCl-0.05% Tween, (ii) Tris-HCl, and (iii) deionized water, then immediately subjected to imaging

### **Binding Validation of Lectin Candidates to Fuca(1-2)Gal by ELLA.**

Nunc Maxisorp 384-well plates were coated overnight at 4°C with lectins (50 ng/well) in carbonate buffer (50 $\mu$ l, 50mM H<sub>2</sub>CO<sub>3</sub>, pH 9.0). The wells were then washed with washing buffer (3 x 100  $\mu$ l, TBS containing 0.03% Tween 20). The washing procedure was repeated

after each incubation throughout the assay. After washing, the wells were filled with serial dilutions of biotinylated polymers (Fuca(1-2)Gal, Gal(1-2)Gal and control (-OH) polymer, 25µl/well, GlycoTech) in binding buffer ( PBS, 1 mM CaCl<sub>2</sub>, 4 mM MgCl<sub>2</sub>) and incubated at rt for 2.5 h. The wells were washed and blocked with 10% Fetal Bovine Serum, FBS (80 µl) at 37°C for 1 hr. After blocking, the plates were incubated with horseradish peroxidase-conjugated streptavidin (1:40000, Pierce) at rt for 1 h, developed with TMB substrate (3,3',5,5'-tetramethylbenzidine, Pierce) and quenched with 2 M H<sub>2</sub>SO<sub>4</sub>. Absorbances were measured at 450 nm using PerkinElmer Victor plate reader and were fitted to a linear regression analysis using KaleidaGraph (version 4.1.2). Experiments were performed in triplicate, and data represent the mean ± SEM.

**Sequence Alignment.** Multiple sequence alignment between SV2a and three other C-type lectins: RSL, ASGR1 and DC-SIGN were carried out using the alignment program T-coffee (V-8.93) (<http://www.ebi.ac.uk/Tools/msa/tcoffee/>). Protein sequences were collected with BLAST by using the query sequences of mouse SV2a (UniProtKB ID: Q9JIS5), rat ASGR1 (UniProtKB ID: P02706), mouse DC-SIGN (UniProtKB ID: Q91ZX1) and croat RSL (UniProtKB ID: P21963).

**Chemoenzymatic Labeling of Cell Lysates.** The cortices of adult C57BL/6, FUT1<sup>-/-</sup> and FUT2<sup>-/-</sup> mice were dissected on ice and lysed in boiling 1% SDS (5 volumes/weight) with sonication until the mixture was homogeneous. Protein was precipitated using methanol/chloroform/water. Briefly, protein was diluted to 200 µL and precipitated by sequential mixing with 600 µL of MeOH, 200 µL of CHCl<sub>3</sub> and 450 µL

H<sub>2</sub>O, after which the mixture was centrifuged at 23,000 x g for 15 min. Precipitated protein was washed with 450  $\mu$ L of MeOH and centrifuged at 23,000 x g for 10 min. After the protein pellet was allowed to dry briefly, the pellet was re-dissolved at 5 mg/mL in 20 mM HEPES pH 7.9 containing 1% SDS, and diluted fivefold into a buffer with the following final concentrations: 20 mM HEPES pH 7.9, 50 mM NaCl, 2% NP-40, 5 mM MnCl<sub>2</sub>. UDP-GalNAz (25  $\mu$ M; Invitrogen) and BgtA (0.16 mg/mL) were added, and the samples were incubated at 4 °C for 16-20 h. The labeled proteins were precipitated as above and resuspended in 50 mM Tris pH 7.4 containing 1% SDS at 4 mg/mL. The resuspended proteins were subsequently reacted with alkyne-TAMRA (Invitrogen) as per the Click-It™ TAMRA Protein Analysis Detection kit instructions (Invitrogen), except that EDTA-free Complete™ protease inhibitors were added during the reaction. Negative controls were performed under identical conditions except that BgtA was omitted from the labeling reaction. After the labeling reactions, protein was precipitated using chloroform/methanol/water as described above and re-dissolved in boiling 2% SDS. This precipitation and resolubilization was then repeated once more to ensure removal of non-specific interactions. TAMRA-labeled proteins were resolved on a NuPAGE 4-12% Bis-Tris gel and transferred to PVDF membrane. The membrane was blocked with 5% milk (Biorad) in TBST (50 mM Tris-HCl pH 7.4, 150 mM NaCl, 0.05% Tween 20) for 1 hr at rt and immunoblotted with rabbit anti-TAMRA (1:1000, Invitrogen) and mouse anti-Tubulin (1:5000, Sigma-Aldrich). Membranes were washed with TBST, incubated with the appropriate Alexa Fluor 680-conjugated (Invitrogen) or IR800-conjugated (Rockland) secondary antibody, and visualized using a LiCOR Odyssey Imaging System.

**Neuronal Cultures for Functional Assay.** For biochemical assay, cortical neuronal cultures were prepared as previously described,<sup>37</sup> except that neurons from E15-16 timed-pregnant C57BL/6, *FUT1*(-/-) and *FUT2*(-/-) mice were plated onto poly-DL-lysine coated 6-well plates (BD Bioscience). Neurons were maintained for up to 10 days in vitro (DIV) in Neurobasal medium (NBM) supplemented with 2 mM Glutamax-I and 2% B-27 (Invitrogen). For staining and imaging, hippocampal neurons were prepared as previously described,<sup>38</sup> except that neurons from E15-16 timed-pregnant mice were plated on poly-DL-lysine coated glass coverslips (Carolina Biological) at a density of 75 cells/mm<sup>2</sup>. Neurons were maintained for up to 10 DIV in NBM supplemented with 2 mM Glutamax-I and, and 2% B-27.

**Assaying SV2a Distribution in cortical neuron.** Ten DIV cortical neuron cultures (C56BL/7, *FUT1*(-/-) and *FUT2*(-/-)) were washed once with ice-cold PBS, gently scraped with trypsin and suspended in DMEM (Dulbecco Modified Eagle Medium) supplemented with 10% FBS (Invitrogen) before being cleared by centrifugation for 10 min at 500 x g at 4°C. Pellets were washed with cold PBS and fractionated using the Qproteome Cell Compartment Kit (Qiagen). The resulting membrane extract protein concentrations were quantified using the BCA assay. Equal amount of proteins were resolved on a NuPAGE 4-12% Bis-Tris gel and transferred to PVDF membrane. The membrane was blocked in 5% milk, immunoblotted with goat anti-SV2a (E-15, 1:200, Santa Cruz) and mouse anti-Synaptophysin (1:800, Sigma-Aldrich) and visualized using a LiCOR Odyssey Imaging System. SV2a distribution in the membrane of *FUT1*(-/-) and *FUT2*(-/-) neurons were expressed relative to the control C57Bl/6 level (n = 3-5), and were reported as the mean ±

SEM. Statistical analysis was performed using the student's unpaired t-test to compare the SV2a level between *FUT2*(-/-) and C57BL/6 neurons.

**Surface Biotinylation.** Ten DIV cortical neuron cultures (C56BL/7, *FUT1*(-/-) and *FUT2*(-/-)) were washed once with ice-cold PBS, pH 8.0, and biotinylated by incubating with 0.5 mg/ml EZ-Link Sulfo-NHS-LC-LC-Biotin (Pierce) for 25 min at 4°C with gentle shaking. Cultures were washed with PBS, pH 7.4, and incubated with 100 mM glycine for 15 min at 4°C to quench the reaction. Neurons were rinsed with ice-cold PBS, pH 7.4, and extracted in solubilization buffer (150 mM NaCl, 50 mM Tris-HCl, 1 mM EDTA, 1% NP-40 and protease inhibitor) for 1 h at 4°C. Insoluble material was removed by ultracentrifugation (19000 x g for 20 min) and the supernatants were subjected to immunoprecipitation by incubating with anti-SV2a (E-15, Santa Cruz) overnight at 4°C. The samples were diluted with solubilization buffer to a final concentration of 1 mg/ml and were incubated with pre-treated (blocked with 0.1% fish gelatin) protein A/G sepharose beads (ThermoFisher) at 4°C for 2h. The resin was washed three times with 10 column volumes of solubilization buffer and captured protein was eluted with loading buffer without boiling. Equal amount of proteins were resolved on a NuPAGE 4-12% Bis-Tris gel and transferred to PVDF membrane. The membrane was blocked in 5% milk and immunoblotted with rabbit anti-SV2a (1:300, Synaptic Systems) for total immunoprecipitated SV2a and streptavidin-HRP (1:1000, pierce) for biotinylated SV2a. Labeled bands were visualized and quantified using a LiCOR Odyssey Imaging System. The proportion of SV2a on the plasma membrane of *FUT2*(-/-) neurons were expressed relative to the control C57BL/6 level (n = 4) as the normalized intensity of biotinylated-

SV2a signal to the total SV2a, and were reported as the mean  $\pm$  SEM. Statistical analysis was performed using the student's unpaired t-test to compare the SV2a level between *FUT2*(-/-) and C57BL/6 neurons.

**Immunostaining and quantification.** The hippocampal neurons on the coverslips were rinsed one time with PBS, fixed in 4% paraformaldehyde/sucrose at rt for 20 min, washed twice with PBS, permeabilized in 0.3% TritonX-100 at rt for 5 min, and washed twice with PBST. Non-specific binding was blocked by incubating with 5% goat serum (GS) in PBST at 4°C for 1 h and then rinsing twice with PBST. Cells were then incubated with rabbit anti-SV2a (1:300, Synaptic Systems) in 5% GS at rt for 2 h. Excess antibody was rinsed away with PBST and cells were further incubated overnight with mouse anti-Synaptophysin (1:300, Millipore) in 5% GS at 4°C. After washing with PBST, The cells were treated with anti-rabbit IgG AlexaFluor 488 (1:1000, Invitrogen) and anti-mouse IgG AlexaFluor568 (1:1000, Invitrogen) in 5% GS at rt for 2 h. The coverslips were mounted onto glass slides and imaged using a LSM510 Meta confocal laser scanning microscope with a 100X 1.40 N.A oil immersion plan apochromat objective lens (Carl Zeiss MicroImaging, Inc.).

Images were analyzed with ImageJ (<http://rsbweb.nih.gov/ij/>) using the JACoP Colocalization plugin and colocalized puncta analysis was performed as previously described<sup>39,40</sup> using the Colocalization Highlighter plugin. Briefly, images of synaptic proteins were thresholded with the same value across experimental conditions so as to include clusters with intensity at least twofold greater than the adjacent dendrite. Puncta were defined as continuous pixel clusters of 0.5–11  $\mu$ m. To determine the degree of

colocalization between two proteins, each channel was thresholded and the distinct puncta in each channel is overlaid to generate colocalized region. Puncta were manually counted as colocalized if the average intensity within the overlaid region exceeded the threshold value. Counted puncta were expressed as puncta density along the neuronal processes and were reported relative to the control sample. Three independent experiments (n = 70-80 images) were conducted and statistical analysis were performed using the student's unpaired t-test.

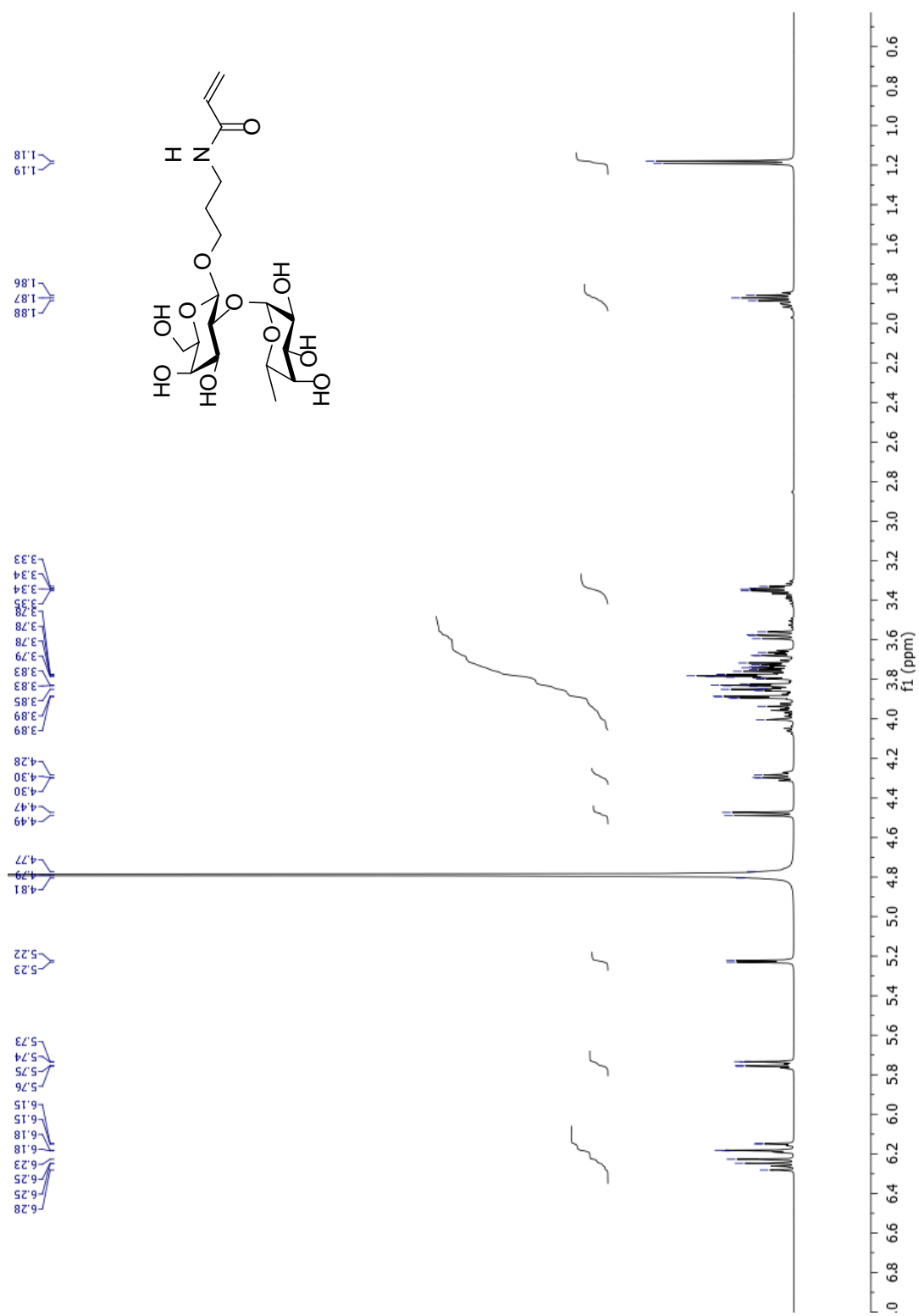
## REFERENCES

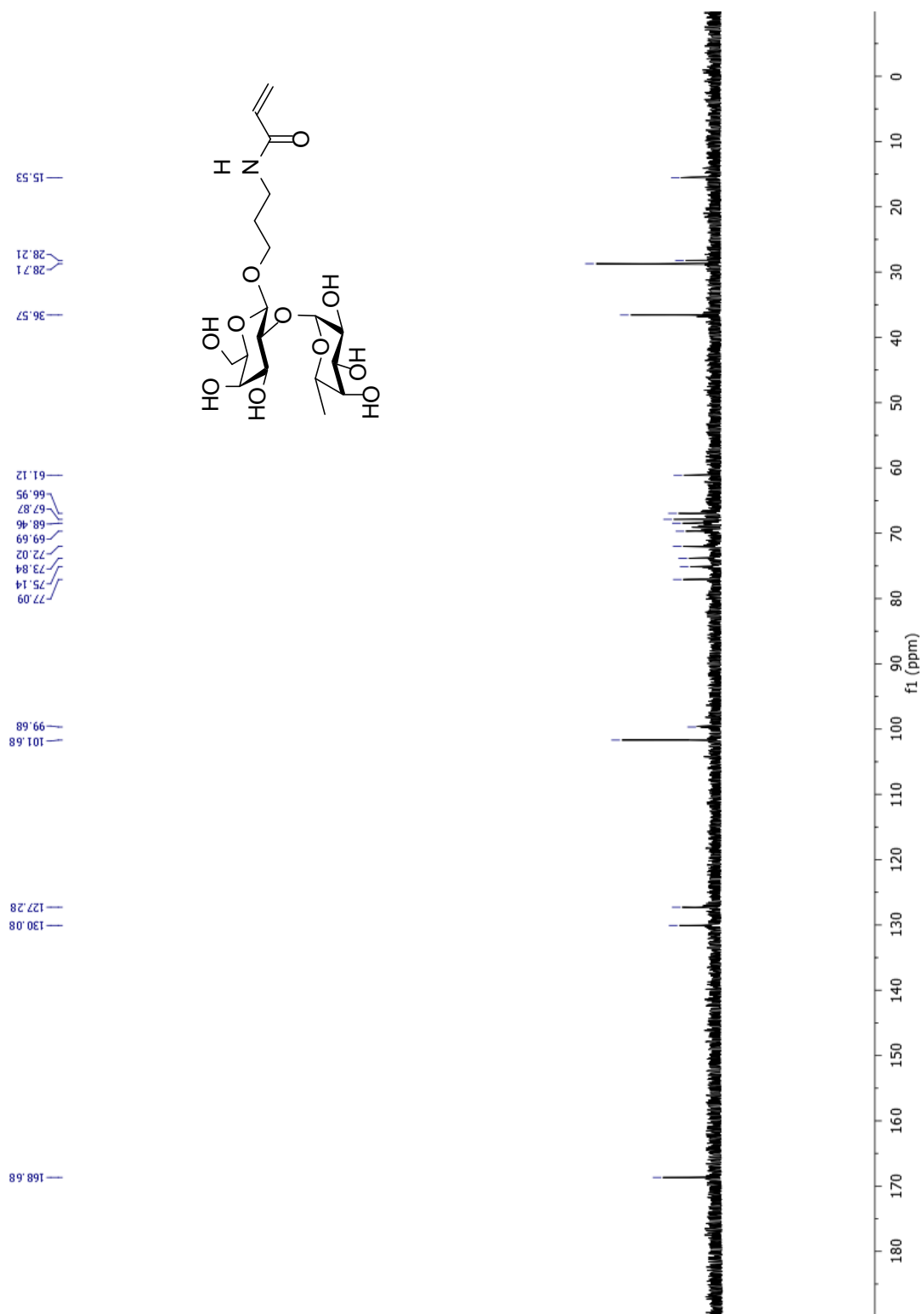
1. Raman, R.; Venkataraman, M.; Ramakrishnan, S.; Lang, W.; Raguram, R. et al. *Glycobiology*. **2006**, 16, 82R
2. Murrey, H. E.; Gama, C. I.; Kalovidouris, S.; Luo, W. I.; Hsieh-Wilson, L. C. *Proc. Natl. Acad. Sci. U.S.A.* **2006**, 103, 21
3. Murrey, H. E.; Ficarro, S. B.; Krishnamurthy, C.; Domino, S. E.; Peters, E. C.; Hsieh-Wilson, L. C. *Biochemistry*. **2009**, 48, 7261
4. Tanaka, T.; Serneo, F. F.; Tseng, H. C.; Kulkarni, A. B.; Tsai, L. H.; Gleeson, J. G. *Neuron*. **2004**, 41, 215
5. Rao, M. S.; Shetty, A. K. *Eur. J. Neurosci.* **2004**, 19, 234
6. Hevroni, D.; Rattner, A.; Bundman, M.; Lederfein, D.; Gabarah, A. et al. *J. Mol. Neurosci.* **1999**, 10, 75
7. Chou, W. H.; Wang, D.; McMahan, T.; Qi, Z. H.; Song, M.; Zhang, C.; Shokat, K. M.; Messing, R. O. *J. Neurosci.* **2010**, 30, 13955
8. Chen, Y.; Cantrell, A. R.; Messing, R. O.; Scheuer, T.; Catterall, W. A. *J. Neurosci.* **2005**, 25, 507
9. Zeidman, R.; Troller, U.; Raghunanth, A.; Pahlman, S.; Larsson, C. *Mol. Biol. Cell.* **2002**, 13, 12
10. Mirotznik, R. R.; Zheng, X.; Stanley, F. F. *J. Neurosci.* **2000**, 20, 7614
11. Nakata, H.; Kozasa, T. *Mol. Pharmacol.* **2005**, 67, 695
12. Chang, W. P.; Sudhof, T. *J. Neurosci.* **2009**, 29, 883
13. Schivell, A. E.; Batchelor, R. H.; Bajjalieh, S. M. *J. Biol. Chem.* **1996**, 271, 27770
14. Manimala, J. C.; Roach, T. A.; Li, Z.; Gildersleeve, J. C. *Angew. Chem. Int. Ed.* **2006**, 45, 3607
15. Chang, C. F.; Pan, J. F.; Lin, C. N.; Wu, I. L.; Wong, C. H. et al. *Glycobiology*. **2011**, 21, 895
16. Buckley, K.; Kelly, R. B. *J. Cell. Biol.* **1985**, 100, 1284
17. Dong, M.; Yeh, F.; Tepp, W. H.; Dean, C.; Johnson, E. A. et al. *Science*. **2006**, 312, 592
18. Janz, R.; Sudhof, T. C. *Neuroscience*. **1999**, 94, 1279
19. Bajjalieh, S. M.; Frantz, G. D.; Weimann, J. M.; McConnel, S. K.; Scheller, R. H. *J. Neurosci.* **1994**, 14, 5223
20. Crowder, K. M.; Gunther, J. M.; Jones, A. T.; Hale, B. D.; Zhang, Z. H. et al. *Proc. Natl. Acad. Sci. U.S.A.* **1999**, 96, 15268
21. Janz, R.; Goda, Y.; Geppert, M.; Missler, M.; Sudhof, T. C. *Neuron*. **1999**, 1003
22. Lynch, B. A.; Lambeng, N.; Nocka, K.; Kensel-Hammes, P.; Bajjalieh, S. M. et al. *Proc. Natl. Acad. Sci. U.S.A.* **2004**, 101, 9861
23. Feinberg, H.; Mitchell, D.; Drickamer, K.; Weis, W. *Science*. **2001**, 294, 2163
24. Guo, Y.; Feinberg, H.; Conroy, E.; Mitchell, D. A.; Alvarez, R. et al. *Nat. Struct. Mol. Biol.* **2004**, 11, 591

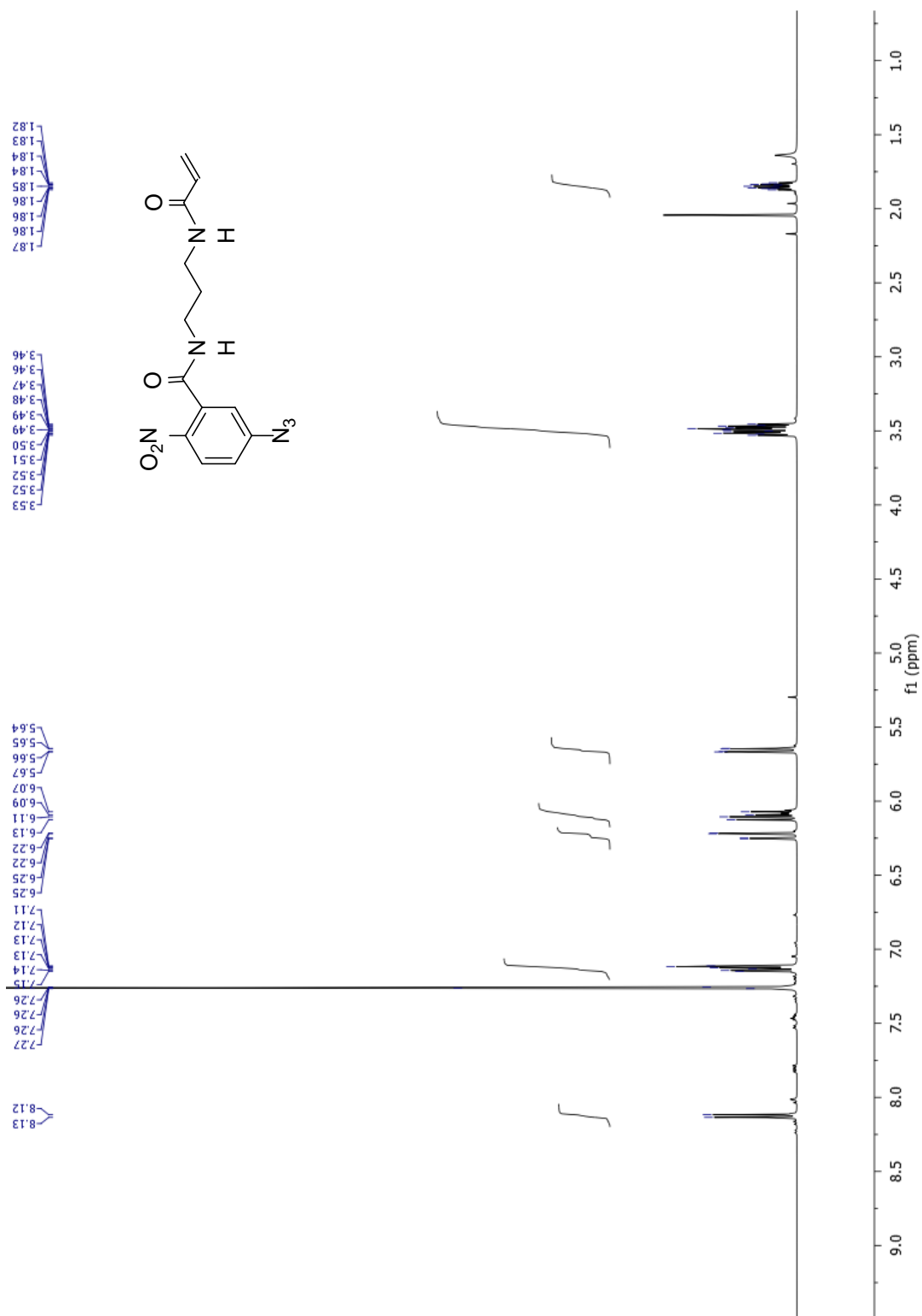
25. Mitchell, D. A.; Fadden, A. J.; Drickamer, K. *J. Biol. Chem.* **2001**, 276, 28939
26. Weigel, P. H.; Jasper, H. N. Y. *Biochim. Biophys. Acta.* **2002**, 1572, 341
27. Young, N. M.; van Faassen, H.; Watson D. C.; MacKenzie, C. R. *Glycoconj. J.* **2011**, 28, 427
28. Zalensky, A. N.; Gready, J. E. *FEBS. J.* **2005**, 272, 6179
29. Zalensky, A. N.; Gready, J. E. *Protein. Struct. Funct. Genet.* **2003**, 52, 466
30. Nowack, A.; Yao, J.; Custer, K. L.; Bajjalieh, S. M. *Am. J. Physiol. Cell. Physiol.* **2010**, 299, C960
31. Iwamori, M.; Domino, S. E. *Biochem. J.* **2004**, 380, 75
32. Domino, S. E.; Zhang, L.; Gillespie, P. J.; Saunders, T. L.; Lowe, J. B. *Mol. Cell. Biol.* **2001**, 21, 8336
33. Chaubard, J.-L.; Khrisnamurthy, C.; Yi, W.; Smith, D.; Hsieh-Wilson, L.C. *J. Am. Chem. Soc.* **2012**, 134, 4489
34. Yao, J.; Nowack, A.; Gardner, R. G.; Kensel-Hammes, P.; Bajjalieh, S. M. *J. Neurosci.* **2010**, 30, 5569
35. Lin, P.T.; Gleeson, J.G.; Corbo, J.C.; Flanagan, L.; Walsh, C.A. *J. Neurosci.* **2000**, 20, 9152
36. Yao, J.; Bajjalieh, S.M. *J. Biol. Chem.* **2008**, 283, 20628
37. Rexach, J.E.; Rodgers, C.J.; Yu, S-H.; Tao, J.; Sun, Y.E.; Hsieh-Wilson, L.C. *Nat. Chem. Biol.* **2010**, 6, 645
38. Rawat, M.; Gama, C.I.; Matson, J.B.; Hsieh-Wilson, L.C. *J. Am. Chem. Soc.* **2008**, 130, 2959
39. Kayser, M.S.; McClelland, A.C.; Hughes, E.G.; Dalva, M.B. *J. Neurosci.* **2006**, 26, 12152.
40. Jones, K.A.; Srivastava, D.P.; Allen, J.A.; Strachan, R.T.; Roth, B.L.; Penzes, P. *Proc. Natl. Acad. Sci.* **2009**, 106, 19575

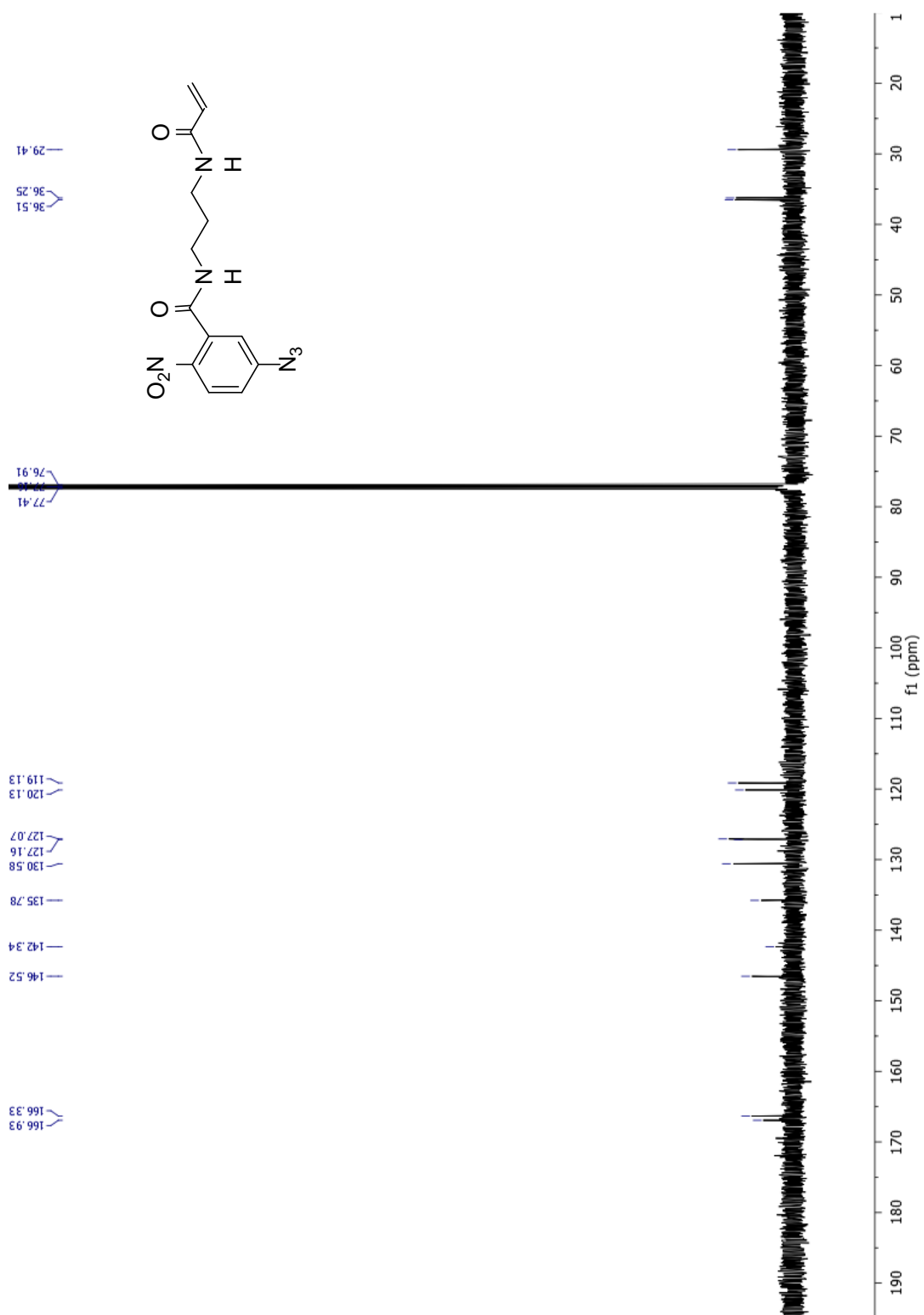
# ***APPENDIX 1***

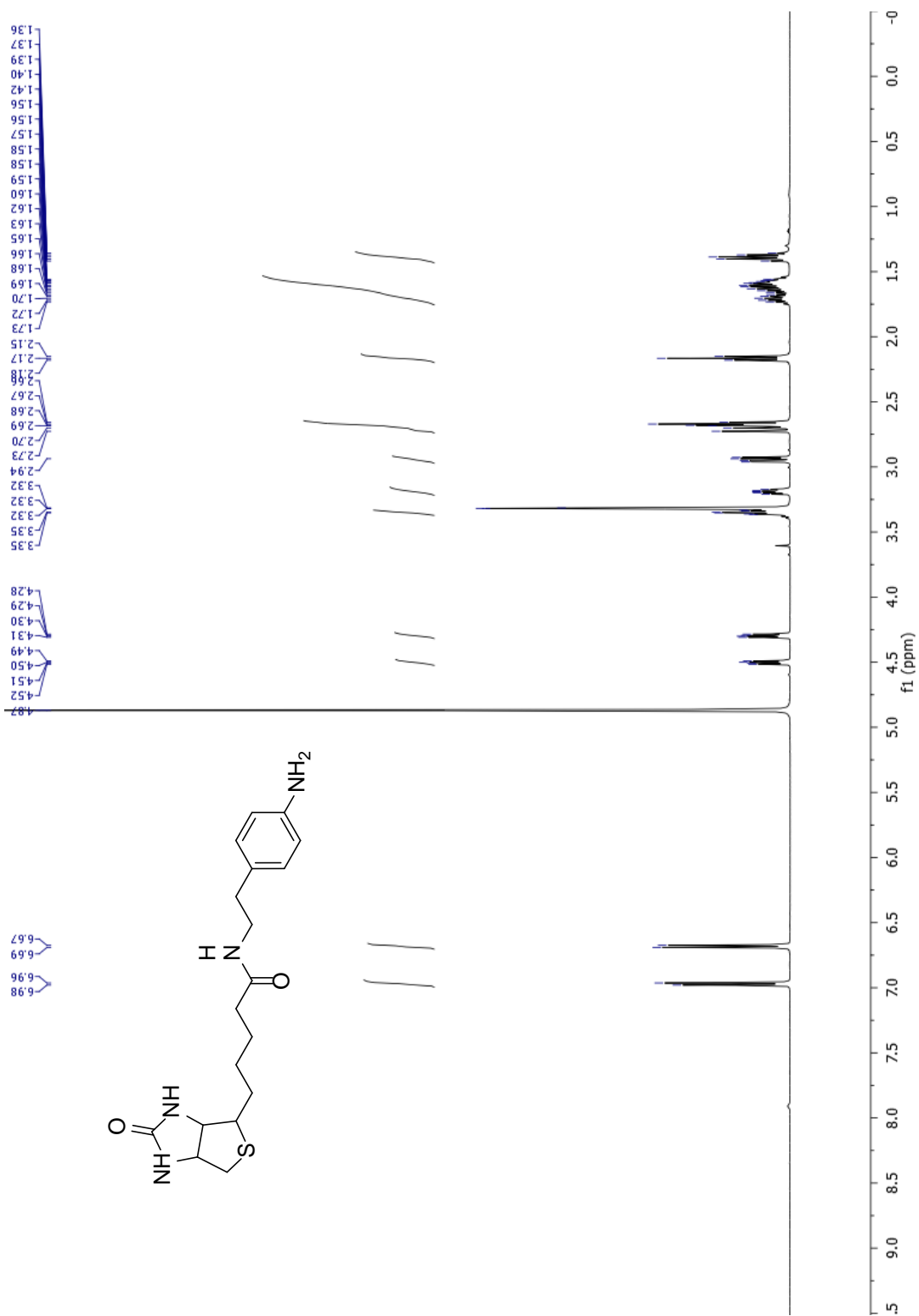
## *SPECTRA FOR POLYMER SYNTHESIS*

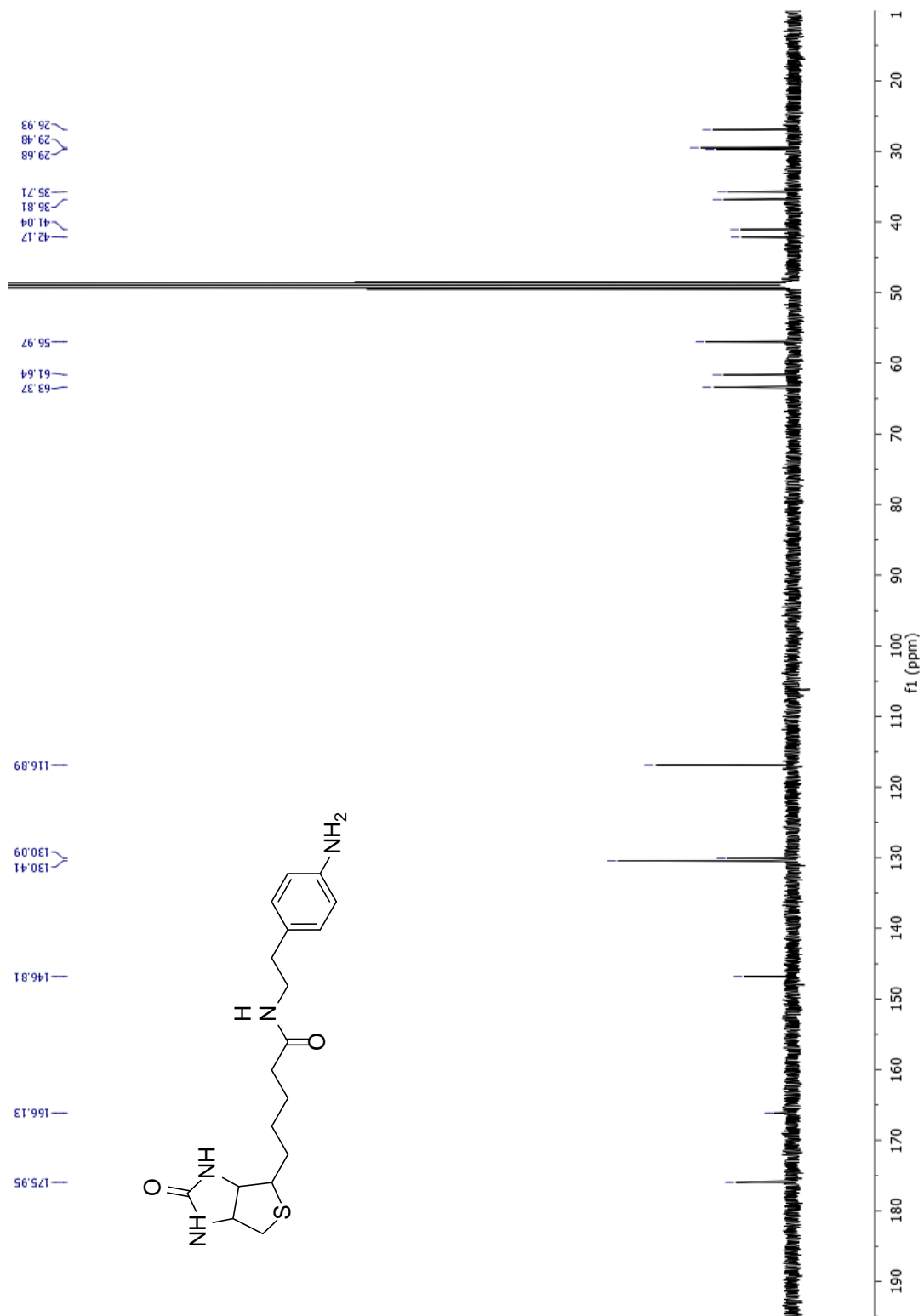


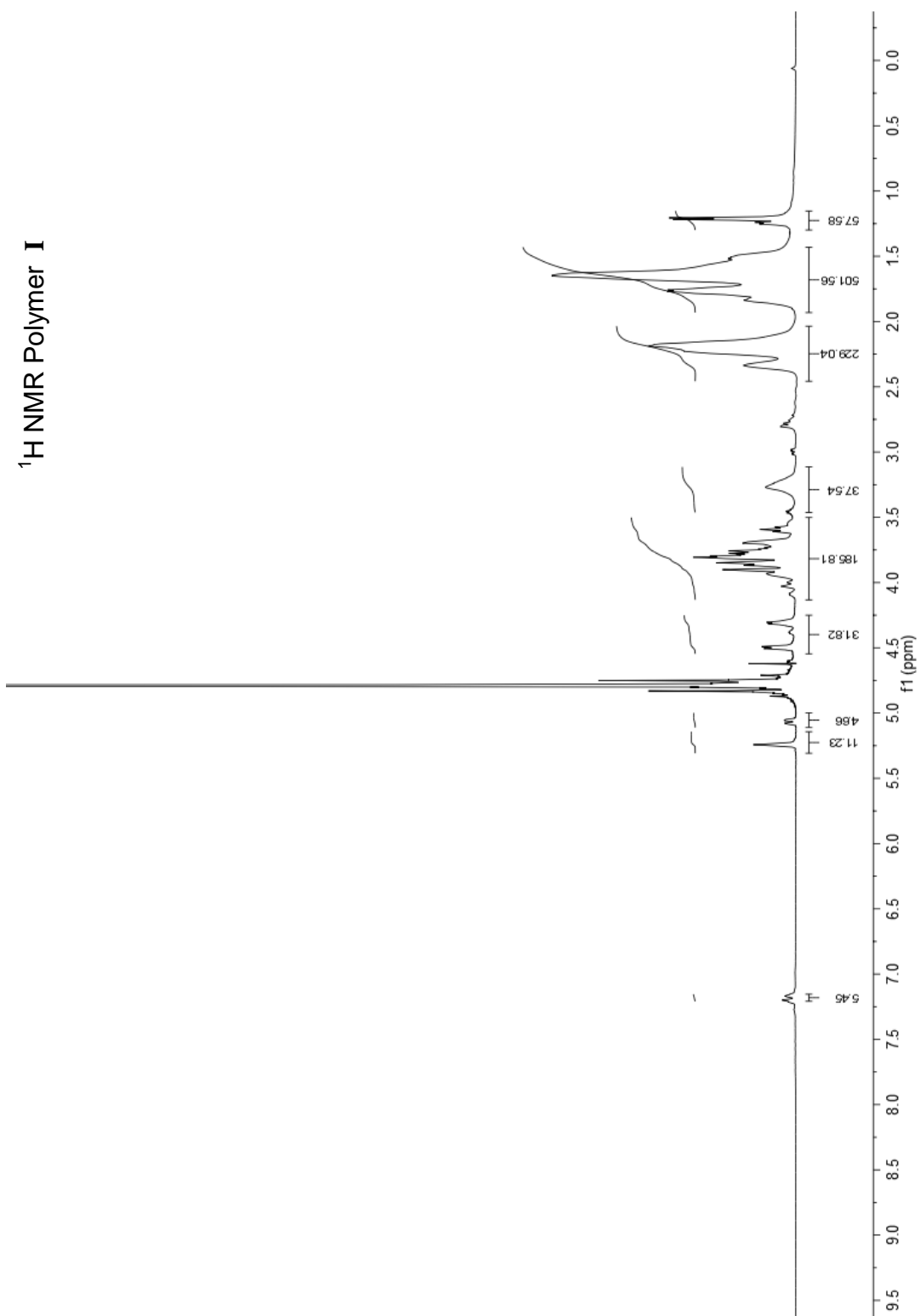


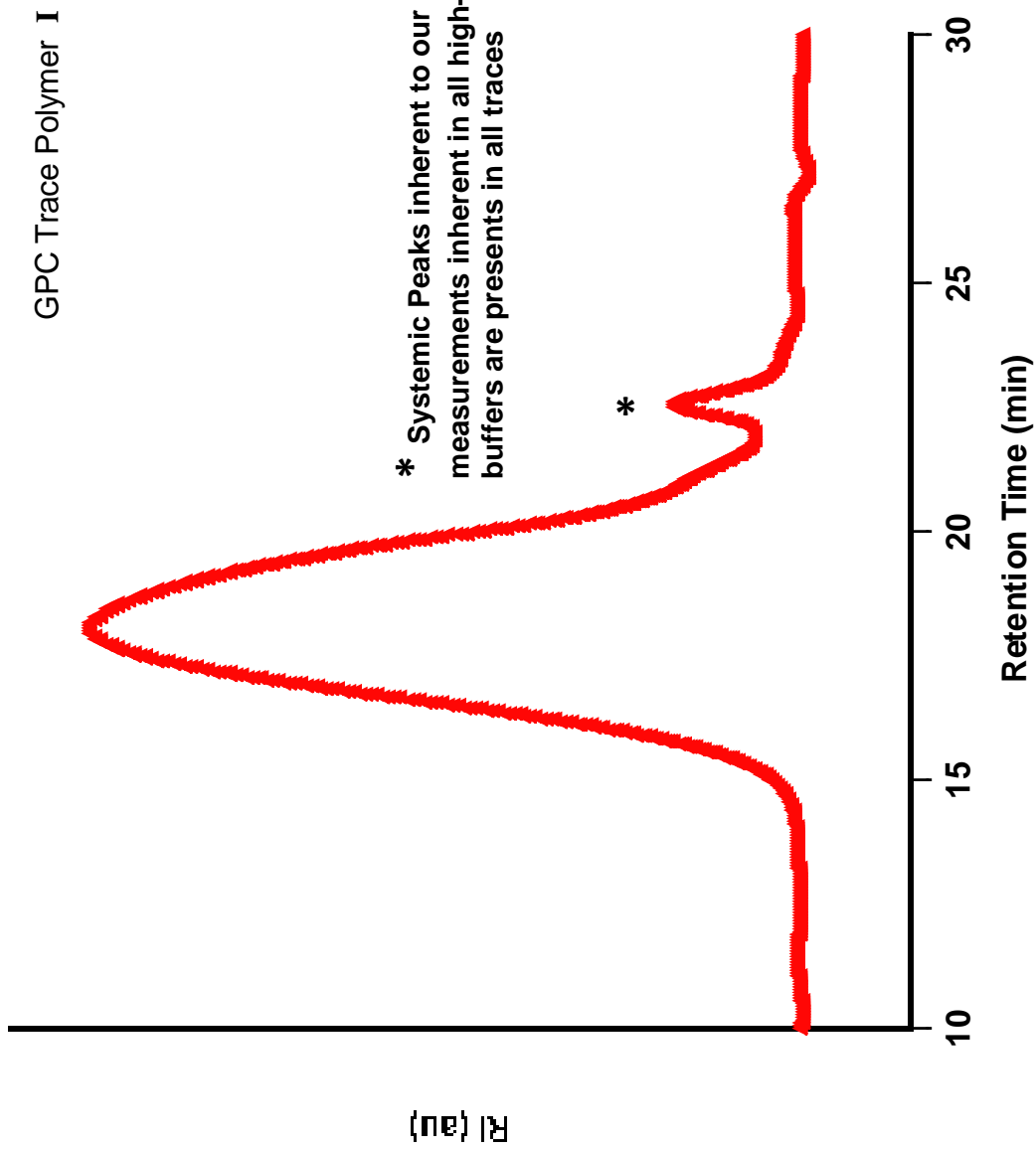




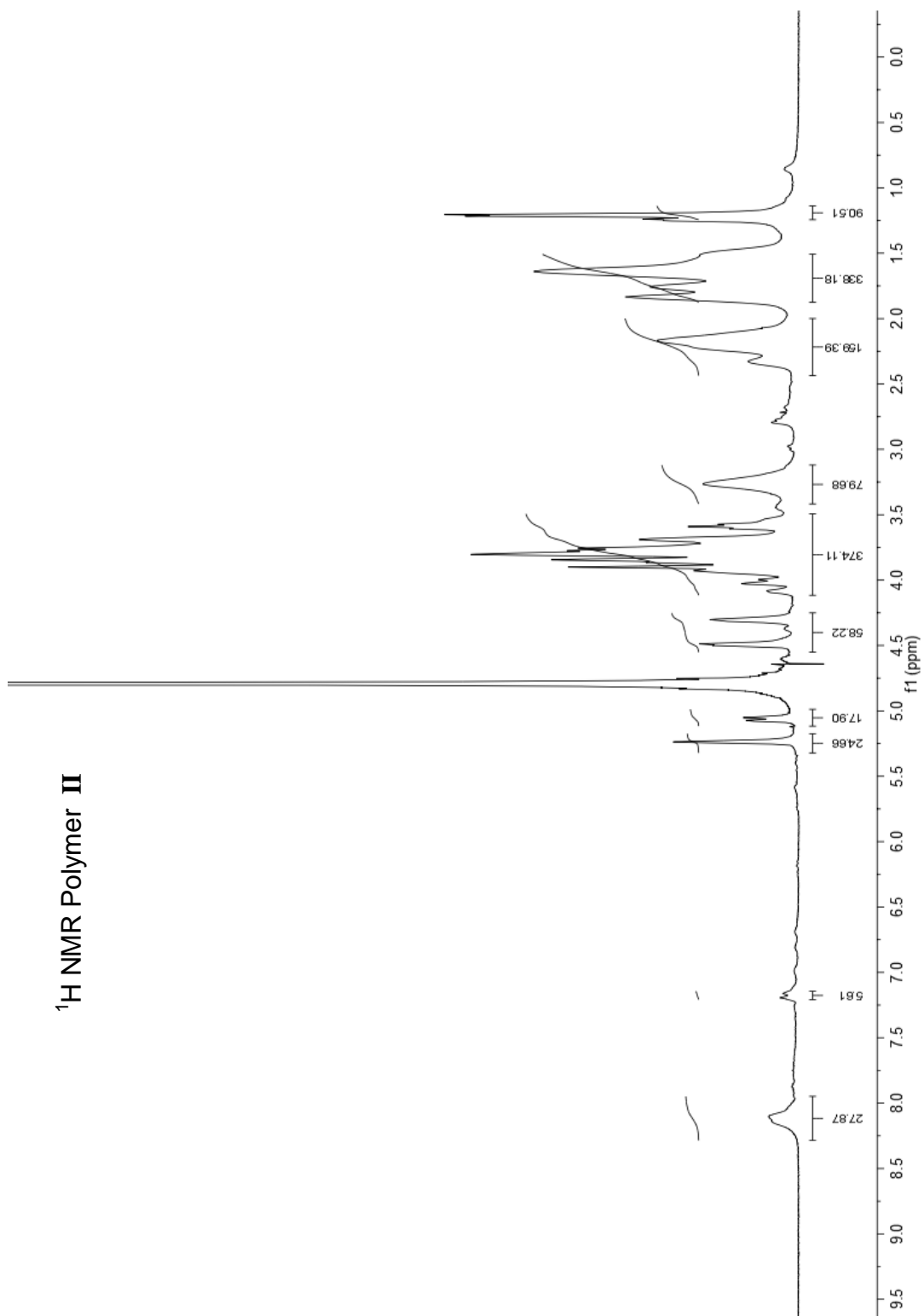


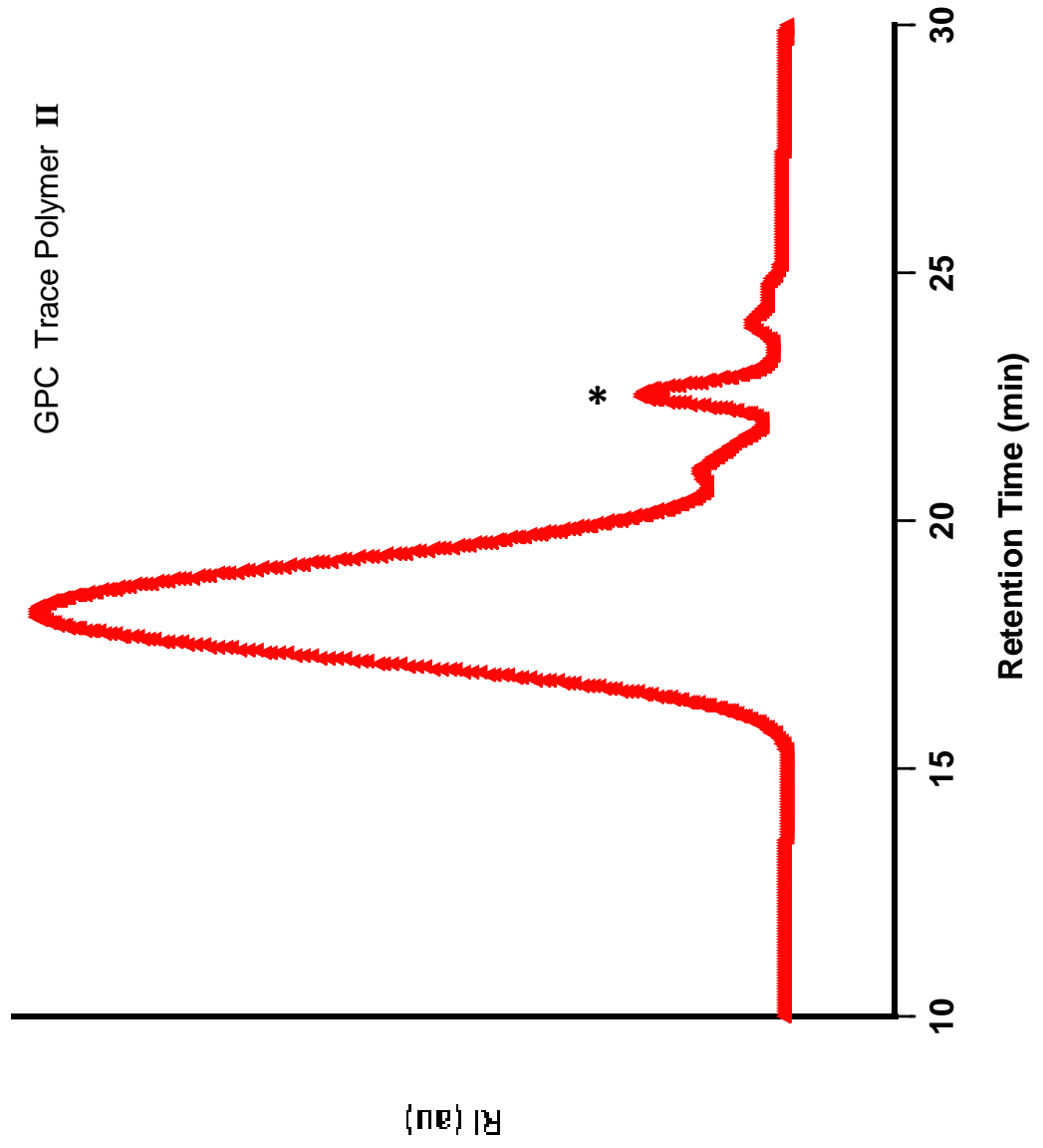


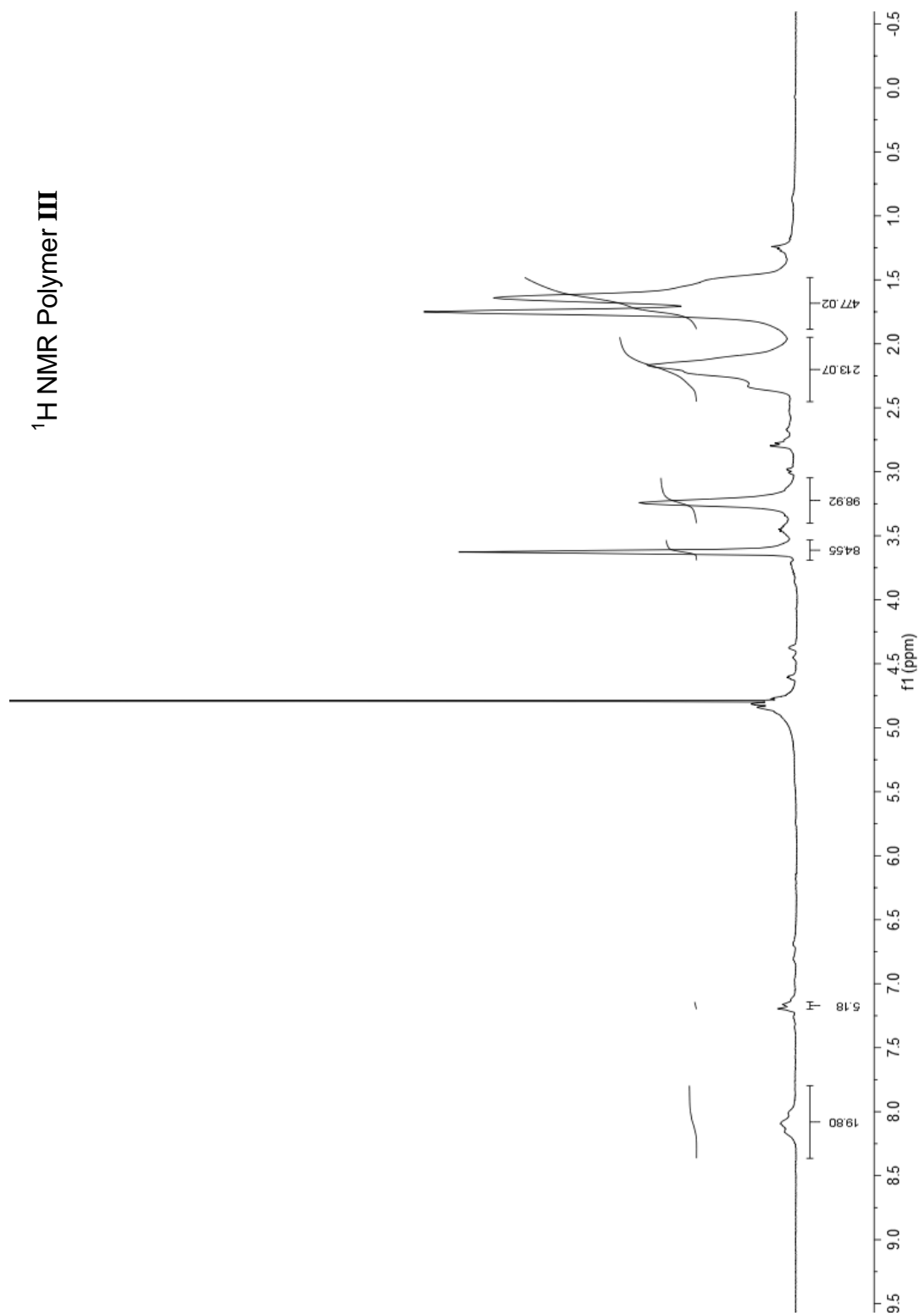




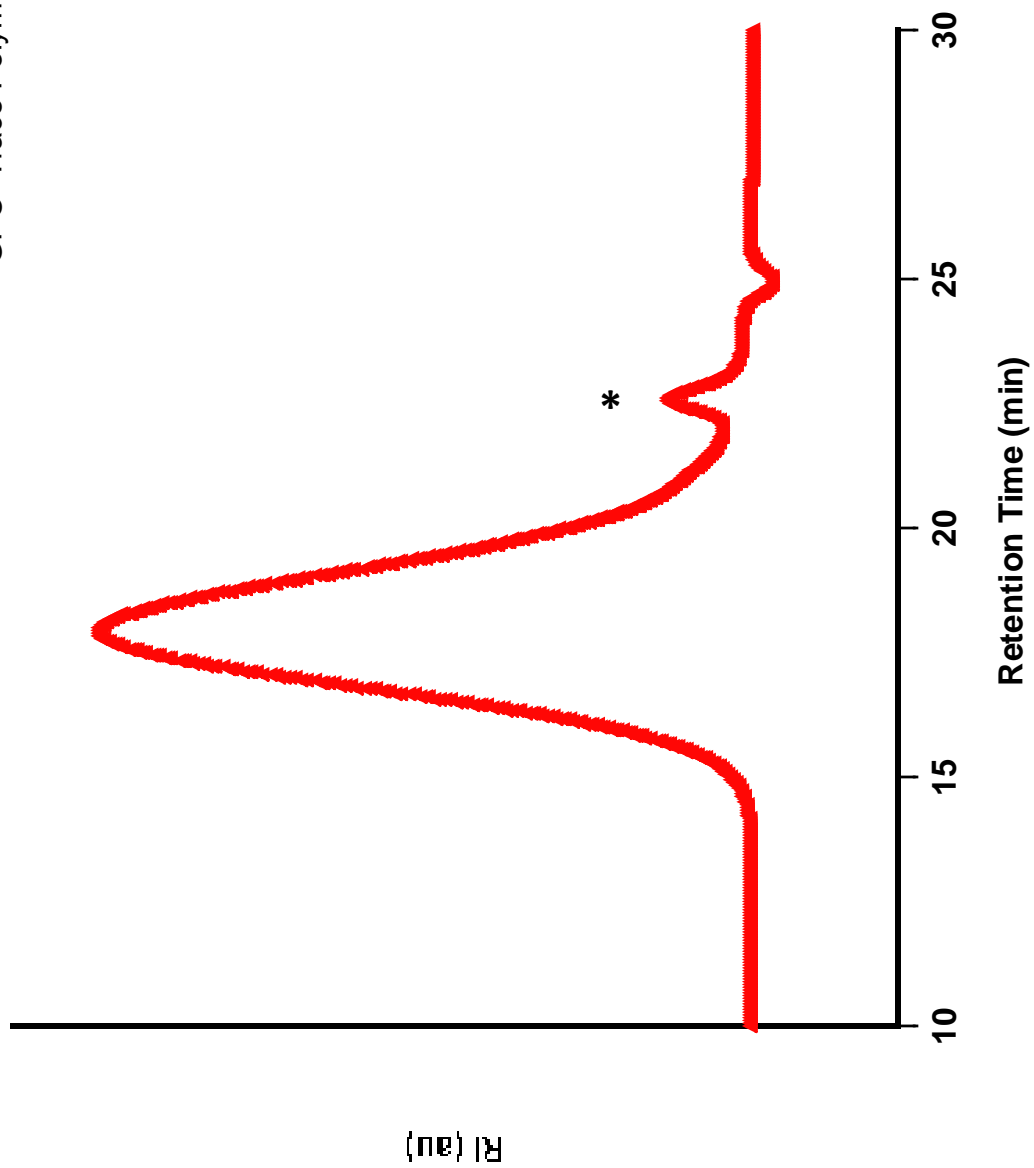
**<sup>1</sup>H NMR Polymer II**







GPC Trace Polymer III



## ***APPENDIX 2***

### ***PROTEOMICS DATA***

GNFGEL488\_AW01-33\_41\_LargeGel\_LTQ\_RatRevDB-converted  
(Membrane)

Identified Proteins	Accession Number	MW	FG	Ct
Tax_Id=10116 Gene_Symbol=Ania4 84 kDa protein	IPI:IPI00778626.1	84 kDa	9	0
Tax_Id=10116 Gene_Symbol=Rpn2 Dolichyl- diphosphooligosaccharide--protein glycosyltransferase 63 kDa subunit precursor	IPI:IPI00188059.2	69 kDa	9	0
Tax_Id=10116 Gene_Symbol=Eif3s6ip Eukaryotic translation initiation factor 3, subunit 6 interacting protein	IPI:IPI00366436.1	67 kDa	9	0
Tax_Id=10116 Gene_Symbol=Kif5b Kinesin heavy chain	IPI:IPI00364904.2	110 kDa	8	0
Tax_Id=10116 Gene_Symbol=Myo1b Isoform C of Myosin-Ib	IPI:IPI00231045.4 (+2)	125 kDa	8	0
Tax_Id=10116 Gene_Symbol=LOC360975 2- oxoglutarate dehydrogenase E1 component, mitochondrial precursor	IPI:IPI00215093.1 (+2)	116 kDa	8	0
Tax_Id=10116 Gene_Symbol=Rnpep Aminopeptidase B	IPI:IPI00193584.7	73 kDa	7	0
Tax_Id=10116 Gene_Symbol=Hspd1 60 kDa heat shock protein, mitochondrial precursor	IPI:IPI00339148.2	61 kDa	6	0
Tax_Id=10116 Gene_Symbol=Aars similar to alanyl- tRNA synthetase	IPI:IPI00363563.3	107 kDa	6	0
Tax_Id=10116 Gene_Symbol=Nars 64 kDa protein	IPI:IPI00565217.3	64 kDa	6	0
Tax_Id=10116 Gene_Symbol=Lrp1 similar to low density lipoprotein receptor-related protein 1	IPI:IPI00369995.2	505 kDa	6	0
Tax_Id=10116 Gene_Symbol=Tubb5 Isoform 1 of Tubulin beta-5 chain	IPI:IPI00197579.2	50 kDa	5	0
Tax_Id=10116 Gene_Symbol=Sv2a Synaptic vesicle glycoprotein 2A	IPI:IPI00208115.4 (+1)	83 kDa	5	0
Tax_Id=10116 Gene_Symbol=Hsph1 Heat shock protein 105 kDa	IPI:IPI00471835.1	96 kDa	5	0
Tax_Id=10116 Gene_Symbol=Nedd4a E3 ubiquitin- protein ligase NEDD4	IPI:IPI00766723.1	103 kDa	5	0
Tax_Id=10116 Gene_Symbol=Cyln2 CAP-Gly domain- containing linker protein 2	IPI:IPI00195929.1 (+1)	115 kDa	5	0
Tax_Id=10116 Gene_Symbol=LOC363309 similar to tubulin-specific chaperone d	IPI:IPI00765967.1	134 kDa	5	0
Tax_Id=10116 Gene_Symbol=Prmt5_predicted similar to protein arginine N-methyltransferase 5	IPI:IPI00359690.3	73 kDa	5	0
Tax_Id=10116 Gene_Symbol=Picalm Isoform 2 of	IPI:IPI00194958.1	65	5	0

Phosphatidylinositol-binding clathrin assembly protein	(+3)	kDa		
Tax_Id=10116 Gene_Symbol=Ipo7_predicted similar to Importin-7	IPI:IPI00206234.2 (+2)	120 kDa	5	0
Tax_Id=10116 Gene_Symbol=Sfpq Splicing factor proline/glutamine rich	IPI:IPI00627068.1 (+1)	75 kDa	5	0
Tax_Id=10116 Gene_Symbol=Xpnpep1 Xaa-Pro aminopeptidase 1	IPI:IPI00200054.1 (+1)	70 kDa	5	0
Tax_Id=10116 Gene_Symbol=Syn2 Isoform IIa of Synapsin-2	IPI:IPI00210036.1	63 kDa	5	0
Tax_Id=10116 Gene_Symbol=- 100 kDa protein	IPI:IPI00192076.3 (+2)	100 kDa	5	0
Tax_Id=10116 Gene_Symbol=Gucy1b3 Guanylate cyclase soluble subunit beta-1	IPI:IPI00324485.6	70 kDa	5	0
Tax_Id=10116 Gene_Symbol=Lphn1 Isoform 4 of Latrophilin-1 precursor	IPI:IPI00208999.1 (+3)	162 kDa	4	0
Tax_Id=10116 Gene_Symbol=Ctnna2_predicted similar to Alpha-2 catenin	IPI:IPI00364916.2 (+1)	100 kDa	4	0
Tax_Id=10116 Gene_Symbol=Prkce Protein kinase C epsilon type	IPI:IPI00551781.4	83 kDa	4	0
Tax_Id=10116 Gene_Symbol=Ctnnd1_predicted similar to Catenin delta-1	IPI:IPI00359491.3 (+2)	105 kDa	4	0
Tax_Id=10116 Gene_Symbol=Immt 82 kDa protein	IPI:IPI00364895.4 (+2)	82 kDa	4	0
Tax_Id=10116 Gene_Symbol=Khsrp Far upstream element-binding protein 2	IPI:IPI00200920.1	74 kDa	4	0
Tax_Id=10116 Gene_Symbol=Kars 68 kDa protein	IPI:IPI00363565.3 (+1)	68 kDa	4	0
Tax_Id=10116 Gene_Symbol=LOC682937 similar to WAS protein family, member 3	IPI:IPI00766566.1	55 kDa	4	0
Tax_Id=10116 Gene_Symbol=Gpd2 Glycerol-3-phosphate dehydrogenase, mitochondrial precursor	IPI:IPI00199663.1 (+1)	81 kDa	4	0
Tax_Id=10116 Gene_Symbol=LOC619561 Hypothetical protein LOC619561	IPI:IPI00203054.2	68 kDa	4	0
Tax_Id=10116 Gene_Symbol=Snx2_predicted similar to sorting nexin 2	IPI:IPI00363187.3 (+1)	59 kDa	4	0
Tax_Id=10116 Gene_Symbol=Lrrc47_predicted similar to leucine rich repeat containing 47	IPI:IPI00359172.2 (+1)	52 kDa	4	0
Tax_Id=10116 Gene_Symbol=Ubqln2_predicted similar to ubiquilin 2	IPI:IPI00362791.3	67 kDa	4	0
Tax_Id=10116 Gene_Symbol=Vac14 VAC14	IPI:IPI00230981.1	88 kDa	4	0
Tax_Id=10116 Gene_Symbol=Anxa6 Annexin A6	IPI:IPI00421888.3 (+1)	76 kDa	4	0
Tax_Id=10116 Gene_Symbol=Rap1ga1 similar to Rap1	IPI:IPI00359567.3	83	4	0

GTPase-activating protein 1		kDa		
Tax_Id=10116 Gene_Symbol=LOC367171 Microtubule-associated protein 4	IPI:IPI00393975.2 (+2)	110 kDa	3	0
Tax_Id=10116 Gene_Symbol=RGD1562629_predicted similar to Protein neurobeachin	IPI:IPI00567941.2	327 kDa	3	0
Tax_Id=10116 Gene_Symbol=Grlf1_predicted Glucocorticoid receptor DNA-binding factor 1	IPI:IPI00198211.2 (+1)	172 kDa	3	0
Tax_Id=10116 Gene_Symbol=Trim28 similar to Transcription intermediary factor 1-beta	IPI:IPI00194567.4 (+1)	89 kDa	3	0
Tax_Id=10116 Gene_Symbol=Eif4g1 175 kDa protein	IPI:IPI00370448.4 (+2)	175 kDa	3	0
Tax_Id=10116 Gene_Symbol=Mtap6 STOP protein	IPI:IPI00210119.1 (+3)	100 kDa	3	0
Tax_Id=10116 Gene_Symbol=Daam1_predicted similar to Disheveled-associated activator of morphogenesis 1	IPI:IPI00367408.3 (+2)	124 kDa	3	0
Tax_Id=10116 Gene_Symbol=Ripx Protein RUFY3	IPI:IPI00204065.1 (+2)	53 kDa	3	0
Tax_Id=10116 Gene_Symbol=RGD1309461 similar to NIK and IKK(beta) binding protein isoform 2	IPI:IPI00361094.4 (+1)	128 kDa	3	0
Tax_Id=10116 Gene_Symbol=Kpna1 Importin subunit alpha-1	IPI:IPI00395277.1 (+1)	60 kDa	3	0
Tax_Id=10116 Gene_Symbol=Sel1h Sel-1 homolog precursor	IPI:IPI00205606.3	89 kDa	3	0
Tax_Id=10116 Gene_Symbol=Uble1b similar to Ubiquitin-like 1-activating enzyme E1B	IPI:IPI00367235.3 (+1)	68 kDa	3	0
Tax_Id=10116 Gene_Symbol=Vcp Transitional endoplasmic reticulum ATPase	IPI:IPI00212014.2 (+1)	90 kDa	3	0
Tax_Id=10116 Gene_Symbol=Camk4 Isoform 1 of Calcium/calmodulin-dependent protein kinase type IV	IPI:IPI00231822.4	53 kDa	3	0
Tax_Id=10116 Gene_Symbol=Camk2b Calmodulin- dependent protein kinase II beta M isoform	IPI:IPI00209824.2 (+6)	73 kDa	3	0
Tax_Id=10116 Gene_Symbol=Farslb Phenylalanine- tRNA synthetase-like, beta subunit	IPI:IPI00202379.1	66 kDa	3	0
Tax_Id=10116 Gene_Symbol=Cdc16 CDC16 cell division cycle 16 homolog	IPI:IPI00190201.5	71 kDa	3	0
Tax_Id=10116 Gene_Symbol=LOC304743 Coiled-coil domain-containing protein 93	IPI:IPI00371846.2	73 kDa	3	0
Tax_Id=10116 Gene_Symbol=Gria2 Isoform Flip of Glutamate receptor 2 precursor	IPI:IPI00231061.5 (+2)	99 kDa	3	0
Tax_Id=10116 Gene_Symbol=Slc8a1 Isoform 1 of Sodium/calcium exchanger 1 precursor	IPI:IPI00206113.3 (+7)	108 kDa	3	0
Tax_Id=10116 Gene_Symbol=Srp68_predicted similar to signal recognition particle 68	IPI:IPI00368134.2	70 kDa	3	0
Tax_Id=10116 Gene_Symbol=Gsp1 G1 to S phase	IPI:IPI00368457.1	69	3	0

transition 1		kDa		
Tax_Id=10116 Gene_Symbol=Fchsd2_predicted similar to FCH and double SH3 domains 2	IPI:IPI00764114.1	144 kDa	3	0
Tax_Id=10116 Gene_Symbol=Cpsf6_predicted similar to cleavage and polyadenylation specific factor 6	IPI:IPI00366220.3 (+1)	59 kDa	3	0
Tax_Id=10116 Gene_Symbol=Igsf8 immunoglobulin superfamily, member 8	IPI:IPI00372709.3 (+1)	64 kDa	2	0
Tax_Id=10116 Gene_Symbol=Stk39 STE20/SPS1-related proline-alanine-rich protein kinase	IPI:IPI00210537.2	60 kDa	2	0
Tax_Id=10116 Gene_Symbol=Tfrc similar to transferrin receptor	IPI:IPI00363550.2	86 kDa	2	0
Tax_Id=10116 Gene_Symbol=Nova2_predicted 50 kDa protein	IPI:IPI00476817.3 (+1)	50 kDa	2	0
Tax_Id=10116 Gene_Symbol=Centg3_predicted similar to centaurin, gamma 3	IPI:IPI00358128.3 (+1)	102 kDa	2	0
Tax_Id=10116 Gene_Symbol=Ppp3cb Serine/threonine-protein phosphatase 2B catalytic subunit beta isoform	IPI:IPI00201407.1 (+4)	59 kDa	2	0
Tax_Id=10116 Gene_Symbol=Snx27 PDZ protein Mrt1a	IPI:IPI00203641.1	61 kDa	2	0
Tax_Id=10116 Gene_Symbol=Aco1 Iron-responsive element-binding protein 1	IPI:IPI00207003.1 (+1)	98 kDa	2	0
Tax_Id=10116 Gene_Symbol=Acadvl Very-long-chain specific acyl-CoA dehydrogenase, mitochondrial precursor	IPI:IPI00213057.2 (+1)	71 kDa	2	0
Tax_Id=10116 Gene_Symbol=G3bp similar to Ras-GTPase-activating protein binding protein 1	IPI:IPI00193648.2	59 kDa	2	0
Tax_Id=10116 Gene_Symbol=Cct8_predicted similar to T-complex protein 1 subunit theta	IPI:IPI00370815.3	60 kDa	2	0
Tax_Id=10116 Gene_Symbol=RGD1560544_predicted similar to Protein C11orf2	IPI:IPI00371469.4 (+2)	77 kDa	1	0
Tax_Id=10116 Gene_Symbol=Prkcb1 Isoform Beta-II of Protein kinase C beta type	IPI:IPI00189278.4 (+1)	77 kDa	1	0

GNFGEL498\_AW20-61\_NotIncl\_Gel3\_LTQ\_RatRevDB-converted  
(Membrane)

Identified Proteins	Accession Number	MW	FG	Ct
Tax_Id=10116 Gene_Symbol=Matr3 Matrin-3	IPI:IPI00555259.4	94 kDa	19	0
Tax_Id=10116 Gene_Symbol=Col6a3_predicted similar to alpha 3 type VI collagen isoform 1 precursor	IPI:IPI00565677.2	289 kDa	19	0
Tax_Id=10116 Gene_Symbol=Vim Vimentin	IPI:IPI00230941.5	54 kDa	14	0
Tax_Id=10116 Gene_Symbol=Kif1a similar to Kinesin-like protein KIF1A	IPI:IPI00559725.2 (+1)	190 kDa	13	0
Tax_Id=10116 Gene_Symbol=Flna_predicted similar to Filamin-A	IPI:IPI00409539.3	281 kDa	13	0
Tax_Id=10116 Gene_Symbol=- Copa protein	IPI:IPI00372458.2	138 kDa	12	0
Tax_Id=10116 Gene_Symbol=Myo1c myosin IC	IPI:IPI00393867.4	120 kDa	12	0
Tax_Id=10116 Gene_Symbol=Kif5c_predicted similar to kinesin family member 5C	IPI:IPI00193402.4	109 kDa	10	0
Tax_Id=10116 Gene_Symbol=Nef3 Neurofilament medium polypeptide	IPI:IPI00325609.4	96 kDa	10	0
Tax_Id=10116 Gene_Symbol=Bdh1 3-hydroxybutyrate dehydrogenase	IPI:IPI00480620.1	38 kDa	10	0
Tax_Id=10116 Gene_Symbol=RGD1305240_predicted similar to nodal modulator 1	IPI:IPI00365744.1	133 kDa	10	0
Tax_Id=10116 Gene_Symbol=Slc25a4 ADP/ATP translocase 1	IPI:IPI00231927.11	33 kDa	9	0
Tax_Id=10116 Gene_Symbol=Tcp1 T-complex protein 1 subunit alpha	IPI:IPI00200847.1	60 kDa	9	0
Tax_Id=10116 Gene_Symbol=Prkce Protein kinase C epsilon type	IPI:IPI00551781.4	83 kDa	9	0
Tax_Id=10116 Gene_Symbol=Col6a1_predicted similar to Collagen alpha-1(VI) chain precursor	IPI:IPI00371853.3	109 kDa	9	0
Tax_Id=10116 Gene_Symbol=Copb2 Coatomer subunit beta'	IPI:IPI00231953.10	103 kDa	9	0
Tax_Id=10116 Gene_Symbol=Dhx9_predicted similar to ATP-dependent RNA helicase A	IPI:IPI00366249.4	150 kDa	9	0
Tax_Id=10116 Gene_Symbol=Plec1 Plectin 10	IPI:IPI00569024.2	518 kDa	8	0
Tax_Id=10116 Gene_Symbol=Spg3a Atlastin-like protein	IPI:IPI00421909.3	63 kDa	8	0
Tax_Id=10116 Gene_Symbol=Atp1a2 Sodium/potassium-transporting ATPase subunit alpha-2 precursor	IPI:IPI00205693.1	112 kDa	7	0
Tax_Id=10116 Gene_Symbol=Atp2b2 Isoform WB of	IPI:IPI00194875.1	137	7	0

Plasma membrane calcium-transporting ATPase 2	(+3)	kDa		
Tax_Id=10116 Gene_Symbol=Slc25a3 Slc25a3 protein	IPI:IPI00209115.2	40 kDa	7	0
Tax_Id=10116 Gene_Symbol=Eprs 170 kDa protein	IPI:IPI00421357.2 (+1)	170 kDa	7	0
Tax_Id=10116 Gene_Symbol=Usp9x_predicted similar to Probable ubiquitin carboxyl-terminal hydrolase FAF-X (Ubiquitin thioesterase FAF-X) (Ubiquitin-specific-processing protease FAF-X) (Deubiquitinating enzyme FAF-X) (Fat facets protein-related, X-linked) (Ubiquitin-specific protease 9, X c	IPI:IPI00204923.4 (+1)	291 kDa	7	0
Tax_Id=10116 Gene_Symbol=Eftud2 similar to 116 kDa U5 small nuclear ribonucleoprotein component	IPI:IPI00370117.3	109 kDa	7	0
Tax_Id=10116 Gene_Symbol=Abce1 similar to ATP-binding cassette sub-family E member 1	IPI:IPI00193816.2	67 kDa	7	0
Tax_Id=10116 Gene_Symbol=Ckap5 similar to cytoskeleton associated protein 5 isoform 1	IPI:IPI00764313.1 (+3)	223 kDa	7	0
Tax_Id=10116 Gene_Symbol=Ywhae 14-3-3 protein epsilon	IPI:IPI00325135.3	29 kDa	7	0
Tax_Id=10116 Gene_Symbol=Ddx1 ATP-dependent RNA helicase DDX1	IPI:IPI00555314.1	82 kDa	7	0
Tax_Id=10116 Gene_Symbol=Lars Leucyl-tRNA synthetase	IPI:IPI00363236.2	134 kDa	6	0
Tax_Id=10116 Gene_Symbol=Capzb F-actin capping protein subunit beta	IPI:IPI00365283.1	31 kDa	6	0
Tax_Id=10116 Gene_Symbol=Atp5c1 ATP synthase gamma chain	IPI:IPI00454288.1	68 kDa	6	0
Tax_Id=10116 Gene_Symbol=Slc25a11 Mitochondrial 2-oxoglutarate/malate carrier protein	IPI:IPI00231261.7	34 kDa	6	0
Tax_Id=10116 Gene_Symbol=Slc25a5 ADP/ATP translocase 2	IPI:IPI00200466.3	33 kDa	6	0
Tax_Id=10116 Gene_Symbol=LOC315676 similar to Dmx-like 2	IPI:IPI00369671.3	344 kDa	6	0
Tax_Id=10116 Gene_Symbol=Cul5 Cullin-5	IPI:IPI00325517.5	91 kDa	6	0
Tax_Id=10116 Gene_Symbol=Gria2 103 kDa protein	IPI:IPI00780113.1	103 kDa	6	0
Tax_Id=10116 Gene_Symbol=Pde10a PDE10A2	IPI:IPI00561300.1	90 kDa	6	0
Tax_Id=10116 Gene_Symbol=Idh3g Isocitrate dehydrogenase [NAD] subunit gamma, mitochondrial precursor	IPI:IPI00194047.3	43 kDa	6	0
Tax_Id=10116 Gene_Symbol=- 102 kDa protein	IPI:IPI00366397.2	102 kDa	6	0
Tax_Id=10116 Gene_Symbol=Strn3 Isoform 1 of Striatin-3	IPI:IPI00760130.2 (+1)	87 kDa	6	0

Tax_Id=10116 Gene_Symbol=Ywhaz 14-3-3 protein zeta/delta	IPI:IPI00324893.4	28 kDa	5	0
Tax_Id=10116 Gene_Symbol=Alg2 similar to Alpha-1,3-mannosyltransferase ALG2	IPI:IPI00367294.2	47 kDa	5	0
Tax_Id=10116 Gene_Symbol=Eif3s10 ZH12 protein	IPI:IPI00372810.4	162 kDa	5	0
Tax_Id=10116 Gene_Symbol=Ctnna2_predicted similar to Alpha-2 catenin	IPI:IPI00364916.2 (+1)	100 kDa	5	0
Tax_Id=10116 Gene_Symbol=Nars 64 kDa protein	IPI:IPI00565217.3	64 kDa	5	0
Tax_Id=10116 Gene_Symbol=Cyln2 111 kDa protein	IPI:IPI00476704.1	111 kDa	5	0
Tax_Id=10116 Gene_Symbol=Dync1li1 Cytoplasmic dynein 1 light intermediate chain 1	IPI:IPI00213552.1	57 kDa	5	0
Tax_Id=10116 Gene_Symbol=Tardbp 45 kDa protein	IPI:IPI00191216.1	45 kDa	5	0
Tax_Id=10116 Gene_Symbol=Dhcr7 7-dehydrocholesterol reductase	IPI:IPI00210431.1	54 kDa	5	0
Tax_Id=10116 Gene_Symbol=LOC362012 similar to Protein FAM40A	IPI:IPI00373402.3 (+3)	99 kDa	5	0
Tax_Id=10116 Gene_Symbol=Ybx1 Ybx1 protein	IPI:IPI00551815.2 (+2)	36 kDa	5	0
Tax_Id=10116 Gene_Symbol=RGD1565486_predicted similar to RNA binding motif protein 25	IPI:IPI00765889.1 (+1)	96 kDa	5	0
Tax_Id=10116 Gene_Symbol=Atp2b4 Isoform XA of Plasma membrane calcium-transporting ATPase 4	IPI:IPI00230910.1 (+1)	129 kDa	5	0
Tax_Id=10116 Gene_Symbol=LOC360975 2-oxoglutarate dehydrogenase E1 component, mitochondrial precursor	IPI:IPI00215093.1 (+2)	116 kDa	5	0
Tax_Id=10116 Gene_Symbol=Ndufa9 similar to NADH dehydrogenase (ubiquinone) 1 alpha subcomplex, 9	IPI:IPI00358441.1	43 kDa	5	0
Tax_Id=10116 Gene_Symbol=Qars Glutaminyl-tRNA synthetase	IPI:IPI00362720.1	88 kDa	5	0
Tax_Id=10116 Gene_Symbol=Fmo1 Dimethylaniline monooxygenase [N-oxide-forming] 1	IPI:IPI00201564.4	60 kDa	5	0
Tax_Id=10116 Gene_Symbol=Aacs Acetoacetyl-CoA synthetase	IPI:IPI00204738.1	75 kDa	5	0
Tax_Id=10116 Gene_Symbol=Cul1_predicted similar to Cullin-1	IPI:IPI00358206.2	90 kDa	5	0
Tax_Id=10116 Gene_Symbol=- 100 kDa protein	IPI:IPI00192076.3 (+2)	100 kDa	5	0
Tax_Id=10116 Gene_Symbol=Slc1a3 Isoform GLAST-1 of Excitatory amino acid transporter 1	IPI:IPI00324377.1	60 kDa	4	0
Tax_Id=10116 Gene_Symbol=Synj1 similar to Synptojanin-1	IPI:IPI00210153.3 (+3)	173 kDa	4	0
Tax_Id=10116 Gene_Symbol=Ddost_predicted	IPI:IPI00471645.1	49 kDa	4	0

Dolichyl-di-phosphooligosaccharide-protein glycotransferase		kDa		
Tax_Id=10116 Gene_Symbol=Ywhab Isoform Long of 14-3-3 protein beta/alpha	IPI:IPI00230837.5 (+1)	28 kDa	4	0
Tax_Id=10116 Gene_Symbol=P4hb Protein disulfide-isomerase precursor	IPI:IPI00198887.1	57 kDa	4	0
Tax_Id=10116 Gene_Symbol=Ikbkap Elongator complex protein 1	IPI:IPI00389755.1	149 kDa	4	0
Tax_Id=10116 Gene_Symbol=Col1a2 Collagen alpha-2(I) chain precursor	IPI:IPI00188921.1	130 kDa	4	0
Tax_Id=10116 Gene_Symbol=Sec23a_predicted similar to Protein transport protein Sec23A	IPI:IPI00207738.2	87 kDa	4	0
Tax_Id=10116 Gene_Symbol=Ndufs2 NADH dehydrogenase (Ubiquinone) Fe-S protein 2	IPI:IPI00471647.1	53 kDa	4	0
Tax_Id=10116 Gene_Symbol=RGD1307525_predicted similar to Temporarily Assigned Gene name family member	IPI:IPI00358840.3 (+2)	179 kDa	4	0
Tax_Id=10116 Gene_Symbol=Hmgcs2 Hydroxymethylglutaryl-CoA synthase, mitochondrial precursor	IPI:IPI00210444.5	57 kDa	4	0
Tax_Id=10116 Gene_Symbol=Ctnnd2 similar to Catenin delta-2	IPI:IPI00553941.3 (+1)	134 kDa	4	0
Tax_Id=10116 Gene_Symbol=Emilin1_predicted similar to elastin microfibril interfacier 1	IPI:IPI00199867.1	108 kDa	4	0
Tax_Id=10116 Gene_Symbol=Lap3 Isoform 1 of Cytosol aminopeptidase	IPI:IPI00471530.2 (+1)	56 kDa	4	0
Tax_Id=10116 Gene_Symbol=Pdhb Pyruvate dehydrogenase E1 component subunit beta, mitochondrial precursor	IPI:IPI00194324.2	39 kDa	4	0
Tax_Id=10116 Gene_Symbol=Etfb Electron transfer flavoprotein subunit beta	IPI:IPI00364321.3	28 kDa	4	0
Tax_Id=10116 Gene_Symbol=Hnrpm Isoform 1 of Heterogeneous nuclear ribonucleoprotein M	IPI:IPI00209148.5 (+1)	74 kDa	4	0
Tax_Id=10116 Gene_Symbol=Acaa2 3-ketoacyl-CoA thiolase, mitochondrial	IPI:IPI00201413.1	42 kDa	4	0
Tax_Id=10116 Gene_Symbol=Sfxn1 Sideroflexin-1	IPI:IPI00213735.3 (+1)	36 kDa	4	0
Tax_Id=10116 Gene_Symbol=LOC681996 similar to AHA1, activator of heat shock 90kDa protein ATPase homolog 1 isoform 2	IPI:IPI00766463.1 (+1)	38 kDa	4	0
Tax_Id=10116 Gene_Symbol=Phyhipl 42 kDa protein	IPI:IPI00361492.2	42 kDa	4	0
Tax_Id=10116 Gene_Symbol=Vdac1 Voltage-dependent anion-selective channel protein 1	IPI:IPI00421874.4	31 kDa	4	0
Tax_Id=10116 Gene_Symbol=Vac14 VAC14	IPI:IPI00230981.1	88 kDa	4	0

Tax_Id=10116 Gene_Symbol=Mthfd1l_predicted similar to methylenetetrahydrofolate dehydrogenase (NADP+ dependent) 1-like	IPI:IPI00365405.3	106 kDa	4	0
Tax_Id=10116 Gene_Symbol=RGD1566215_predicted similar to Coatomer gamma-2 subunit	IPI:IPI00767794.1	98 kDa	4	0
Tax_Id=10116 Gene_Symbol=Sf3b3_predicted similar to splicing factor 3b, subunit 3	IPI:IPI00363568.3	114 kDa	4	0
Tax_Id=10116 Gene_Symbol=Rps3 40S ribosomal protein S3	IPI:IPI00212776.1	27 kDa	4	0
Tax_Id=10116 Gene_Symbol=Centg3_predicted similar to centaurin, gamma 3	IPI:IPI00358128.3	102 kDa	4	0
Tax_Id=10116 Gene_Symbol=Txndc1 Thioredoxin domain containing 1	IPI:IPI00365626.3	31 kDa	4	0
Tax_Id=10116 Gene_Symbol=Galk1 Galactokinase 1	IPI:IPI00188671.1	42 kDa	4	0
Tax_Id=10116 Gene_Symbol=Exoc8 Exocyst complex component 8	IPI:IPI00199846.1	81 kDa	4	0
Tax_Id=10116 Gene_Symbol=Sarm1_predicted similar to sterile alpha and TIR motif containing 1	IPI:IPI00369913.2	80 kDa	4	0
Tax_Id=10116 Gene_Symbol=Ayt12_predicted 1-acylglycerophosphocholine O-acyltransferase 1	IPI:IPI00365394.2 (+1)	60 kDa	4	0
Tax_Id=10116 Gene_Symbol=Nnt 76 kDa protein	IPI:IPI00390435.1 (+1)	76 kDa	4	0
Tax_Id=10116 Gene_Symbol=Bgn Biglycan precursor	IPI:IPI00191090.1	42 kDa	4	0
Tax_Id=10116 Gene_Symbol=Serpinh1 Serpin H1 precursor	IPI:IPI00204703.5	47 kDa	4	0
Tax_Id=10116 Gene_Symbol=Fdft1 Squalene synthetase	IPI:IPI00210233.1	48 kDa	4	0
Tax_Id=10116 Gene_Symbol=Nid2 similar to nidogen 2 isoform 2	IPI:IPI00372786.5 (+1)	153 kDa	4	0
Tax_Id=10116 Gene_Symbol=Ap3b2_predicted similar to adaptor-related protein complex 3, beta 2 subunit	IPI:IPI00368200.2 (+1)	124 kDa	4	0
Tax_Id=10116 Gene_Symbol=Ywhah 14-3-3 protein eta	IPI:IPI00231677.5	28 kDa	4	0
Tax_Id=10116 Gene_Symbol=Suclg2 similar to succinate-Coenzyme A ligase, GDP-forming, beta subunit isoform 4	IPI:IPI00471539.4 (+4)	47 kDa	4	0
Tax_Id=10116 Gene_Symbol=RGD1306534_predicted similar to Phosphatidylinositol 3,4,5-trisphosphate-dependent Rac exchanger 1 protein	IPI:IPI00365036.4	185 kDa	4	0
Tax_Id=10116 Gene_Symbol=Abr_predicted similar to active BCR-related gene isoform 3	IPI:IPI00370314.2	98 kDa	3	0
Tax_Id=10116 Gene_Symbol=Gna13 Galpha13	IPI:IPI00422053.1	44 kDa	3	0
Tax_Id=10116 Gene_Symbol=RGD1309586_predicted	IPI:IPI00196210.3	73 kDa	3	0

similar to Putative ATP-dependent RNA helicase Pl10	(+1)	kDa		
Tax_Id=10116 Gene_Symbol=Crat Carnitine O-acetyltransferase	IPI:IPI00360158.4	72 kDa	3	0
Tax_Id=10116 Gene_Symbol=Gnai1 Guanine nucleotide-binding protein G(i), alpha-1 subunit	IPI:IPI00231733.7	40 kDa	3	0
Tax_Id=10116 Gene_Symbol=LOC296318 Similar to Ndr3 protein	IPI:IPI00464777.1 (+2)	42 kDa	3	0
Tax_Id=10116 Gene_Symbol=Cadps Calcium-dependent secretion activator 1	IPI:IPI00199577.5 (+2)	146 kDa	3	0
Tax_Id=10116 Gene_Symbol=Snx6_predicted similar to sorting nexin 6	IPI:IPI00365613.2	47 kDa	3	0
Tax_Id=10116 Gene_Symbol=Arhgap1_predicted similar to Rho GTPase activating protein 1	IPI:IPI00363427.3	55 kDa	3	0
Tax_Id=10116 Gene_Symbol=Atp1b3 Sodium/potassium-transporting ATPase subunit beta-3	IPI:IPI00208061.3	32 kDa	3	0
Tax_Id=10116 Gene_Symbol=Gsk3a Glycogen synthase kinase-3 alpha	IPI:IPI00189904.1	51 kDa	3	0
Tax_Id=10116 Gene_Symbol=Pdcd6ip similar to Programmed cell death 6-interacting protein	IPI:IPI00767837.1	97 kDa	3	0
Tax_Id=10116 Gene_Symbol=Map2k1 Dual specificity mitogen-activated protein kinase kinase 1	IPI:IPI00231247.9	43 kDa	3	0
Tax_Id=10116 Gene_Symbol=Gls Glutaminase kidney isoform, mitochondrial precursor	IPI:IPI00199465.1	74 kDa	3	0
Tax_Id=10116 Gene_Symbol=Slc25a20 Mitochondrial carnitine/acylcarnitine carrier protein	IPI:IPI00205413.1 (+1)	33 kDa	3	0
Tax_Id=10116 Gene_Symbol=Lancl2_predicted LanC (Bacterial lantibiotic synthetase component C)-like 2	IPI:IPI00192484.2	51 kDa	3	0
Tax_Id=10116 Gene_Symbol=Scfd1 Sec1 family domain-containing protein 1	IPI:IPI00210389.1 (+1)	72 kDa	3	0
Tax_Id=10116 Gene_Symbol=Dncli2 Cytoplasmic dynein 1 light intermediate chain 2	IPI:IPI00207202.1 (+1)	55 kDa	3	0
Tax_Id=10116 Gene_Symbol=Psat1 Phosphoserine aminotransferase	IPI:IPI00331919.5	41 kDa	3	0
Tax_Id=10116 Gene_Symbol=Clptm1_predicted similar to cleft lip and palate associated transmembrane protein 1	IPI:IPI00193869.1 (+1)	75 kDa	3	0
Tax_Id=10116 Gene_Symbol=Acsl3 Isoform Long of Long-chain-fatty-acid--CoA ligase 3	IPI:IPI00205908.1 (+1)	80 kDa	3	0
Tax_Id=10116 Gene_Symbol=Gnb1 Guanine nucleotide-binding protein G(I)/G(S)/G(T) subunit beta 1	IPI:IPI00212655.4	37 kDa	3	0
Tax_Id=10116 Gene_Symbol=Cndp2 Cytosolic non-specific dipeptidase	IPI:IPI00421899.1 (+1)	53 kDa	3	0
Tax_Id=10116 Gene_Symbol=Syn2 Isoform Ila of Synapsin-2	IPI:IPI00210036.1 (+1)	63 kDa	3	0

Tax_Id=10116 Gene_Symbol=Eef1b2_predicted similar to eukaryotic translation elongation factor 1 beta 2	IPI:IPI00476899.1	25 kDa	3	0
Tax_Id=10116 Gene_Symbol=Vat1 Vesicle amine transport protein 1 homolog	IPI:IPI00201969.1	43 kDa	3	0
Tax_Id=10116 Gene_Symbol=Col1a1 Collagen alpha-1(I) chain precursor	IPI:IPI00188909.2 (+2)	138 kDa	3	0
Tax_Id=10116 Gene_Symbol=Prkcsh_predicted similar to Glucosidase II beta subunit precursor	IPI:IPI00388209.2 (+1)	59 kDa	3	0
Tax_Id=10116 Gene_Symbol=Slc8a1 Isoform 1 of Sodium/calcium exchanger 1 precursor	IPI:IPI00206113.3 (+7)	108 kDa	3	0
Tax_Id=10116 Gene_Symbol=Ap3d1 similar to adaptor-related protein complex 3, delta 1 subunit	IPI:IPI00198486.3	136 kDa	3	0
Tax_Id=10116 Gene_Symbol=Cope_predicted similar to epsilon subunit of coatomer protein complex	IPI:IPI00201137.1	35 kDa	3	0
Tax_Id=10116 Gene_Symbol=MGC93997 Similar to PRUNEM1	IPI:IPI00368646.1	50 kDa	3	0
Tax_Id=10116 Gene_Symbol=Psmc3 Proteasome (Prosome, macropain) 26S subunit, non-ATPase, 3	IPI:IPI00370009.1	61 kDa	3	0
Tax_Id=10116 Gene_Symbol=Pde2a cGMP-dependent 3',5'-cyclic phosphodiesterase	IPI:IPI00199076.2 (+3)	105 kDa	3	0
Tax_Id=10116 Gene_Symbol=Pck2_predicted similar to mitochondrial phosphoenolpyruvate carboxykinase 2	IPI:IPI00388232.4	83 kDa	3	0
Tax_Id=10116 Gene_Symbol=RGD1305915 similar to SVH protein	IPI:IPI00372341.3 (+2)	33 kDa	3	0
Tax_Id=10116 Gene_Symbol=Hsd17b12 Estradiol 17-beta-dehydrogenase 12	IPI:IPI00208645.6 (+1)	35 kDa	3	0
Tax_Id=10116 Gene_Symbol=Scamp3 similar to Secretory carrier-associated membrane protein 3	IPI:IPI00206037.6 (+2)	39 kDa	3	0
Tax_Id=10116 Gene_Symbol=Nlgn2 Isoform 1 of Neuroligin-2 precursor	IPI:IPI00209308.1 (+1)	91 kDa	3	0
Tax_Id=10116 Gene_Symbol=Eif3s6 Eukaryotic translation initiation factor 3 subunit 6	IPI:IPI00366398.2	52 kDa	3	0
Tax_Id=10116 Gene_Symbol=Stch Stress 70 protein chaperone microsomal-associated 60 kDa protein precursor	IPI:IPI00206300.2	52 kDa	3	0
Tax_Id=10116 Gene_Symbol=Kif3b_predicted similar to Kinesin-like protein KIF3B (Microtubule plus end-directed kinesin motor 3B) isoform 2	IPI:IPI00765754.1 (+1)	85 kDa	3	0
Tax_Id=10116 Gene_Symbol=Prpf40a_predicted similar to Pre-mRNA-processing factor 40 homolog A	IPI:IPI00372759.3	109 kDa	3	0
Tax_Id=10116 Gene_Symbol=Gna11 Guanine nucleotide-binding protein alpha-11 subunit	IPI:IPI00200437.1	42 kDa	3	0
Tax_Id=10116 Gene_Symbol=Vps16 Vacuolar protein sorting 16	IPI:IPI00471668.2	95 kDa	3	0

Tax_Id=10116 Gene_Symbol=Trim2 similar to tripartite motif protein TRIM2	IPI:IPI00373220.4 (+2)	87 kDa	3	0
Tax_Id=10116 Gene_Symbol=Ranbp1_predicted similar to Ran-specific GTPase-activating protein	IPI:IPI00363569.3	24 kDa	3	0
Tax_Id=10116 Gene_Symbol=Eif3s4 Eukaryotic translation initiation factor 3, subunit 4	IPI:IPI00365487.2	36 kDa	3	0
Tax_Id=10116 Gene_Symbol=Ptpn23 162 kDa protein	IPI:IPI00214150.2 (+1)	162 kDa	3	0
Tax_Id=10116 Gene_Symbol=Madd MAP kinase-activating death domain protein	IPI:IPI00196614.1 (+4)	178 kDa	3	0
Tax_Id=10116 Gene_Symbol=Arbp 60S acidic ribosomal protein P0	IPI:IPI00200147.1	34 kDa	3	0
Tax_Id=10116 Gene_Symbol=Dscr3_predicted similar to Down syndrome critical region protein 3 homolog (Down syndrome critical region protein A homolog) isoform 1	IPI:IPI00763791.1	33 kDa	3	0
Tax_Id=10116 Gene_Symbol=Kb2 Keratin, type II cytoskeletal 2 epidermal	IPI:IPI00551558.2 (+1)	69 kDa	2	0
Tax_Id=10116 Gene_Symbol=RGD1309571 Similar to RNA-binding protein isoform G3BP-2a	IPI:IPI00464529.1 (+1)	51 kDa	2	0
Tax_Id=10116 Gene_Symbol=Marcksl1 MARCKS-related protein	IPI:IPI00189061.3	20 kDa	2	0
Tax_Id=10116 Gene_Symbol=Hsph1 Heat shock protein 105 kDa	IPI:IPI00471835.1 (+3)	96 kDa	2	0
Tax_Id=10116 Gene_Symbol=Kb4 Keratin, type II cytoskeletal 4	IPI:IPI00421778.1	58 kDa	2	0
Tax_Id=10116 Gene_Symbol=Robo2 Robo2 (Fragment)	IPI:IPI00215029.1 (+1)	117 kDa	2	0
Tax_Id=10116 Gene_Symbol=Adsl_predicted similar to adenylosuccinate lyase	IPI:IPI00361216.2	55 kDa	2	0
Tax_Id=10116 Gene_Symbol=Prg-2 Plasticity-related protein PRG-2	IPI:IPI00382123.1	77 kDa	2	0
Tax_Id=10116 Gene_Symbol=Aldh6a1 Methylmalonate-semialdehyde dehydrogenase [acylating], mitochondrial precursor	IPI:IPI00205018.2	58 kDa	2	0
Tax_Id=10116 Gene_Symbol=Ppp3ca Isoform 1 of Serine/threonine-protein phosphatase 2B catalytic subunit alpha isoform	IPI:IPI00201410.1 (+1)	59 kDa	2	0
Tax_Id=10116 Gene_Symbol=Tuba6 Tubulin alpha-1C chain	IPI:IPI00364046.2	50 kDa	2	0
Tax_Id=10116 Gene_Symbol=Kab 174 kDa protein	IPI:IPI00776774.1	174 kDa	2	0
Tax_Id=10116 Gene_Symbol=Farp1_predicted similar to FERMRhoGEF (Arhgef) and pleckstrin domain protein 1	IPI:IPI00373724.3 (+1)	164 kDa	2	0
Tax_Id=10116 Gene_Symbol=Bat3 Large proline-rich	IPI:IPI00203181.2	115	2	0

protein BAT3	(+1)	kDa		
Tax_Id=10116 Gene_Symbol=Txnl2 Isoform 1 of Thioredoxin-like protein 2	IPI:IPI00553899.1	38 kDa	2	0
Tax_Id=10116 Gene_Symbol=Gucy1a3 Guanylate cyclase soluble subunit alpha-3	IPI:IPI00851136.1	78 kDa	2	0
Tax_Id=10116 Gene_Symbol=Cdk5 Cell division protein kinase 5	IPI:IPI00231092.3	33 kDa	2	0
Tax_Id=10116 Gene_Symbol=Sucla2_predicted similar to succinate-Coenzyme A ligase, ADP-forming, beta subunit	IPI:IPI00364431.2	50 kDa	2	0
Tax_Id=10116 Gene_Symbol=Sqstm1 Isoform 1 of Sequestosome-1	IPI:IPI00194561.1 (+2)	48 kDa	2	0
Tax_Id=10116 Gene_Symbol=Vdp General vesicular transport factor p115	IPI:IPI00324618.3	107 kDa	2	0
Tax_Id=10116 Gene_Symbol=Sccpdh Probable saccharopine dehydrogenase	IPI:IPI00372804.2 (+1)	47 kDa	2	0
Tax_Id=10116 Gene_Symbol=Bcat1 Branched-chain-amino-acid aminotransferase, cytosolic	IPI:IPI00215523.1 (+1)	46 kDa	2	0
Tax_Id=10116 Gene_Symbol=Ywhag 14-3-3 protein gamma	IPI:IPI00230835.5	28 kDa	2	0
Tax_Id=10116 Gene_Symbol=Hsd11 Hydroxysteroid dehydrogenase like 1	IPI:IPI00365202.1	37 kDa	2	0
Tax_Id=10116 Gene_Symbol=RGD1307235_predicted hypothetical protein	IPI:IPI00360079.4	135 kDa	2	0
Tax_Id=10116 Gene_Symbol=Snx2_predicted similar to sorting nexin 2	IPI:IPI00769194.1	74 kDa	2	0
Tax_Id=10116 Gene_Symbol=Col6a2 similar to procollagen, type VI, alpha 2	IPI:IPI00372839.3	110 kDa	2	0
Tax_Id=10116 Gene_Symbol=Dnpep Aspartyl aminopeptidase	IPI:IPI00358059.2	53 kDa	2	0
Tax_Id=10116 Gene_Symbol=Epm2aip1_predicted similar to EPM2A (laforin) interacting protein 1	IPI:IPI00371118.3 (+1)	70 kDa	2	0
Tax_Id=10116 Gene_Symbol=Actn1 Alpha-actinin-1	IPI:IPI00209082.1 (+3)	103 kDa	2	0
Tax_Id=10116 Gene_Symbol=Bzw1 Basic leucine zipper and W2 domain-containing protein 1	IPI:IPI00366953.1	48 kDa	2	0
Tax_Id=10116 Gene_Symbol=Ruvbl2 RuvB-like 2	IPI:IPI00364340.2	51 kDa	2	0
Tax_Id=10116 Gene_Symbol=Eif2s2 Eukaryotic translation initiation factor 2, subunit 2	IPI:IPI00373164.1	38 kDa	2	0
Tax_Id=10116 Gene_Symbol=RGD1559864_predicted 45 kDa protein	IPI:IPI00560515.2	45 kDa	2	0
Tax_Id=10116 Gene_Symbol=Capza2 F-actin capping protein subunit alpha-2	IPI:IPI00370681.1	33 kDa	2	0
Tax_Id=10116 Gene_Symbol=Rpl5 60S ribosomal protein L5	IPI:IPI00230914.5 (+1)	34 kDa	2	0

Tax_Id=10116 Gene_Symbol=Ptprrd Leukocyte common antigen-related phosphatase precursor	IPI:IPI00214375.1 (+1)	207 kDa	2	0
Tax_Id=10116 Gene_Symbol=Cars_predicted similar to Cysteinyl-tRNA synthetase	IPI:IPI00371408.2	95 kDa	2	0
Tax_Id=10116 Gene_Symbol=Dnm2 Isoform IIBA of Dynamin-2	IPI:IPI00210319.2 (+2)	98 kDa	2	0
Tax_Id=10116 Gene_Symbol=Sgpl1 Sphingosine-1-phosphate lyase 1	IPI:IPI00193172.1	64 kDa	2	0
Tax_Id=10116 Gene_Symbol=Srp68_predicted similar to signal recognition particle 68	IPI:IPI00368134.2	70 kDa	2	0
Tax_Id=10116 Gene_Symbol=Fus Fusion, derived from t(12;16) malignant liposarcoma	IPI:IPI00362587.3	53 kDa	2	0
Tax_Id=10116 Gene_Symbol=Itsn1 similar to Intersectin-1	IPI:IPI00554196.3	194 kDa	2	0
Tax_Id=10116 Gene_Symbol=Hnrpl Hnrpl protein	IPI:IPI00364061.4 (+1)	64 kDa	2	0
Tax_Id=10116 Gene_Symbol=Irgq_predicted similar to FKSG27	IPI:IPI00367047.3	59 kDa	2	0
Tax_Id=10116 Gene_Symbol=- Ab2-076	IPI:IPI00382233.1 (+1)	103 kDa	2	0
Tax_Id=10116 Gene_Symbol=Tnpo2_predicted similar to transportin 2	IPI:IPI00205920.4	101 kDa	2	0
Tax_Id=10116 Gene_Symbol=Unr Cold shock domain-containing protein E1	IPI:IPI00190971.1 (+1)	89 kDa	2	0
Tax_Id=10116 Gene_Symbol=Rph3a Rabphilin-3A	IPI:IPI00189927.1 (+1)	76 kDa	2	0
Tax_Id=10116 Gene_Symbol=Wdr7 Isoform 1 of WD repeat protein 7	IPI:IPI00190963.1 (+1)	163 kDa	2	0
Tax_Id=10116 Gene_Symbol=Pabpc1 Polyadenylate-binding protein 1	IPI:IPI00189074.3	71 kDa	2	0
Tax_Id=10116 Gene_Symbol=RGD1303066 35 kDa protein	IPI:IPI00214510.2 (+3)	35 kDa	2	0
Tax_Id=10116 Gene_Symbol=Strn4_predicted similar to Striatin-4	IPI:IPI00213355.1	81 kDa	2	0
Tax_Id=10116 Gene_Symbol=Nes Isoform 1 of Nestin	IPI:IPI00194103.2 (+1)	209 kDa	2	0
Tax_Id=10116 Gene_Symbol=Ppfia3 similar to Liprin-alpha-3	IPI:IPI00365736.3 (+1)	150 kDa	2	0
Tax_Id=10116 Gene_Symbol=Becn1 beclin 1	IPI:IPI00325272.3	52 kDa	2	0
Tax_Id=10116 Gene_Symbol=Cse1l_predicted similar to chromosome segregation 1-like	IPI:IPI00193247.1	110 kDa	2	0
Tax_Id=10116 Gene_Symbol=Arpc1a Actin-related protein 2/3 complex subunit 1A	IPI:IPI00200845.1	42 kDa	2	0
Tax_Id=10116 Gene_Symbol=Syngr1 21 kDa protein	IPI:IPI00188732.2 (+1)	21 kDa	2	0

Tax_Id=10116 Gene_Symbol=Safb Scaffold attachment factor B	IPI:IPI00209618.2	105 kDa	2	0
Tax_Id=10116 Gene_Symbol=Rdh11 LRRGT00111	IPI:IPI00421314.1 (+1)	45 kDa	2	0
Tax_Id=10116 Gene_Symbol=Ptges2_predicted similar to prostaglandin E synthase 2	IPI:IPI00197369.1	43 kDa	2	0
Tax_Id=10116 Gene_Symbol=Grin1 Isoform A of Glutamate [NMDA] receptor subunit zeta-1 precursor	IPI:IPI00198625.5 (+2)	106 kDa	2	0
Tax_Id=10116 Gene_Symbol=Slc25a1 Tricarboxylate transport protein, mitochondrial precursor	IPI:IPI00327694.3	34 kDa	2	0
Tax_Id=10116 Gene_Symbol=Pmpcb Mitochondrial-processing peptidase subunit beta, mitochondrial precursor	IPI:IPI00209980.6	54 kDa	2	0
Tax_Id=10116 Gene_Symbol=Mtap6 STOP protein	IPI:IPI00210119.1 (+1)	100 kDa	2	0
Tax_Id=10116 Gene_Symbol=Slc27a4 similar to solute carrier family 27 (fatty acid transporter), member 4	IPI:IPI00372070.2	72 kDa	2	0
Tax_Id=10116 Gene_Symbol=LOC362015 similar to adenosine monophosphate deaminase 2	IPI:IPI00554244.3	95 kDa	2	0
Tax_Id=10116 Gene_Symbol=Ppp1cc Isoform Gamma-1 of Serine/threonine-protein phosphatase PP1-gamma catalytic subunit	IPI:IPI00203358.1 (+2)	37 kDa	2	0
Tax_Id=10116 Gene_Symbol=LOC362855 UPF0027 protein C22orf28 homolog	IPI:IPI00209916.1	55 kDa	2	0
Tax_Id=10116 Gene_Symbol=Cnp1 2',3'-cyclic-nucleotide 3'-phosphodiesterase	IPI:IPI00199394.2	47 kDa	2	0
Tax_Id=10116 Gene_Symbol=Lasp1 LIM and SH3 domain protein 1	IPI:IPI00198567.1	30 kDa	2	0
Tax_Id=10116 Gene_Symbol=Timm44 Import inner membrane translocase subunit TIM44, mitochondrial precursor	IPI:IPI00205394.1	51 kDa	2	0
Tax_Id=10116 Gene_Symbol=Preb Prolactin regulatory element-binding protein	IPI:IPI00553950.3	45 kDa	2	0
Tax_Id=10116 Gene_Symbol=RGD1306694_predicted similar to Hook-related protein 1	IPI:IPI00763697.1	212 kDa	2	0
Tax_Id=10116 Gene_Symbol=RGD1307966_predicted hypothetical protein	IPI:IPI00370116.3	67 kDa	2	0
Tax_Id=10116 Gene_Symbol=Vapa Vesicle-associated membrane protein-associated protein A	IPI:IPI00209290.3	28 kDa	2	0
Tax_Id=10116 Gene_Symbol=Acsl6 Acyl-CoA synthetase isoform 6 variant2	IPI:IPI00421952.2	81 kDa	2	0
Tax_Id=10116 Gene_Symbol=Clic1 Chloride intracellular channel 1	IPI:IPI00421995.1	27 kDa	2	0
Tax_Id=10116 Gene_Symbol=Ddah2 NG,NG-dimethylarginine dimethylaminohydrolase 2	IPI:IPI00215294.1	30 kDa	2	0
Tax_Id=10116 Gene_Symbol=Pdk1 [Pyruvate	IPI:IPI00204957.1	49 kDa	2	0

dehydrogenase [lipoamide]] kinase isozyme 1, mitochondrial precursor	(+1)	kDa		
Tax_Id=10116 Gene_Symbol=Dnm3 Dynamin-3	IPI:IPI00213318.4 (+2)	96 kDa	2	0
Tax_Id=10116 Gene_Symbol=Inpp1 Inositol polyphosphate-1-phosphatase	IPI:IPI00362407.2	43 kDa	2	0
Tax_Id=10116 Gene_Symbol=Lamc1 similar to Laminin gamma-1 chain precursor	IPI:IPI00363849.2	177 kDa	2	0
Tax_Id=10116 Gene_Symbol=Cul2_predicted similar to Cullin-2	IPI:IPI00364910.1	87 kDa	2	0
Tax_Id=10116 Gene_Symbol=Syncrip 70 kDa protein	IPI:IPI00557424.3 (+4)	70 kDa	2	0
Tax_Id=10116 Gene_Symbol=RGD1563580_predicted similar to AP2 associated kinase 1	IPI:IPI00556943.2 (+2)	104 kDa	2	0
Tax_Id=10116 Gene_Symbol=Acbd3 Golgi resident protein GCP60	IPI:IPI00339079.6	60 kDa	2	0
Tax_Id=10116 Gene_Symbol=Tollip_predicted Toll interacting protein	IPI:IPI00366104.2 (+1)	30 kDa	2	0
Tax_Id=10116 Gene_Symbol=Dsp similar to desmoplakin isoform I isoform 2	IPI:IPI00366081.3	332 kDa	2	0
Tax_Id=10116 Gene_Symbol=Dnaja1 DnaJ homolog subfamily A member 1	IPI:IPI00210884.1	45 kDa	2	0
Tax_Id=10116 Gene_Symbol=Ube4a Ab2-232	IPI:IPI00369411.1 (+1)	124 kDa	2	0
Tax_Id=10116 Gene_Symbol=Dfna5h similar to Nonsyndromic hearing impairment protein 5 homolog	IPI:IPI00382346.3 (+1)	57 kDa	2	0
Tax_Id=10116 Gene_Symbol=Osbp11_predicted similar to oxysterol binding protein-like 11	IPI:IPI00362151.5 (+2)	84 kDa	2	0
Tax_Id=10116 Gene_Symbol=Lamb1_predicted similar to Laminin beta-1 chain precursor	IPI:IPI00365542.3 (+1)	203 kDa	2	0
Tax_Id=10116 Gene_Symbol=Fkbp4 similar to FK506-binding protein 4	IPI:IPI00358443.3 (+1)	62 kDa	2	0
Tax_Id=10116 Gene_Symbol=Uble1b similar to Ubiquitin-like 1-activating enzyme E1B	IPI:IPI00768246.1	71 kDa	2	0
Tax_Id=10116 Gene_Symbol=RGD1565416_predicted similar to talin 2	IPI:IPI00370137.2 (+3)	273 kDa	2	0
Tax_Id=10116 Gene_Symbol=LOC682967 similar to Protein disulfide-isomerase TXNDC10 precursor	IPI:IPI00769287.1	66 kDa	2	0
Tax_Id=10116 Gene_Symbol=Gpiap1 GPI-anchored membrane protein 1	IPI:IPI00560977.2	78 kDa	2	0
Tax_Id=10116 Gene_Symbol=Sel1h Sel-1 homolog precursor	IPI:IPI00205606.3 (+1)	89 kDa	2	0
Tax_Id=10116 Gene_Symbol=Rcn1_predicted similar to Reticulocalbin-1 precursor	IPI:IPI00192912.1	38 kDa	2	0
Tax_Id=10116 Gene_Symbol=- 72 kDa protein	IPI:IPI00476922.3 (+1)	72 kDa	2	0

Tax_Id=10116 Gene_Symbol=Gria1 Isoform Flip of Glutamate receptor 1 precursor	IPI:IPI00231012.2	102 kDa	2	0
Tax_Id=10116 Gene_Symbol=Camk2d Isoform Delta 1 of Calcium/calmodulin-dependent protein kinase type II delta chain	IPI:IPI00212226.1 (+3)	60 kDa	2	0
Tax_Id=10116 Gene_Symbol=Nsdhl NAD(P) dependent steroid dehydrogenase-like	IPI:IPI00360954.1	40 kDa	2	0
Tax_Id=10116 Gene_Symbol=Tuba4 Tubulin alpha-4A chain	IPI:IPI00362927.1	50 kDa	2	0
Tax_Id=10116 Gene_Symbol=Pitpnm1 Membrane-associated phosphatidylinositol transfer protein 1	IPI:IPI00366129.3	135 kDa	2	0
Tax_Id=10116 Gene_Symbol=Ppp2r5d similar to delta isoform of regulatory subunit B56, protein phosphatase 2A isoform 1	IPI:IPI00366908.3	77 kDa	2	0
Tax_Id=10116 Gene_Symbol=Sf3b1 similar to splicing factor 3b, subunit 1 isoform 1	IPI:IPI00366952.3	147 kDa	2	0
Tax_Id=10116 Gene_Symbol=Snip 135 kDa protein	IPI:IPI00190619.3 (+2)	135 kDa	2	0
Tax_Id=10116 Gene_Symbol=RGD1311196 RGD1311196 protein	IPI:IPI00370637.3	62 kDa	2	0
Tax_Id=10116 Gene_Symbol=Ehd3 EH-domain containing protein 2	IPI:IPI00200258.2	61 kDa	2	0
Tax_Id=10116 Gene_Symbol=Hrmt1l2 Protein arginine N-methyltransferase 1	IPI:IPI00205168.2	42 kDa	2	0

GNFGEL498\_AW54-91\_NotIncl\_Gel4\_LTQ\_RatRevDB-converted  
(Membrane)

Identified Proteins	Accession Number	MW	FG	Ct
Tax_Id=10116 Gene_Symbol=Acta1 Actin, alpha skeletal muscle	IPI:IPI00189813.1 (+1)	42 kDa	7	0
Tax_Id=10116 Gene_Symbol=Slc25a4 ADP/ATP translocase 1	IPI:IPI00231927.11	33 kDa	6	0
Tax_Id=10116 Gene_Symbol=Sv2a Synaptic vesicle glycoprotein 2A	IPI:IPI00208115.4 (+1)	83 kDa	6	0
Tax_Id=10116 Gene_Symbol=Slc1a3 Isoform GLAST-1A of Excitatory amino acid transporter 1	IPI:IPI00230956.1 (+1)	54 kDa	5	0
Tax_Id=10116 Gene_Symbol=Eif4a1 Eukaryotic translation initiation factor 4A1	IPI:IPI00369618.1	46 kDa	5	0
Tax_Id=10116 Gene_Symbol=Ehd1 EH-domain containing 1	IPI:IPI00360340.3 (+1)	61 kDa	5	0
Tax_Id=10116 Gene_Symbol=RGD1560871_predicted	IPI:IPI00358371.3	212	5	0

similar to plexin A1		kDa		
Tax_Id=10116 Gene_Symbol=Kb36 Type II keratin Kb36	IPI:IPI00421780.1	60 kDa	5	0
Tax_Id=10116 Gene_Symbol=RGD1306694_predicted similar to Hook-related protein 1	IPI:IPI00763697.1	212 kDa	5	0
Tax_Id=10116 Gene_Symbol=Sbf1_predicted similar to SET binding factor 1 isoform a	IPI:IPI00764860.1 (+1)	210 kDa	5	0
Tax_Id=10116 Gene_Symbol=Hmgcs2 Hydroxymethylglutaryl-CoA synthase, mitochondrial precursor	IPI:IPI00210444.5	57 kDa	4	0
Tax_Id=10116 Gene_Symbol=Idh3a Isocitrate dehydrogenase [NAD] subunit alpha, mitochondrial precursor	IPI:IPI00198720.1	40 kDa	4	0
Tax_Id=10116 Gene_Symbol=Kif3a similar to Kinesin-like protein KIF3A (Microtubule plus end-directed kinesin motor 3A) isoform 6	IPI:IPI00326085.4 (+6)	80 kDa	4	0
Tax_Id=10116 Gene_Symbol=LOC367171 Microtubule-associated protein 4	IPI:IPI00393975.2 (+2)	110 kDa	4	0
Tax_Id=10116 Gene_Symbol=Cct5 T-complex protein 1 subunit epsilon	IPI:IPI00470301.1	60 kDa	4	0
Tax_Id=10116 Gene_Symbol=RGD1308307_predicted similar to pyruvate dehydrogenase phosphatase regulatory subunit isoform 1	IPI:IPI00359656.3	99 kDa	4	0
Tax_Id=10116 Gene_Symbol=LOC315676 similar to Dmx-like 2	IPI:IPI00369671.3	344 kDa	4	0
Tax_Id=10116 Gene_Symbol=Prkacb cAMP-dependent protein kinase, beta-catalytic subunit	IPI:IPI00560492.1	46 kDa	4	0
Tax_Id=10116 Gene_Symbol=Epm2aip1_predicted similar to EPM2A (laforin) interacting protein 1	IPI:IPI00766207.1	70 kDa	4	0
Tax_Id=10116 Gene_Symbol=Gnas Isoform Gnas-1 of Guanine nucleotide-binding protein G(s) subunit alpha isoforms short	IPI:IPI00199872.2 (+1)	46 kDa	4	0
Tax_Id=10116 Gene_Symbol=Gnaq guanine nucleotide binding protein, alpha q polypeptide	IPI:IPI00230868.4	42 kDa	4	0
Tax_Id=10116 Gene_Symbol=Adsl_predicted similar to adenylosuccinate lyase	IPI:IPI00361216.2	55 kDa	4	0
Tax_Id=10116 Gene_Symbol=Phgdh D-3-phosphoglycerate dehydrogenase	IPI:IPI00475835.3	56 kDa	4	0
Tax_Id=10116 Gene_Symbol=RGD1560544_predicted similar to Protein C11orf2 (Another new gene 2 protein) isoform 1	IPI:IPI00762984.1 (+1)	86 kDa	4	0
Tax_Id=10116 Gene_Symbol=Vac14 VAC14	IPI:IPI00230981.1	88 kDa	4	0
Tax_Id=10116 Gene_Symbol=Centg3_predicted similar to centaurin, gamma 3	IPI:IPI00358128.3	102 kDa	4	0
Tax_Id=10116 Gene_Symbol=Cand2 Isoform 1 of	IPI:IPI00326431.1	140 kDa	3	0

Cullin-associated NEDD8-dissociated protein 2	(+2)	kDa		
Tax_Id=10116 Gene_Symbol=Sqstm1 Isoform 1 of Sequestosome-1	IPI:IPI00194561.1 (+2)	48 kDa	3	0
Tax_Id=10116 Gene_Symbol=LOC686545 similar to slit homolog 1	IPI:IPI00768734.1	81 kDa	3	0
Tax_Id=10116 Gene_Symbol=Ptpcd Leukocyte common antigen-related phosphatase precursor	IPI:IPI00214375.1 (+1)	207 kDa	3	0
Tax_Id=10116 Gene_Symbol=Ddx1 ATP-dependent RNA helicase DDX1	IPI:IPI00555314.1	82 kDa	3	0
Tax_Id=10116 Gene_Symbol=Ctnnd1_predicted similar to Catenin delta-1	IPI:IPI00359491.3 (+2)	105 kDa	3	0
Tax_Id=10116 Gene_Symbol=Vps18_predicted similar to Vacuolar protein sorting 18	IPI:IPI00197453.1	110 kDa	3	0
Tax_Id=10116 Gene_Symbol=Ywhaq 14-3-3 protein theta	IPI:IPI00196661.1	28 kDa	3	0
Tax_Id=10116 Gene_Symbol=RGD1307235_predicted hypothetical protein	IPI:IPI00360079.4	135 kDa	3	0
Tax_Id=10116 Gene_Symbol=Vars2 Valyl-tRNA synthetase	IPI:IPI00372557.2	141 kDa	3	0
Tax_Id=10116 Gene_Symbol=Synj1 similar to Synaptojanin-1	IPI:IPI00210153.3 (+3)	173 kDa	3	0
Tax_Id=10116 Gene_Symbol=Acdb3 Golgi resident protein GCP60	IPI:IPI00339079.6	60 kDa	3	0
Tax_Id=10116 Gene_Symbol=Pde10a PDE10A11	IPI:IPI00213904.5 (+3)	96 kDa	3	0
Tax_Id=10116 Gene_Symbol=P4hb Protein disulfide-isomerase precursor	IPI:IPI00198887.1	57 kDa	3	0
Tax_Id=10116 Gene_Symbol=Ankfy1_predicted similar to Ankyrin repeat and FYVE domain protein 1	IPI:IPI00364871.3	129 kDa	3	0
Tax_Id=10116 Gene_Symbol=Kif5a Kinesin heavy chain isoform 5A	IPI:IPI00417753.1	117 kDa	3	0
Tax_Id=10116 Gene_Symbol=Ipo9_predicted similar to Importin-9	IPI:IPI00195818.3	117 kDa	2	0
Tax_Id=10116 Gene_Symbol=Wdr7 Isoform 1 of WD repeat protein 7	IPI:IPI00190963.1 (+1)	163 kDa	2	0
Tax_Id=10116 Gene_Symbol=Ap2a2 Adaptor protein complex AP-2, alpha 2 subunit	IPI:IPI00471901.3	104 kDa	2	0
Tax_Id=10116 Gene_Symbol=Cct6a Chaperonin subunit 6a	IPI:IPI00188111.1	58 kDa	2	0
Tax_Id=10116 Gene_Symbol=Rasa1 Ras GTPase-activating protein 1	IPI:IPI00203320.1	115 kDa	2	0
Tax_Id=10116 Gene_Symbol=Fdft1 Squalene synthetase	IPI:IPI00210233.1	48 kDa	2	0
Tax_Id=10116 Gene_Symbol=Atp2b4 Isoform XA of Plasma membrane calcium-transporting ATPase 4	IPI:IPI00230910.1 (+1)	129 kDa	2	0
Tax_Id=10116 Gene_Symbol=Bin1 Isoform AMPH2-1	IPI:IPI00196509.2	65	2	0

of Myc box-dependent-interacting protein 1	(+2)	kDa		
Tax_Id=10116 Gene_Symbol=Itsn1 Isoform 2 of Intersectin-1	IPI:IPI00231962.1 (+2)	129 kDa	2	0
Tax_Id=10116 Gene_Symbol=Dctn1 Dynactin subunit 1	IPI:IPI00196703.1	142 kDa	2	0
Tax_Id=10116 Gene_Symbol=Cask Peripheral plasma membrane protein CASK	IPI:IPI00388752.3 (+1)	103 kDa	2	0
Tax_Id=10116 Gene_Symbol=Clptm1_predicted similar to cleft lip and palate associated transmembrane protein 1	IPI:IPI00193869.1 (+1)	75 kDa	2	0
Tax_Id=10116 Gene_Symbol=LOC362012 similar to Protein FAM40A	IPI:IPI00373402.3 (+3)	99 kDa	2	0
Tax_Id=10116 Gene_Symbol=Cct4 T-complex protein 1 subunit delta	IPI:IPI00337168.5	58 kDa	2	0
Tax_Id=10116 Gene_Symbol=Gpd2 Glycerol-3-phosphate dehydrogenase, mitochondrial precursor	IPI:IPI00199663.1	81 kDa	2	0
Tax_Id=10116 Gene_Symbol=Nsdhl NAD(P) dependent steroid dehydrogenase-like	IPI:IPI00360954.1	40 kDa	2	0
Tax_Id=10116 Gene_Symbol=Slc25a3 Slc25a3 protein	IPI:IPI00209115.2 (+1)	40 kDa	2	0
Tax_Id=10116 Gene_Symbol=Hdac6 similar to Histone deacetylase 6	IPI:IPI00200498.5	126 kDa	2	0
Tax_Id=10116 Gene_Symbol=Add2 Isoform 1 of Beta-adducin	IPI:IPI00192626.3 (+1)	81 kDa	2	0
Tax_Id=10116 Gene_Symbol=Hnrpl Hnrpl protein	IPI:IPI00364061.4 (+1)	64 kDa	2	0
Tax_Id=10116 Gene_Symbol=Nlgn1 Isoform 1 of Neuroligin-1 precursor	IPI:IPI00208218.1 (+6)	94 kDa	2	0
Tax_Id=10116 Gene_Symbol=Sars1 61 kDa protein	IPI:IPI00373410.3 (+1)	61 kDa	2	0
Tax_Id=10116 Gene_Symbol=Kit Tyrosine-protein kinase receptor	IPI:IPI00205775.1	109 kDa	2	0
Tax_Id=10116 Gene_Symbol=Exoc2 Exocyst complex component 2	IPI:IPI00324275.3 (+1)	104 kDa	2	0
Tax_Id=10116 Gene_Symbol=Kif21b_predicted similar to Kinesin family member 21B	IPI:IPI00363445.4 (+1)	181 kDa	2	0
Tax_Id=10116 Gene_Symbol=RGD1306534_predicted similar to Phosphatidylinositol 3,4,5-trisphosphate-dependent Rac exchanger 1 protein	IPI:IPI00365036.4	185 kDa	2	0
Tax_Id=10116 Gene_Symbol=Robo2 similar to Roundabout homolog 2 precursor	IPI:IPI00558943.2	161 kDa	2	0
Tax_Id=10116 Gene_Symbol=Pgm3_predicted similar to Phosphoacetylglucosamine mutase	IPI:IPI00205603.3 (+1)	60 kDa	2	0
Tax_Id=10116 Gene_Symbol=Csk Tyrosine-protein kinase CSK	IPI:IPI00188950.1	51 kDa	2	0
Tax_Id=10116 Gene_Symbol=Ikbkap Elongator	IPI:IPI00389755.1	149	2	0

complex protein 1		kDa		
Tax_Id=10116 Gene_Symbol=Fthfd 10-formyltetrahydrofolate dehydrogenase	IPI:IPI00196725.5	99 kDa	2	0
Tax_Id=10116 Gene_Symbol=Cnp1 2',3'-cyclic-nucleotide 3'-phosphodiesterase	IPI:IPI00199394.2	47 kDa	2	0
Tax_Id=10116 Gene_Symbol=Ntrk2 Isoform GP145-TrkB of BDNF/NT-3 growth factors receptor precursor	IPI:IPI00210944.1 (+2)	92 kDa	2	0
Tax_Id=10116 Gene_Symbol=Pcbp2 Poly(RC) binding protein 2	IPI:IPI00464805.2 (+1)	39 kDa	2	0
Tax_Id=10116 Gene_Symbol=- 94 kDa protein	IPI:IPI00368857.4	94 kDa	2	0
Tax_Id=10116 Gene_Symbol=Ube2o_predicted similar to ubiquitin-conjugating enzyme E2O	IPI:IPI00361541.3 (+1)	143 kDa	2	0
Tax_Id=10116 Gene_Symbol=Rasgrp2_predicted RAS guanyl releasing protein 2	IPI:IPI00372470.2 (+1)	70 kDa	2	0
Tax_Id=10116 Gene_Symbol=RGD1560587_predicted similar to Eph receptor A4	IPI:IPI00361893.2 (+1)	110 kDa	2	0
Tax_Id=10116 Gene_Symbol=RGD1560511_predicted similar to vacuolar protein sorting 41	IPI:IPI00768079.1	99 kDa	2	0
Tax_Id=10116 Gene_Symbol=Ayt12_predicted 1-acylglycerophosphocholine O-acyltransferase 1	IPI:IPI00365394.2 (+1)	60 kDa	2	0
Tax_Id=10116 Gene_Symbol=Spnb2 Non-erythrocyte beta-spectrin	IPI:IPI00373419.2 (+1)	251 kDa	2	0
Tax_Id=10116 Gene_Symbol=Txnl2 Isoform 1 of Thioredoxin-like protein 2	IPI:IPI00553899.1	38 kDa	2	0
Tax_Id=10116 Gene_Symbol=Sh3glb1 43 kDa protein	IPI:IPI00363770.2 (+1)	43 kDa	2	0
Tax_Id=10116 Gene_Symbol=Ap3b2_predicted similar to adaptor-related protein complex 3, beta 2 subunit	IPI:IPI00368200.2 (+1)	124 kDa	2	0
Tax_Id=10116 Gene_Symbol=Xpo7 similar to exportin 7 isoform 1	IPI:IPI00768094.1 (+1)	125 kDa	2	0
Tax_Id=10116 Gene_Symbol=Gnai2 Guanine nucleotide-binding protein G(i), alpha-2 subunit	IPI:IPI00231925.8	41 kDa	2	0
Tax_Id=10116 Gene_Symbol=Plaa Phospholipase A-2-activating protein	IPI:IPI00562304.2 (+1)	87 kDa	2	0
Tax_Id=10116 Gene_Symbol=RGD1559939_predicted similar to peroxisome biogenesis factor 1	IPI:IPI00388336.3 (+1)	148 kDa	2	0
Tax_Id=10116 Gene_Symbol=Vps53_predicted similar to vacuolar protein sorting 53	IPI:IPI00369705.3 (+2)	94 kDa	2	0
Tax_Id=10116 Gene_Symbol=RGD1560248_predicted similar to formin-like 2 isoform B	IPI:IPI00389912.2 (+3)	65 kDa	2	0
Tax_Id=10116 Gene_Symbol=lvd Isovaleryl-CoA dehydrogenase, mitochondrial precursor	IPI:IPI00193716.1	46 kDa	2	0
Tax_Id=10116 Gene_Symbol=Birc6_predicted similar to baculoviral IAP repeat-containing 6	IPI:IPI00360081.4 (+2)	551 kDa	2	0
Tax_Id=10116 Gene_Symbol=Pde2a cGMP-dependent	IPI:IPI00199076.2	105 kDa	2	0

3',5'-cyclic phosphodiesterase	(+3)	kDa		
Tax_Id=10116 Gene_Symbol=Ptk2b Isoform 1 of Protein tyrosine kinase 2 beta	IPI:IPI00190485.1 (+1)	116 kDa	2	0
Tax_Id=10116 Gene_Symbol=Rrm1 Ribonucleoside-diphosphate reductase	IPI:IPI00361151.2	90 kDa	2	0
Tax_Id=10116 Gene_Symbol=RGD1306143_predicted similar to CG9339-PE, isoform E	IPI:IPI00368722.3 (+1)	63 kDa	2	0
Tax_Id=10116 Gene_Symbol=Igsf3_predicted similar to immunoglobulin superfamily, member 3	IPI:IPI00368876.3	140 kDa	2	0
Tax_Id=10116 Gene_Symbol=Pgap1 GPI inositol-deacylase	IPI:IPI00409514.1	104 kDa	2	0
Tax_Id=10116 Gene_Symbol=Trim2 similar to tripartite motif protein TRIM2	IPI:IPI00373220.4 (+2)	87 kDa	2	0

#GNFGEL507\_AW01-43\_GelA\_RatRevDB  
(Synaptosome)

Identified Proteins	Accession Number	MW	FG	Ct
Tax_Id=10116 Gene_Symbol=Atp1a3 Sodium/potassium-transporting ATPase subunit alpha-3	IPI:IPI00231451.4	112 kDa	19	0
Tax_Id=10116 Gene_Symbol=Dync1h1 Dynein heavy chain, cytosolic	IPI:IPI00327630.1	532 kDa	21	0
Tax_Id=10116 Gene_Symbol=Fasn Fatty acid synthase	IPI:IPI00200661.1	273 kDa	14	0
Tax_Id=10116 Gene_Symbol=Atp5a1 ATP synthase subunit alpha, mitochondrial precursor	IPI:IPI00396910.1	60 kDa	7	0
Tax_Id=10116 Gene_Symbol=Lrp1rc Leucine rich protein 157	IPI:IPI00360075.2	157 kDa	8	0
Tax_Id=10116 Gene_Symbol=Dcx Neuronal migration protein doublecortin	IPI:IPI00324409.3	41 kDa	5	0
Tax_Id=10116 Gene_Symbol=Acly Isoform 1 of ATP-citrate synthase	IPI:IPI00214665.2 (+1)	121 kDa	8	0
Tax_Id=10116 Gene_Symbol=Ania4 84 kDa protein	IPI:IPI00778626.1	84 kDa	10	0
Tax_Id=10116 Gene_Symbol=Map1b similar to Microtubule-associated protein 1B	IPI:IPI00372009.3	270 kDa	5	0
Tax_Id=10116 Gene_Symbol=Kif5c_predicted similar to kinesin family member 5C	IPI:IPI00193402.4	109 kDa	8	0
Tax_Id=10116 Gene_Symbol=Kif21b_predicted similar to Kinesin family member 21B	IPI:IPI00363445.4 (+1)	181 kDa	6	0
Tax_Id=10116 Gene_Symbol=Tubb3 Tubulin beta-3 chain	IPI:IPI00362160.1	50 kDa	7	0
Tax_Id=10116 Gene_Symbol=Hspd1 60 kDa heat	IPI:IPI00339148.2	61 kDa	8	0

shock protein, mitochondrial precursor		kDa		
Tax_Id=10116 Gene_Symbol=Cltc Clathrin heavy chain	IPI:IPI00193983.3 (+1)	192 kDa	8	0
Tax_Id=10116 Gene_Symbol=Cand1 Cullin-associated NEDD8-dissociated protein 1	IPI:IPI00205466.1	136 kDa	8	0
Tax_Id=10116 Gene_Symbol=Crmp1 Dihydropyrimidinase-related protein 1	IPI:IPI00561065.2	74 kDa	8	0
Tax_Id=10116 Gene_Symbol=Hk1 Hexokinase-1	IPI:IPI00202543.1	102 kDa	10	0
Tax_Id=10116 Gene_Symbol=Jup Junction plakoglobin	IPI:IPI00421429.3	82 kDa	3	0
Tax_Id=10116 Gene_Symbol=Epb4.1l1 Isoform S of Band 4.1-like protein 1	IPI:IPI00203237.2 (+2)	98 kDa	4	0
Tax_Id=10116 Gene_Symbol=Dctn1 Dynactin subunit 1	IPI:IPI00196703.1	142 kDa	6	0
Tax_Id=10116 Gene_Symbol=Dnm1 Dynamin-1	IPI:IPI00782657.1	96 kDa	6	0
Tax_Id=10116 Gene_Symbol=Hspcb Heat shock protein HSP 90-beta	IPI:IPI00471584.7	83 kDa	8	0
Tax_Id=10116 Gene_Symbol=Opa1 Isoform 3 of Dynamin-like 120 kDa protein, mitochondrial precursor	IPI:IPI00192639.5 (+1)	116 kDa	6	0
Tax_Id=10116 Gene_Symbol=Atp1a1 Sodium/potassium-transporting ATPase subunit alpha-1 precursor	IPI:IPI00326305.3	113 kDa	4	0
Tax_Id=10116 Gene_Symbol=Gnao Guanine nucleotide-binding protein G(o) subunit alpha 1	IPI:IPI00231505.5	40 kDa	5	0
Tax_Id=10116 Gene_Symbol=LOC314432 Similar to ubiquitin-protein ligase (EC 6.3.2.19) E1-mouse	IPI:IPI00368347.2	118 kDa	6	0
Tax_Id=10116 Gene_Symbol=Gap43 Neuromodulin	IPI:IPI00212320.1	24 kDa	3	0
Tax_Id=10116 Gene_Symbol=Usp9x_predicted similar to Probable ubiquitin carboxyl-terminal hydrolase FAF-X (Ubiquitin thioesterase FAF-X) (Ubiquitin-specific-processing protease FAF-X) (Deubiquitinating enzyme FAF-X) (Fat facets protein-related, X-linked) (Ubiquitin-specific protease 9, X c	IPI:IPI00204923.4 (+1)	291 kDa	6	0
Tax_Id=10116 Gene_Symbol=LOC360975 2-oxoglutarate dehydrogenase E1 component, mitochondrial precursor	IPI:IPI00215093.1 (+2)	116 kDa	7	0
Tax_Id=10116 Gene_Symbol=Aco2 Aconitate hydratase, mitochondrial precursor	IPI:IPI00421539.3	85 kDa	5	0
Tax_Id=10116 Gene_Symbol=Eef2 Elongation factor 2	IPI:IPI00203214.6	95 kDa	7	0
Tax_Id=10116 Gene_Symbol=Tufm_predicted similar to Tu translation elongation factor, mitochondrial	IPI:IPI00371236.3	50 kDa	4	0

Tax_Id=10116 Gene_Symbol=Uqcrc2 Ubiquinol-cytochrome-c reductase complex core protein 2, mitochondrial precursor	IPI:IPI00188924.4	48 kDa	4	0
Tax_Id=10116 Gene_Symbol=Spnb3 Spectrin beta chain, brain 2	IPI:IPI00327662.3	271 kDa	7	0
Tax_Id=10116 Gene_Symbol=Ripx Protein RUFY3	IPI:IPI00204065.1 (+2)	53 kDa	5	0
Tax_Id=10116 Gene_Symbol=Mtap2 Isoform MAP2x of Microtubule-associated protein 2	IPI:IPI00206171.1 (+2)	202 kDa	5	0
Tax_Id=10116 Gene_Symbol=Cyln2 CAP-Gly domain-containing linker protein 2	IPI:IPI00195929.1 (+1)	115 kDa	4	0
Tax_Id=10116 Gene_Symbol=RGD1566016_predicted similar to SLIT-ROBO Rho GTPase-activating protein 2	IPI:IPI00363832.3	121 kDa	5	0
Tax_Id=10116 Gene_Symbol=Aldh1l2_predicted similar to aldehyde dehydrogenase 1 family, member L2	IPI:IPI00361193.5	102 kDa	4	0
Tax_Id=10116 Gene_Symbol=Atp2a2 Isoform SERCA2B of Sarcoplasmic/endoplasmic reticulum calcium ATPase 2	IPI:IPI00190020.3 (+1)	115 kDa	4	0
Tax_Id=10116 Gene_Symbol=Phgdh D-3-phosphoglycerate dehydrogenase	IPI:IPI00475835.3	56 kDa	5	0
Tax_Id=10116 Gene_Symbol=Hsph1 Heat shock protein 105 kDa	IPI:IPI00471835.1	96 kDa	3	0
Tax_Id=10116 Gene_Symbol=Ndufs1 NADH-ubiquinone oxidoreductase 75 kDa subunit, mitochondrial precursor	IPI:IPI00358033.1	79 kDa	6	0
Tax_Id=10116 Gene_Symbol=Cct3 T-complex protein 1 subunit gamma	IPI:IPI00372388.1	61 kDa	6	0
Tax_Id=10116 Gene_Symbol=Prss15 Lon protease homolog, mitochondrial precursor	IPI:IPI00205076.1	106 kDa	7	0
Tax_Id=10116 Gene_Symbol=Hmgcs1 Hydroxymethylglutaryl-CoA synthase, cytoplasmic	IPI:IPI00188158.1	57 kDa	3	0
Tax_Id=10116 Gene_Symbol=Gprin1_predicted similar to G protein-regulated inducer of neurite outgrowth 1	IPI:IPI00360030.4 (+1)	94 kDa	4	0
Tax_Id=10116 Gene_Symbol=Aars similar to alanyl-tRNA synthetase	IPI:IPI00363563.3	107 kDa	4	0
Tax_Id=10116 Gene_Symbol=LOC367171 Microtubule-associated protein 4	IPI:IPI00393975.2 (+2)	110 kDa	3	0
Tax_Id=10116 Gene_Symbol=Centg3_predicted similar to centaurin, gamma 3	IPI:IPI00358128.3	102 kDa	4	0
Tax_Id=10116 Gene_Symbol=Trio similar to triple functional domain	IPI:IPI00360644.3 (+1)	348 kDa	5	0
Tax_Id=10116 Gene_Symbol=Ckap5 similar to cytoskeleton associated protein 5 isoform 1	IPI:IPI00764313.1 (+3)	223 kDa	5	0
Tax_Id=10116 Gene_Symbol=Dpysl3 Isoform 2 of	IPI:IPI00203250.1	74 kDa	4	0

Dihydropyrimidinase-related protein 3	(+1)	kDa		
Tax_Id=10116 Gene_Symbol=Acaca Isoform 1 of Acetyl-CoA carboxylase 1	IPI:IPI00194102.2 (+1)	265 kDa	3	0
Tax_Id=10116 Gene_Symbol=LOC363309 similar to tubulin-specific chaperone d	IPI:IPI00765967.1	134 kDa	3	0
Tax_Id=10116 Gene_Symbol=Exoc4 Exocyst complex component 4	IPI:IPI00209144.1 (+2)	111 kDa	3	0
Tax_Id=10116 Gene_Symbol=Kab 174 kDa protein	IPI:IPI00776774.1	174 kDa	4	0
Tax_Id=10116 Gene_Symbol=Eno1 Alpha-enolase	IPI:IPI00464815.11 (+2)	47 kDa	5	0
Tax_Id=10116 Gene_Symbol=Kif5b Kinesin heavy chain	IPI:IPI00364904.2	110 kDa	4	0
Tax_Id=10116 Gene_Symbol=Cct8_predicted similar to T-complex protein 1 subunit theta	IPI:IPI00370815.3	60 kDa	4	0
Tax_Id=10116 Gene_Symbol=Ap2b1 Isoform 2 of AP-2 complex subunit beta-1	IPI:IPI00231502.3 (+2)	106 kDa	4	0
Tax_Id=10116 Gene_Symbol=Lancl2_predicted LanC (Bacterial lantibiotic synthetase component C)-like 2	IPI:IPI00192484.2	51 kDa	4	0
Tax_Id=10116 Gene_Symbol=Vps18_predicted similar to Vacuolar protein sorting 18	IPI:IPI00197453.1	110 kDa	3	0
Tax_Id=10116 Gene_Symbol=Hip1 similar to huntingtin interacting protein 1 isoform 2	IPI:IPI00370335.3 (+1)	116 kDa	3	0
Tax_Id=10116 Gene_Symbol=Cyfp1_predicted similar to cytoplasmic FMR1 interacting protein 1	IPI:IPI00367829.4	145 kDa	3	0
Tax_Id=10116 Gene_Symbol=Afap Actin filament associated protein	IPI:IPI00206325.1	81 kDa	3	0
Tax_Id=10116 Gene_Symbol=Tpp2 Tripeptidyl-peptidase 2	IPI:IPI00213579.3 (+1)	138 kDa	4	0
Tax_Id=10116 Gene_Symbol=Npepps similar to aminopeptidase puromycin sensitive	IPI:IPI00372700.1 (+3)	103 kDa	4	0
Tax_Id=10116 Gene_Symbol=Cad_mapped similar to carbamoyl-phosphate synthetase 2, aspartate transcarbamylase, and dihydroorotase isoform 4	IPI:IPI00365582.3 (+2)	243 kDa	4	0
Tax_Id=10116 Gene_Symbol=Vps35_mapped similar to vacuolar protein sorting 35	IPI:IPI00363493.2	92 kDa	3	0
Tax_Id=10116 Gene_Symbol=Plaa Phospholipase A-2-activating protein	IPI:IPI00562304.2	87 kDa	3	0
Tax_Id=10116 Gene_Symbol=Tra1_predicted 93 kDa protein	IPI:IPI00365985.4 (+1)	93 kDa	3	0
Tax_Id=10116 Gene_Symbol=Wdr47 similar to WD repeat domain 47	IPI:IPI00768998.1	102 kDa	3	0
Tax_Id=10116 Gene_Symbol=Spna2 Spectrin alpha chain, brain	IPI:IPI00209258.4	285 kDa	3	0
Tax_Id=10116 Gene_Symbol=Ap2a2 Adaptor protein complex AP-2, alpha 2 subunit	IPI:IPI00471901.3	104 kDa	3	0

Tax_Id=10116 Gene_Symbol=Cct6a Chaperonin subunit 6a	IPI:IPI00188111.1	58 kDa	3	0
Tax_Id=10116 Gene_Symbol=Pygb similar to Glycogen phosphorylase, brain form	IPI:IPI00357945.1	97 kDa	3	0
Tax_Id=10116 Gene_Symbol=RGD1562629_predicted similar to Protein neurobeachin	IPI:IPI00567941.2	327 kDa	3	0
Tax_Id=10116 Gene_Symbol=Immt 82 kDa protein	IPI:IPI00364895.4 (+1)	82 kDa	3	0

#GNFGEL517\_AW01-59\_Gelf\_RatRevDB  
(Synaptosome)

Identified Proteins	Accession Number	MW	FG	Ct
Tax_Id=10116 Gene_Symbol=Dync1h1 Dynein heavy chain, cytosolic	IPI:IPI00327630.1	532 kDa	43	0
Tax_Id=10116 Gene_Symbol=Fasn Fatty acid synthase	IPI:IPI00200661.1	273 kDa	9	0
Tax_Id=10116 Gene_Symbol=Kif5c_predicted similar to kinesin family member 5C	IPI:IPI00193402.4	109 kDa	9	0
Tax_Id=10116 Gene_Symbol=Crmp1 Dihydropyrimidinase-related protein 1	IPI:IPI00561065.2	74 kDa	8	0
Tax_Id=10116 Gene_Symbol=Stxbp1 Isoform 1 of Syntaxin-binding protein 1	IPI:IPI00205372.3 (+1)	68 kDa	7	0
Tax_Id=10116 Gene_Symbol=Hspcb Heat shock protein HSP 90-beta	IPI:IPI00471584.7	83 kDa	7	0
Tax_Id=10116 Gene_Symbol=Ania4 84 kDa protein	IPI:IPI00778626.1	84 kDa	7	0
Tax_Id=10116 Gene_Symbol=Atp5a1 ATP synthase subunit alpha, mitochondrial precursor	IPI:IPI00396910.1	60 kDa	6	0
Tax_Id=10116 Gene_Symbol=Tubb3 Tubulin beta-3 chain	IPI:IPI00362160.1	50 kDa	6	0
Tax_Id=10116 Gene_Symbol=Lrp1rc Leucine rich protein 157	IPI:IPI00360075.2	157 kDa	6	0
Tax_Id=10116 Gene_Symbol=Aco2 Aconitate hydratase, mitochondrial precursor	IPI:IPI00421539.3	85 kDa	6	0
Tax_Id=10116 Gene_Symbol=Tubb2b Tubulin beta-2B chain	IPI:IPI00655259.1	50 kDa	5	0
Tax_Id=10116 Gene_Symbol=LOC681252 similar to Myristoylated alanine-rich C-kinase substrate	IPI:IPI00371946.3 (+1)	30 kDa	5	0
Tax_Id=10116 Gene_Symbol=Mtap2 Isoform MAP2x of Microtubule-associated protein 2	IPI:IPI00206171.1 (+2)	202 kDa	5	0
Tax_Id=10116 Gene_Symbol=LOC362587 831 kDa protein	IPI:IPI00359003.4 (+1)	831 kDa	5	0
Tax_Id=10116 Gene_Symbol=Dctn1 Dynactin subunit	IPI:IPI00196703.1	142	5	0

1		kDa		
Tax_Id=10116 Gene_Symbol=Gnao Guanine nucleotide-binding protein G(o) subunit alpha 2	IPI:IPI00204843.2 (+1)	40 kDa	5	0
Tax_Id=10116 Gene_Symbol=Cand1 Cullin-associated NEDD8-dissociated protein 1	IPI:IPI00205466.1	136 kDa	5	0
Tax_Id=10116 Gene_Symbol=Dpysl3 Isoform 2 of Dihydropyrimidinase-related protein 3	IPI:IPI00203250.1 (+1)	74 kDa	4	0
Tax_Id=10116 Gene_Symbol=RGD1565889_predicted similar to Calcium-binding mitochondrial carrier protein Aralar2	IPI:IPI00358163.3	74 kDa	4	0
Tax_Id=10116 Gene_Symbol=Dpysl2 similar to Dihydropyrimidinase-related protein 2	IPI:IPI00192034.2	73 kDa	4	0
Tax_Id=10116 Gene_Symbol=Hspd1 60 kDa heat shock protein, mitochondrial precursor	IPI:IPI00339148.2	61 kDa	4	0
Tax_Id=10116 Gene_Symbol=Hk1 Hexokinase-1	IPI:IPI00202543.1	102 kDa	4	0
Tax_Id=10116 Gene_Symbol=Hspa8 Heat shock cognate 71 kDa protein	IPI:IPI00208205.1 (+1)	71 kDa	4	0
Tax_Id=10116 Gene_Symbol=Hadha Trifunctional enzyme subunit alpha, mitochondrial precursor	IPI:IPI00212622.1	83 kDa	4	0
Tax_Id=10116 Gene_Symbol=Dcd Dermcidin	IPI:IPI00421832.1	11 kDa	3	0
Tax_Id=10116 Gene_Symbol=Dbn1 Isoform A of Drebrin	IPI:IPI00231407.4 (+1)	77 kDa	3	0
Tax_Id=10116 Gene_Symbol=Map1b similar to Microtubule-associated protein 1B	IPI:IPI00372009.3	270 kDa	3	0
Tax_Id=10116 Gene_Symbol=Camkv CaM kinase-like vesicle-associated protein	IPI:IPI00205056.1	54 kDa	3	0
Tax_Id=10116 Gene_Symbol=Dync1li1 Cytoplasmic dynein 1 light intermediate chain 1	IPI:IPI00213552.1	57 kDa	3	0
Tax_Id=10116 Gene_Symbol=Atp2b1 Isoform D of Plasma membrane calcium-transporting ATPase 1	IPI:IPI00194873.1 (+5)	139 kDa	3	0
Tax_Id=10116 Gene_Symbol=Uqcrc2 Ubiquinol-cytochrome-c reductase complex core protein 2, mitochondrial precursor	IPI:IPI00188924.4	48 kDa	3	0
Tax_Id=10116 Gene_Symbol=Prss15 Lon protease homolog, mitochondrial precursor	IPI:IPI00205076.1	106 kDa	3	0
Tax_Id=10116 Gene_Symbol=Cad_mapped similar to carbamoyl-phosphate synthetase 2, aspartate transcarbamylase, and dihydroorotase isoform 4	IPI:IPI00365582.3 (+3)	243 kDa	3	0
Tax_Id=10116 Gene_Symbol=Add1 Isoform 2 of Alpha-adducin	IPI:IPI00231810.1 (+2)	70 kDa	3	0
Tax_Id=10116 Gene_Symbol=Gprin1_predicted similar to G protein-regulated inducer of neurite outgrowth 1	IPI:IPI00360030.4	94 kDa	2	0
Tax_Id=10116 Gene_Symbol=Slc25a4 ADP/ATP	IPI:IPI00231927.11	33	2	0

translocase 1		kDa		
Tax_Id=10116 Gene_Symbol=Syn1 Isoform IA of Synapsin-1	IPI:IPI00191335.1 (+2)	74 kDa	2	0
Tax_Id=10116 Gene_Symbol=Pkm2 Isoform M1 of Pyruvate kinase isozymes M1/M2	IPI:IPI00231929.6 (+3)	58 kDa	2	0
Tax_Id=10116 Gene_Symbol=RGD1562629_predicted similar to Protein neurobeachin	IPI:IPI00567941.2	327 kDa	2	0
Tax_Id=10116 Gene_Symbol=Hspa12a_predicted similar to heat shock protein 12A	IPI:IPI00358537.2	75 kDa	2	0
Tax_Id=10116 Gene_Symbol=Exoc4 Exocyst complex component 4	IPI:IPI00209144.1	111 kDa	2	0
Tax_Id=10116 Gene_Symbol=Gna13 Galpha13	IPI:IPI00422053.1 (+1)	44 kDa	2	0
Tax_Id=10116 Gene_Symbol=Ndufs1 NADH-ubiquinone oxidoreductase 75 kDa subunit, mitochondrial precursor	IPI:IPI00358033.1	79 kDa	2	0
Tax_Id=10116 Gene_Symbol=Eef2 Elongation factor 2	IPI:IPI00203214.6	95 kDa	2	0
Tax_Id=10116 Gene_Symbol=Tubb4 similar to tubulin, beta 4	IPI:IPI00765366.1	50 kDa	2	0
Tax_Id=10116 Gene_Symbol=Hspa9a_predicted Stress-70 protein, mitochondrial precursor	IPI:IPI00363265.3	74 kDa	2	0
Tax_Id=10116 Gene_Symbol=Mark3 81 kDa protein	IPI:IPI00206262.3 (+2)	81 kDa	2	0

#GNFGEL524\_AW01-47\_GelH\_RatRevDB  
(Synaptosome)

Identified Proteins	Accession Number	MW	FG	Ct
Tax_Id=10116 Gene_Symbol=Mtap2 Microtubule-associated protein	IPI:IPI00328017.4	199 kDa	6	0
Tax_Id=10116 Gene_Symbol=Ania4 84 kDa protein	IPI:IPI00778626.1	84 kDa	6	0
Tax_Id=10116 Gene_Symbol=Dpysl5 Dihydropyrimidinase-related protein 5	IPI:IPI00331981.7	62 kDa	5	0
Tax_Id=10116 Gene_Symbol=Camkv CaM kinase-like vesicle-associated protein	IPI:IPI00205056.1	54 kDa	5	0
Tax_Id=10116 Gene_Symbol=Hspa12a_predicted similar to heat shock protein 12A	IPI:IPI00358537.2	75 kDa	5	0
Tax_Id=10116 Gene_Symbol=RGD1311640_predicted similar to centrosome protein cep290	IPI:IPI00560237.2	290 kDa	4	0
Tax_Id=10116 Gene_Symbol=LOC362587 831 kDa protein	IPI:IPI00359003.4 (+1)	831 kDa	4	0
Tax_Id=10116 Gene_Symbol=Hmgcs1	IPI:IPI00188158.1	57	4	0

Hydroxymethylglutaryl-CoA synthase, cytoplasmic		kDa		
Tax_Id=10116 Gene_Symbol=Syn1 Isoform IA of Synapsin-1	IPI:IPI00191335.1 (+2)	74 kDa	4	0
Tax_Id=10116 Gene_Symbol=Tufm_predicted similar to Tu translation elongation factor, mitochondrial	IPI:IPI00371236.3	50 kDa	4	0
Tax_Id=10116 Gene_Symbol=Kns2 kinesin light chain 1 isoform B	IPI:IPI00231498.2	63 kDa	3	0
Tax_Id=10116 Gene_Symbol=Ndufv1 NADH dehydrogenase (Ubiquinone) flavoprotein 1	IPI:IPI00191913.1	51 kDa	3	0
Tax_Id=10116 Gene_Symbol=Vdac1 Voltage-dependent anion-selective channel protein 1	IPI:IPI00421874.4	31 kDa	3	0
Tax_Id=10116 Gene_Symbol=Acad9 similar to very-long-chain acyl-CoA dehydrogenase VLCAD homolog isoform 1	IPI:IPI00337099.2 (+1)	69 kDa	3	0
Tax_Id=10116 Gene_Symbol=Phgdh D-3-phosphoglycerate dehydrogenase	IPI:IPI00475835.3	56 kDa	3	0
Tax_Id=10116 Gene_Symbol=Acot7 Isoform 1 of Cytosolic acyl coenzyme A thioester hydrolase	IPI:IPI00213571.1 (+2)	38 kDa	3	0
Tax_Id=10116 Gene_Symbol=Gnaq guanine nucleotide binding protein, alpha q polypeptide	IPI:IPI00230868.4	42 kDa	3	0
Tax_Id=10116 Gene_Symbol=Camk2b Calmodulin-dependent protein kinase II beta M isoform	IPI:IPI00209824.2 (+3)	73 kDa	3	0
Tax_Id=10116 Gene_Symbol=Pfkm 6-phosphofructokinase, muscle type	IPI:IPI00231293.7	86 kDa	3	0
Tax_Id=10116 Gene_Symbol=Vps35_mapped similar to vacuolar protein sorting 35	IPI:IPI00363493.2	92 kDa	3	0
Tax_Id=10116 Gene_Symbol=Idh1 Isocitrate dehydrogenase [NADP] cytoplasmic	IPI:IPI00194045.1 (+1)	47 kDa	3	0
Tax_Id=10116 Gene_Symbol=Myh10 234 kDa protein	IPI:IPI00391300.3	234 kDa	3	0
Tax_Id=10116 Gene_Symbol=Spnb2 Non-erythrocyte beta-spectrin	IPI:IPI00373419.2	251 kDa	2	0
Tax_Id=10116 Gene_Symbol=Ncdn NORBIN	IPI:IPI00205396.1	79 kDa	2	0
Tax_Id=10116 Gene_Symbol=Dync1li1 Cytoplasmic dynein 1 light intermediate chain 1	IPI:IPI00213552.1	57 kDa	2	0
Tax_Id=10116 Gene_Symbol=Npepps similar to aminopeptidase puromycin sensitive	IPI:IPI00372700.1 (+1)	103 kDa	2	0
Tax_Id=10116 Gene_Symbol=Ppp2ca Serine/threonine-protein phosphatase 2A catalytic subunit alpha isoform	IPI:IPI00200391.1 (+1)	36 kDa	2	0
Tax_Id=10116 Gene_Symbol=Eno1 Alpha-enolase	IPI:IPI00464815.11 (+2)	47 kDa	2	0